AD

# USAAVLABS TECHNICAL REPORT 68-19
# INVESTIGATION OF THE LATERAL/DIRECTIONAL STABILITY CHARACTERISTICS OF A FOUR-PROPELLER TILT-WING VTOL MODEL

By

Richmond P. Boyden

Howard C. Curtiss, Jr.

April 1968

# U. S. ARMY AVIATION MATERIEL LABORATORIES
# FORT EUSTIS, VIRGINIA

CONTRACT DA 44-177-AMC-8(T)

PRINCETON UNIVERSITY

PRINCETON, NEW JERSEY

109

This report has been reviewed by the U. S. Army Aviation
Materiel Laboratories and is considered to be technically
sound. It is published for the exchange of information
and the stimulation of further ideas and understanding in
determining the dynamic stability of V/STOL aircraft.

INVESTIGATION OF THE LATERAL/DIRECTIONAL
STABILITY CHARACTERISTICS OF A
FOUR-PROPELLER TILT-WING VTOL MODEL

Final Report

Aerospace Research Report 743

By

Richmond P. Boyden
Howard C. Curtiss, Jr.

Prepared by

Princeton University
Princeton, New Jersey

for

U. S. ARMY AVIATION MATERIEL LABORATORIES
FORT EUSTIS, VIRGINIA

# SUMMARY

Results of an experimental investigation to determine the lateral/
directional stability characteristics of a four-propeller tilt-wing VTOL
aircraft using a one-tenth scale dynamically similar model are presented.
Test conditions include wing incidences of $89^\circ$, $70^\circ$, and $30^\circ$. Measure-
ments of the transient motion of the model in the lateral/directional
degrees of freedom and the static lateral/directional stability deriva-
tives were made using the Princeton Dynamic Model Track.

The transient and steady-state data are analyzed assuming that the motions
of the vehicle may be described by linearized equations, and the resulting
static and dynamic derivatives are presented. The characteristics of the
lateral/directional dynamic motion of the full-scale vehicle as predicted
by the tests of the dynamically similar model are determined and discussed.
All data are presented for a center-of-gravity position of 9-percent MAC,
which is ahead of the most forward C.G. position of the aircraft (15-
percent MAC), and the horizontal tail and flap programs differ from those
presently used on the aircraft.

The model results indicate that the full-scale aircraft would have an un-
stable lateral oscillation with a period of about 13 seconds at a wing
incidence of $89^\circ$. At $30^\circ$ wing incidence, the lateral/directional motion
is made up of a stable, lightly damped, Dutch-roll oscillation; a rolling
convergence; and a spiral divergence with a time to double amplitude of
about 6 seconds.

## FOREWORD

This research was performed by the Department of Aerospace and Mechanical Sciences, Princeton University, under the sponsorship of the United States Army Aviation Materiel Laboratories Contract DA 44-177-AMC-8(T), with financial support from the United States Navy, Bureau of Weapons, and the Air Force Flight Dynamics Laboratory. The research was monitored by Lt. F. E. LaCasse and Mr. William E. Sickles of the United States Army Aviation Materiel Laboratories.

The experiments described in this report were conducted by Mr. W. F. Putman and Mr. J. J. Traybar.

The research was conducted by Assistant Professor H. C. Curtiss, Jr., and R. P. Boyden of Princeton University.

# CONTENTS

## LIST OF FIGURES

# LIST OF TABLES

# LIST OF SYMBOLS

$A_T$       lift curve slope of vertical tail, per radian

$g$       acceleration due to gravity, 32.2 feet per second squared

$i$       $= \sqrt{-1}$

$i_T$       incidence of horizontal tail, degrees

$i_w$       wing incidence, degrees

$I_x$       moment of inertia about X-axis, slug-feet squared

$I_y$       moment of inertia about Y-axis, slug-feet squared

$I_z$       moment of inertia about Z-axis, slug-feet squared

$I_{xz}$       product of inertia with respect to X-Z axes, slug-feet squared

$L$       rolling moment, positive right wing down, foot-pounds

$L_v, L_{\dot{v}}, L_\varphi,$       rate of change of rolling moment with variable indicated in
$L_{\dot{\varphi}}, L_\psi, L_{\dot{\psi}}$       subscript, divided by moment of inertia in roll

$M$       pitching moment, positive nose up, foot-pounds

MAC       mean aerodynamic chord of wing

$m'$       effective scale mass of model $\left(-\dfrac{Z_0}{g}\right)$, slugs

$m_T$       traveling mass of model; sum of mass of model, support tube and error link, slugs

$N$       yawing moment, positive nose right, foot-pounds

$N_v, N_\varphi, N_{\dot{\varphi}},$       rate of change of yawing moment with variable indicated in
$N_\psi, N_{\dot{\psi}}$       subscript, divided by moment of inertia in yaw

$p$       roll rate about body axis, positive right wing down, radians per second

$q$       pitch rate about body axis, positive nose up, radians per second

$r$       yaw rate, positive nose right, radians per second

| | |
|---|---|
| S | wing area, square feet |
| s | $= \sigma + i\omega$, root of characteristic equation, per second |
| t | time, seconds |
| $T_2$ | time required for exponential function to double amplitude, seconds |
| $T_{1/2}$ | time required for exponential function to half its amplitude, seconds |
| $U_0$ | trim speed, feet per second (also carriage velocity) |
| $v'$ | lateral velocity with respect to fixed-space (motion to the right is positive), feet per second |
| v | lateral velocity with respect to body axes (motion to the right is positive), feet per second |
| Y | sideforce, force to the right is positive, pounds |
| $Y_v, Y_\psi$ | rate of change of sideforce with variable indicated in subscript, divided by effective scale mass of model $(m')$ |
| $Z_0$ | vertical aerodynamic force in steady flight, pounds |
| $\beta$ | sideslip angle, positive for positive lateral velocity, radians |
| $\beta_{.75R}$ | propeller blade angle at 3/4 radius, degrees or radians |
| $\delta_f$ | flap deflection, degrees |
| $\lambda$ | linear scale factor $= \dfrac{\text{full-scale linear dimension}}{\text{model linear dimension}}$ |
| $\rho$ | air density, slugs per foot cubed |
| $\sigma$ | damping, real part of "s", per second |
| $\theta$ | pitch angle, positive nose up, radians |
| $\varphi$ | roll angle, positive right wing down, radians or degrees (see Figure 4) |
| $\Psi$ | yaw angle, positive nose right, radians or degrees (see Figure 4) |
| $\omega$ | frequency, imaginary part of "s", per second |

| | |
|---|---|
| $\Omega$ | propeller rotational speed, radians per second or revolutions per minute |
| $C_T$ | propeller thrust coefficient, $\dfrac{T}{\rho \pi R^2 (\Omega R)^2}$, propeller rotational speed in radians per second |
| $T$ | propeller thrust, pounds |
| $R$ | propeller radius, feet |
| $(\bar{\ })$ | amplitude of envelope of variable |
| $(\dot{\ })$ | derivative with respect to time |
| $(\ )_B$ | with respect to body axes |
| $(\ )_0$ | initial or trim value |

# INTRODUCTION

The current interest in tilt-wing VTOL aircraft is accompanied by a lack of quantitative data on the dynamic motions and stability derivatives of these VTOL aircraft at low forward speeds. The experimental data and analysis presented here represent part of a continuing effort at the Princeton Dynamic Model Track to provide information of this nature. The results include the first quantitative information published on the lateral/directional dynamic derivatives of tilt-wing VTOL aircraft at low forward speeds. Longitudinal experiments on this same model are presented in Reference 7, and some lateral/directional characteristics of a similar model are described in Reference 9.

The experimental results were obtained using the model and apparatus shown in Figures 2 and 3. The following measurements were made: variation of sideforce, rolling moment, and yawing moment with lateral velocity; and transient response of the model in the three lateral/directional degrees of freedom and in various restricted lateral/directional degrees of freedom. These data were taken at three wing incidence angles: $89°$, $70°$, and $30°$. The general form and nature of the data indicated that for the flight conditions investigated, the transient motions could be approximated by linearized equations.

The experiments conducted to evaluate the stability characteristics of a model using the Princeton Dynamic Model Track fall into two categories. The first is similar to wind tunnel testing, and the data that result are referred to in the following as static data. Total forces and moments acting on the model as a function of flight condition were measured. Since the primary aim of the experiments was to obtain information on the stability of the vehicle, emphasis was placed on the force and moment variations about level, unaccelerated flight. The second category consisted of direct measurements of the transient response of the model by using a servo-controlled tracking carriage. The model employed in this study was dynamically similar to a full-scale vehicle. The carriage permits semifree flight of the model in selected degrees of freedom and is described in detail in References 4 and 5. The data resulting from the latter experiments are referred to as dynamic data and are similar in nature to flight-test data.

The four-propeller tilt-wing transport model is a one-tenth scale dynamic model of the LTV XC-142, based on full-scale aircraft characteristics given in Reference 1. The general arrangement of the model is shown in Figure 5. Details of the flap geometry are given in Figure 6a, and the propeller blade characteristics are shown in Figure 7. The model differs in the following respects from the present configuration of the XC-142A described in Reference 2:

a.  Krüger flaps, as shown in Figure 6b, were installed on the model. The leading edge slats presently in use were not installed on the model.

b.  All experiments were conducted at a center-of-gravity position of 9-percent MAC, ahead of the most forward center-of-gravity position of the aircraft (15-percent MAC).

c.  The inboard and outboard propeller thrust lines are parallel on the model. The inboard thrust line of the XC-142A is located at a negative incidence of $2°6'$ with respect to the outboard thrust line.

d.  The wing airfoil section of the XC-142A is a NASA 63-318 with a modified trailing edge. The model airfoil section is an unmodified NASA 63-318.

e.  The horizontal tail incidence and flap deflection with wing incidence differ from those presently in use on the aircraft as shown in Figure 9.

These differences originate from the fact that model design and construction were concurrent with the design and construction of the full-scale aircraft.

Only limited comparison of model data with flight test is possible at this time. A wing incidence versus trim speed comparison is shown in Figure 10. The model exhibits somewhat higher equivalent full-scale trim speeds than the aircraft. The primary model configuration difference of those described above that may influence the trim speed is the absence of leading edge slats. Leading edge slats will promote improved flow conditions over the wing at low speeds and therefore would be expected to reduce the model trim speeds. With respect to this comparison, it should also be noted that the airspeed measuring system on the full-scale aircraft has not been calibrated at low speeds (Reference 3).

The transient response data were analyzed in conjunction with the force and moment data, using servo analysis techniques as described in Appendix I, to determine the stability derivatives of the model. These data were converted to full scale as discussed in Appendix II, and are presented in Figure 1.

## DESCRIPTION OF APPARATUS

### TEST FACILITY

The Princeton Dynamic Model Track is a unique facility designed expressly for the study of the dynamic motions of helicopter and VTOL models at low forward speeds. Equivalent flight speeds up to 75 knots can be investigated with a one-tenth scale model. Basic components of the facility include a 750-foot track and a servo-driven carriage located in a building with a test cross section of 30 by 30 feet. The carriage has an acceleration potential of 0.6g, and steady sustained carriage speeds of up to 40 feet per second are possible. The facility is described in detail in References 4, 5, and 6.

A variety of different booms may be used to attach models to the carriage. Two of these are the lateral and longitudinal mounts. The longitudinal mount is shown in Figure 2. It permits relative motion of the model in the horizontal and vertical directions with respect to the carriage. Horizontal relative motion is sensed and used to command the carriage to follow the model in a closed-loop fashion. Vertical position of the model with respect to the boom moves the boom assembly vertically with respect to the carriage. This servo operation of the carriage and boom allows the model to fly "free" in the longitudinal degrees of freedom with no restraints imposed on the model in those degrees of freedom being investigated.

The lateral mount is shown in Figure 3. This boom configuration permits the model to fly "free" in the lateral/directional degrees of freedom. A schematic drawing of the lateral/directional mount is shown in Figure 4. Relative motion is permitted between the model support linkage and the lateral servo-driven carriage. This lateral displacement of the model and support linkage is sensed and used to position the lateral servo-driven carriage along the lateral boom. Yaw freedom is provided by a pivot mounting that permits angular rotation between the vertical tube supporting the model and the lateral servo-driven carriage. Roll freedom is provided by a pivot mounting located within the fuselage of the model that permits angular motion in roll with respect to the vertical support tube. It should be noted that yaw freedom is provided about a space-fixed axis, and roll freedom is provided about a body-fixed axis. Mechanically, it is not possible to provide two body-fixed axis freedoms. The effects of this linkage configuration are considered in detail in Appendix III.

One-, two-, or three-degree-of-freedom motion can be investigated longitudinally or laterally by restraining various degrees of freedom.

In addition to dynamic testing as described above, testing to determine the static stability derivatives is conducted by programming carriage or model movement in accordance with preselected variations of a particular flight variable (sideslip and side velocity in these experiments). The

3

model is rigidly mounted on the carriage, and forces and moments acting on the model are measured with strain gauges. Although this type of testing is similar to wind tunnel testing, this facility offers a 30-by-30-foot test section with a uniform air velocity, free from turbulence. Precise speed control over a range of speeds from backward flight through hover to forward flight is available. This technique is called quasi-steady-state testing.

MODEL

A three-view drawing of the model constructed for these experiments is shown in Figure 5, and its pertinent dimensions are given in Table IV. The model was based on the full-scale aircraft configuration given in Reference 1.

The fuselage is constructed of an inner and outer Fiberglas skin, vacuum molded and bonded to a Styrofoam core. An aluminum box spar is the main structural member of the wing. Mahogany ribs and a vacuum-molded Fiberglas wing surface form the external airfoil shape. The double-slotted flaps are constructed of low-density Styrofoam with a Fiberglas covering.

The model drive motor is a 200-volt, 400-cycle, 3-phase electric motor, rated at 5 horsepower, mounted on a bulkhead in the fuselage. Power for the four propellers is transmitted to a central transmission and from thence to right-angle gearboxes located in the wing by flexible shafting. A separate power takeoff is used to drive the tail rotor. Propeller gearboxes and housings are mounted directly on the wing spar. The propeller blades were constructed of Fiberglas by the Hamilton Standard Division of the United Aircraft Corporation. The geometric characteristics of the propellers are shown in Figure 7. The static thrust characteristics of the propellers are given in Figure 8.

Model control positions are set from a control console on the carriage. The model incorporates electrically controllable blade angles on each of the four propellers. The collective pitch system is arranged so that the left and right propellers are separately controllable. This provides differential collective pitch for roll trim. The blade angle of the tail rotor is also variable to provide pitching moment trim. Wing incidence, flaps, ailerons, and the horizontal tail are also power operated so that transition runs may be made with selected programming of all required controls. All of these systems are closed-loop position controls.

The complexity of the model, due to the components required for control and such details as double-slotted flaps, made meeting the scaling requirements on model weight and moments of inertia difficult. A comparison of scaled model characteristics with desired full-scale values is shown in Table IV. The corrections necessary to account for these differences on the full-scale vehicle are discussed in later sections. Dynamic model scaling relationships may be found in References 4 and 5, and the resulting model/full-scale relationships are given in Table VI.

4

## DATA RECORDING

All data are transmitted via a telemetering system from the moving carriage to a ground station located in a control room near the track. Data transducers provide signals to a telemeter transmitter mounted on the carriage. The telemetering system provides 20 samples of data per channel per second, with a maximum of 43 channels available. Real-time monitoring of all data quantities is provided by a monitor scope in the telemeter ground station; the data are presented on multi-channel Sanborn recorders and/or X-Y plotters and are simultaneously recorded on an Ampex model 309 tape recorder.

# EXPERIMENTAL RESULTS

This section contains a discussion of the experimental data and the general nature of the results. The techniques used to analyze and interpret the data and the results of the analysis are considered in detail in Appendix I. To minimize the presence of various conversion factors, all discussion in this section is given in terms of model parameters. Then, in the following section, corresponding full-scale results are presented on the basis of scaling described in Appendix II.

## HOVER

### Static Tests

For experiments near hover, the model was mounted on the longitudinal servo boom (Figure 2) with the longitudinal axis of the model yawed $90^\circ$ from the centerline of the track. Carriage velocity then corresponded to model lateral velocity.

The sideforce, rolling moment, and yawing moment variations with lateral velocity were measured by a quasi-steady-state procedure discussed previously. The model was restrained to the carriage by strain gauges to measure rolling moment, yawing moment, and sideforce. With the model trimmed for hover, the carriage was programmed to accelerate slowly to a velocity of approximately 8 feet per second in one direction, then to decelerate through hover to a velocity of 8 feet per second in the other direction, and to return to hover. The carriage acceleration during the experiments varied between 0.4 and 0.7 foot per second per second. Runs were made with the tail rotor running and not running to determine the effect on sideforce, rolling moment, and yawing moment. The only tail rotor contribution apparent in any of the tests was a change in the yawing moment variation with lateral velocity, as illustrated in Figure 11.

Although, in principle, the velocity of the model should be steady for each datum point around the trim condition to determine the static stability derivatives, previous experience has shown that the technique of quasi-steady-state testing - that is, programming the carriage for very small accelerations - yields data that are identical to those obtained with point-by-point measurements at constant velocity. The quasi-steady technique results in a considerable reduction in testing time, and it is valid as long as the carriage accelerations involved are small. A limited number of the data points presented were verified by steady-state measurements at constant velocities.

The noise level present in the force and moment data taken in this quasi-steady-state fashion was of such a magnitude as to require filtering of the data. Disturbances arise from irregularities in track alignment caused by deformations due to ambient temperature variations and carriage mass as well as the presence of expansion joints in the track. The

6

moving carriage is subjected to small acceleration inputs which are transferred through the boom to the model and sensed by the force and moment instrumentation. Viscous dampers in the model restraint linkage, shock mounting of the boom with respect to the carriage, and mass balancing have been used with success to alleviate extraneous inputs from the carriage. These methods are discussed in References 4 and 5. Later development of a shock-mounted carriage, specifically for static testing, has essentially eliminated these problems.

Sideforce, rolling moment, and yawing moment versus sideslip velocity near hover are shown in Figure 11. These data were plotted directly from recorded data using an Autograf X-Y plotter. The data were filtered by a low-pass filter with a corner frequency of 1 cycle per second. The stability derivatives $Y_v$ and $L_v$ were determined by taking a straight-line approximation to the slope of these curves in the neighborhood of zero lateral velocity. The range of values and the average value taken as representative for $Y_v$ and $L_v$ are listed in Table II. The yawing moment versus lateral velocity is nonlinear, and therefore no slope is given. Although the data for yawing moment appear to be quite irregular, they were reasonably consistent over a number of runs.

Dynamic Tests

Single-degree-of-freedom responses were used to determine the roll damping, $L_{\dot{\phi}}$, and the yaw damping, $N_{\dot{\psi}}$. To measure roll damping, the model was locked in yaw, and mechanical springs were attached between the model support tube and the model to provide a restoring moment about the roll axis. The equation of motion for the rigid-body oscillation of the model in roll with the mechanical spring moment, aerodynamic damping, and model mounting friction acting on the model is

$$I_x \, \ddot{\phi} - \left(\frac{\partial L}{\partial \dot{\phi}} + \text{friction}\right) \dot{\phi} - \frac{\partial L}{\partial \phi} \, \phi = 0 \tag{1}$$

The contribution of the friction term to these experiments was neglibible. The spring constant, $\frac{\partial L}{\partial \phi}$, arises from the mechanical spring and the model center-of-gravity position.

The roll damping runs were conducted by releasing the model with propellers running from an initial roll angle offset and recording the resulting roll angle versus time. A flow deflector was used to delay the effects of downwash recirculation as discussed in Reference 8. A selection of the roll damping runs is shown in Figure 12a. From the spring constant and the measured frequency of oscillation of the model in roll, the moment of inertia about the roll axis was determined. Of eight runs, two indicated no damping. An exponential decay was fitted to two of the six runs. The

variation between runs is attributed to the presence of downwash recirculation in spite of the use of a flow deflector. The damping in roll is small, and the effects of random disturbances are therefore particularly noticeable in causing this scatter. The values obtained for roll damping are given in Table VII.

A similar procedure was used to determine the moment of inertia about the yaw axis and the yaw damping. These data were more consistent than the roll measurements due to the larger magnitude of the damping. Figure 12b shows typical responses, and the values of yaw damping that result are listed in Table VII.

Self-excited transient responses were measured for two degrees of freedom (roll angle and lateral velocity) and three degrees of freedom (roll angle, lateral velocity, and yaw angle). The model was fixed to the carriage while the model motor was brought up to speed. Then, the required degrees of freedom were released by unlocking mechanical restraints. The resulting transient motion was recorded. No deliberate inputs were used to excite the model, since the transient motion was unstable and small random disturbances were sufficient to excite the motion.

Typical time histories for the two-degree-of-freedom responses are reproduced in Figures 13a and b. The period and damping of two runs with at least two peaks in the data are given in Table VII. The average values measured for two degrees of freedom (roll and side velocity) were a period of 6.2 seconds and a damping of + 0.59 per second (damping ratio of - 0.51).

Responses in three degrees of freedom, conducted in the same manner as the two-degree-of-freedom runs with yaw angle also released, are shown in Figures 13c and d. The values of the period and damping for three degrees of freedom are included in Table VII. The roll and lateral velocity motions were oscillatory; however, the yaw motion increased monotonically with time and was thus apparently uncoupled from the roll, lateral velocity motions. The average period for the oscillatory motion in roll and lateral velocity was 6.8 seconds with an average damping of + 0.56 per second (damping ratio of - 0.52).

FORWARD FLIGHT

Static Tests

The forward flight experiments were conducted using the lateral mount (Figure 3). Trim conditions corresponding to two wing incidence settings, $70^\circ$ and $30^\circ$, were investigated at model forward velocities of 9.5 and 23 feet per second, respectively, corresponding to full-scale speeds of 17.8 and 43 knots. At $70^\circ$ wing incidence, the model was in a level flight trim condition as determined from previous longitudinal measurements (Reference 3). However, the $30^\circ$ wing incidence case represented a trim condition suggested by the LTV Aerospace Corporation. The exact flight

8

condition was not known, since no horizontal force measurements were made at $30^\circ$ incidence. Extrapolation of data from Reference 7 indicates that the flight condition was equivalent to a slow climb. Test conditions are summarized in Table V.

The variation of sideforce, rolling moment, and yawing moment with lateral velocity was measured by the quasi-steady-state procedure, described previously. While the carriage was traveling at a selected speed, the model was programmed to yaw $(\Psi = -\beta)$ slowly from $0^\circ$ yaw angle to about $+20^\circ$, then to $-20^\circ$, and back to $0^\circ$. The yaw rate for this maneuver was limited to between $2^\circ$ and $6^\circ$ per second to eliminate any unsteady effects and the appearance of yaw damping in the data. The data from these experiments (sideforce, rolling moment, and yawing moment versus sideslip angle) were plotted from the recorded data using an Autograf X-Y plotter. Samples of these curves for wing incidences of $70^\circ$ and $30^\circ$ are shown in Figure 14. These data were filtered to reduce noise due to extraneous track inputs, as previously mentioned. At $30^\circ$ wing incidence, the programmed yaw rate of $6^\circ$ per second was quite large, and so the data presented in Figure 14f include a noticeable contribution from the yaw damping, causing a relative displacement of the yawing moment as a function of sideslip angle due to the sign of the yaw rate.

The noise level present in the rolling moment measurements for both forward flight conditions was high. Figure 14e is presented only to indicate the trend of this derivative. No detailed conclusions should be drawn from the shape of these curves. For this reason, $L_\beta$ is considered as an unknown parameter in the following discussion.

The variation of sideforce, rolling moment, and yawing moment with sideslip angle exhibited an approximately linear character. The stability derivatives $Y_\beta$, $L_\beta$, and $N_\beta$ were determined by taking the linear slope from these graphs in the neighborhood of zero sideslip angle. The relationships between the stability derivatives taken with respect to lateral velocity and sideslip are given by $Y_\beta = - U_0 Y_v$, $L_\beta = - U_0 L_v$, and $N_\beta = - U_0 N_v$. The lateral velocity derivatives at wing incidences of $70^\circ$ and $30^\circ$ are given in Table VIII.

For wing incidences of $89^\circ$ and $30^\circ$, the roll moments of inertia differed by less than 1 percent and the yaw moments of inertia differed by less than 3 percent. Because of this small variation, average values of $I_x = 2.65$ slug-feet$^2$ and $I_z = 3.55$ slug-feet$^2$ were used for all three wing incidences.

## Dynamic Tests

The lateral/directional transient response measurements at forward speed were conducted in the following degrees of freedom:

$\underline{i_w = 70^0}$

Three degrees of freedom in roll, yaw, and lateral velocity

$\underline{i_w = 30^0}$

One degree of freedom in roll
One degree of freedom in yaw ($\Psi = -\beta$)
Two degrees of freedom in roll and yaw ($\Psi = -\beta$)
Three degrees of freedom in roll, yaw, and lateral velocity

The test procedure was to bring the model motor up to speed with the carriage stationary and the model locked with respect to the boom. After the carriage had accelerated and was traveling at the trim speed, timers were used to unlock the mechanical restraints of the desired degrees of freedom. The model was then able to "fly" free in roll, yaw, and sideslip, or in combinations thereof. At a wing incidence of $70^0$, no predetermined inputs were used to excite the model in the majority of the runs, since the response was dominated by an unstable oscillation. Usually some small random disturbance was sufficient to start the motion. However, an initial sideslip angle was used to excite the model motion in the majority of the $30^0$ wing incidence runs, since the motion was stable in the one-degree-of-freedom yaw tests and was marginally stable in the two- and three-degree-of-freedom tests. The amount of initial sideslip angle used as an "input" varied from $2^0$ to $10^0$.

Sample traces at a wing incidence of $70^0$ with three degrees of freedom are shown in Figure 16. The period and damping determined are listed in Table VIII. The average period of the oscillatory motion at $70^0$ wing incidence was 5.4 seconds; the average damping was + 0.48 per second (damping ratio of - 0.38). In these three-degree-of-freedom runs, the yawing moment equation of motion was coupled with the sideforce and rolling moment equations; this is in contrast to hover, where it was uncoupled.

Single-degree-of-freedom runs in yaw ($\Psi = -\beta$) at a wing incidence of $30^0$ are included in Figure 16a. The characteristics of these runs are listed in Table VIII. These runs were characterized by a damped oscillation with an average period of 4.4 seconds and a damping of - 0.50 per second (damping ratio of + 0.33).

Two-degree-of-freedom tests in roll and yaw ($\Psi = -\beta$) at $30^0$ wing incidence gave an average period of 4.8 seconds and an average damping of zero. Typical runs are shown in Figures 16b and c, and the characteristics of each run are listed in Table VIII.

Typical time histories of the three-degree-of-freedom motion are shown in Figures 17d and e. Period and damping as measured from the traces are listed in Table VIII. As is evident from Figures 17d and e, there was some difficulty in obtaining data on the lateral velocity response. Precise trim settings were necessary to keep the lateral displacements of the model

10

within the freedom allowed by the lateral boom. In run 436 (shown in Figure 17e), however, the model hit the boom limits, rebounded, and then after a delay of several seconds went through a complete cycle of motion which appeared in all three variables. The period of the oscillatory motion in run 436 was 4.0 seconds with zero damping. This was the only run for $30^\circ$ wing incidence in which the oscillatory motion in lateral velocity was clearly discernible. The characteristics of the oscillatory motion of the series of five runs in three degrees of freedom were an average period of 4.4 seconds and a damping of zero.

The experimental values of the characteristic roots of the model oscillatory motion at wing incidences of $89^\circ$, $70^\circ$, and $30^\circ$ are summarized in Figure 18.

## DYNAMICS OF THE FULL-SCALE AIRCRAFT

The full-scale aircraft stability derivatives, as determined from the experiments using the analysis discussed in Appendix I and the scaling discussed in Appendix II, are shown as a function of wing incidence in Figure 1. The dashed lines indicate the probable trends of the derivatives. The following points may be noted with respect to the stability derivatives:

The Sideforce due to Lateral Velocity $(Y_v)$. This derivative was found to be small and of minor importance in determining the characteristic modes of motion of the aircraft in the range investigated.

The Dihedral Effect $(L_v)$. This derivative is stable (negative) over the range of test conditions. Its value in hover is quite large, causing a roll-lateral velocity motion in hover that is very similar to the pitch-forward velocity motion discussed in Reference 7.

The Directional Stability $(N_v)$. The aircraft is directionally stable (positive) at forward speeds greater than 17 knots. Near hover, the yawing moment was a nonlinear function of lateral velocity. The measured value of $N_v$ at a wing incidence of $30°$ is approximately twice the value calculated from the rough approximation that the primary contribution to this derivative is the effect of the free-stream velocity on the vertical tail. If it is assumed that the sidewash is negligible, and that the vertical tail efficiency factor is one, the directional stability is equal to (Reference 8)

$$N_v \cong \frac{q \; S_T \; A_T \; \ell_T}{I_z \; U_0}$$

which is about one-half the value shown in Figure 1. The following values are used:

$S_T$ = 130 square feet

$A_T$ = 2 per radian

$\ell_T$ = 23.5 feet

$U_0$ = 43 knots (72.5 feet per second)

$I_z$ = 270,000 slug-feet squared

$N_v$ = 0.0024 per foot-second

12

Note also the slope reversal that appears in the data at sideslip angles greater than about $15^{o}$ (Figure 14f). The measured variation in yawing moment differs from that presented in Reference 9 on a similar configuration at lower wing incidence, in that there is apparently no flat spot near zero sideslip for the data presented here.

The Roll Damping $(L_{\dot{\phi}})$. This derivative is fairly small and increases in a stable sense as wing incidence is reduced.

The Yaw Damping $(N_{\dot{\psi}})$. This derivative increases in a stable sense as wing incidence is reduced.

The Rolling Moment due to Yaw Rate $(L_{\dot{\psi}})$. This derivative increases as wing incidence is reduced and is positive, as is typical of conventional aircraft (Reference 8).

The Yawing Moment due to Roll Rate $(N_{\dot{\phi}})$. This derivative is positive and the magnitudes indicated have only a small effect on the characteristic roots of the aircraft. The positive sign is opposite the sign normally present on a conventional aircraft (Reference 8).

These data indicate that the dynamic motion of the full-scale aircraft in hover would consist of a divergent oscillation in roll angle and lateral velocity with a period of 12.7 seconds and a time to double amplitude of 3.6 seconds. The motion of the vehicle in yaw is uncoupled from the roll and lateral velocity. The third root of the characteristic equation corresponding to the rolling convergence mode gives a time to one-half amplitude of 1.0 second. The divergent oscillation in roll and lateral velocity shows that the vehicle would be sensitive to lateral gusts due to the presence of the comparatively large dihedral effect $(L_v)$. The model period of 6.2 seconds near hover agrees well with the data given in Reference 9 for a similar dynamic model with similar rolling inertia. The full-scale period given above is shorter than that presented in Reference 9 because the difference between scaled model and true full-scale inertia has been taken into account here.

Incomplete data at $70^{o}$ wing incidence prevented a detailed analysis of the lateral/directional dynamics of the full-scale aircraft. However, the model results indicate that all three degrees of freedom were coupled and that the transient motion would be dominated by a divergent oscillation which would be less unstable than at hover.

For $30^{o}$ wing incidence, the model results indicate that the full-scale aircraft would exhibit a stable Dutch-roll-type oscillation, with a period of 9.2 seconds and a time to one-half amplitude of 6.3 seconds. The rolling convergence would have a time to one-half amplitude of 0.85 second, while the spiral mode would be divergent, with a time to double amplitude of 6.3 seconds.
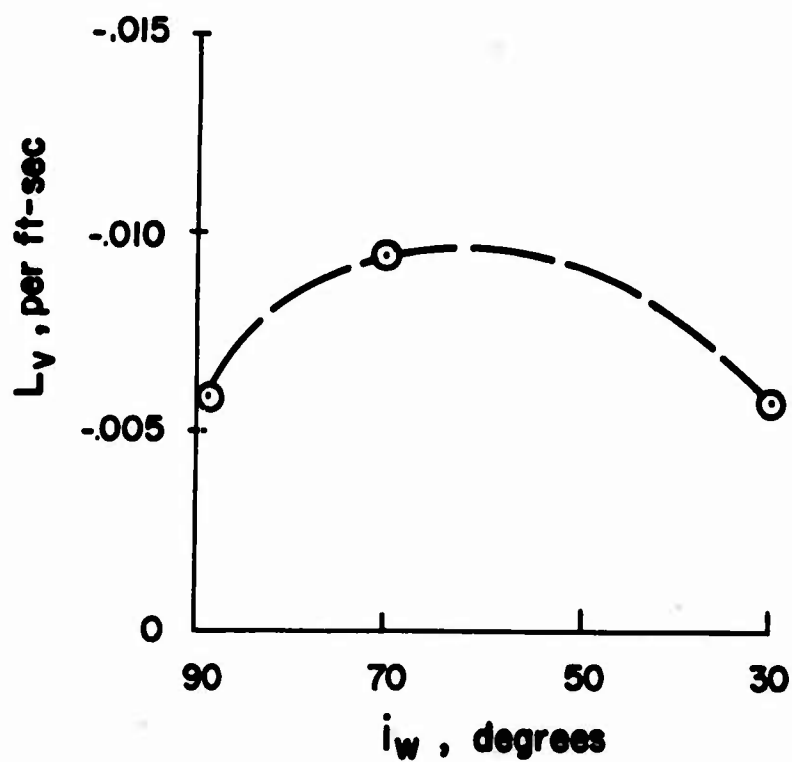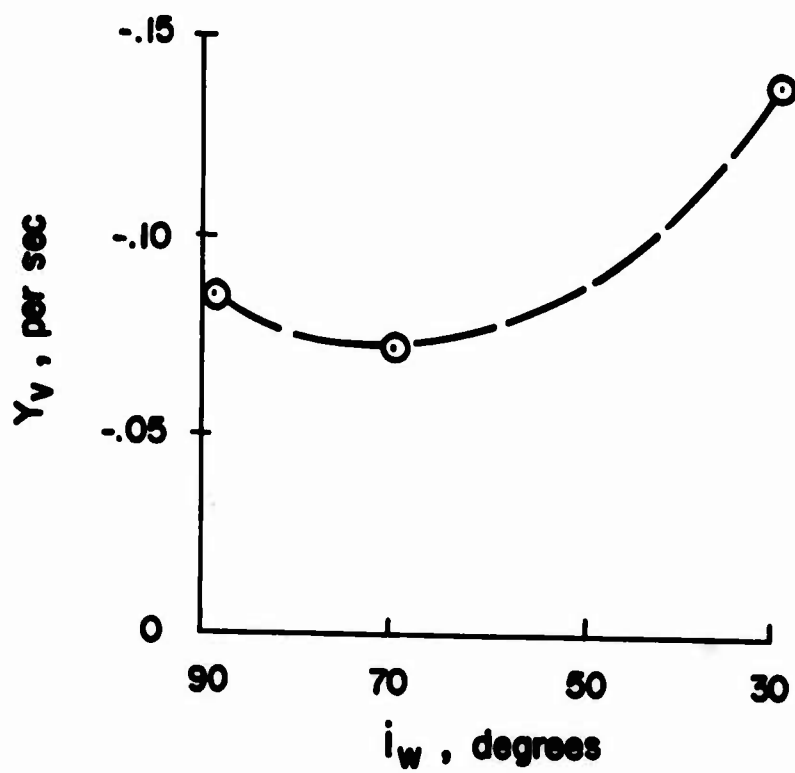
13

Figure 1. Full-Scale Stability Derivatives.
(See Table V, Page 51, for Test Conditions)

Figure 1. Continued.

15

Figure 1. Continued.

16

Figure 1. Continued.

17
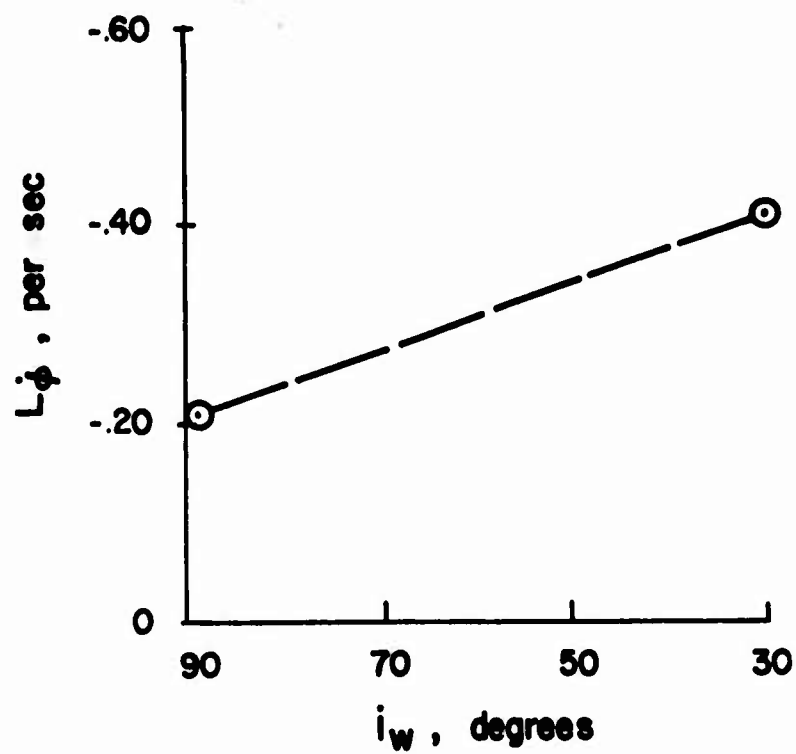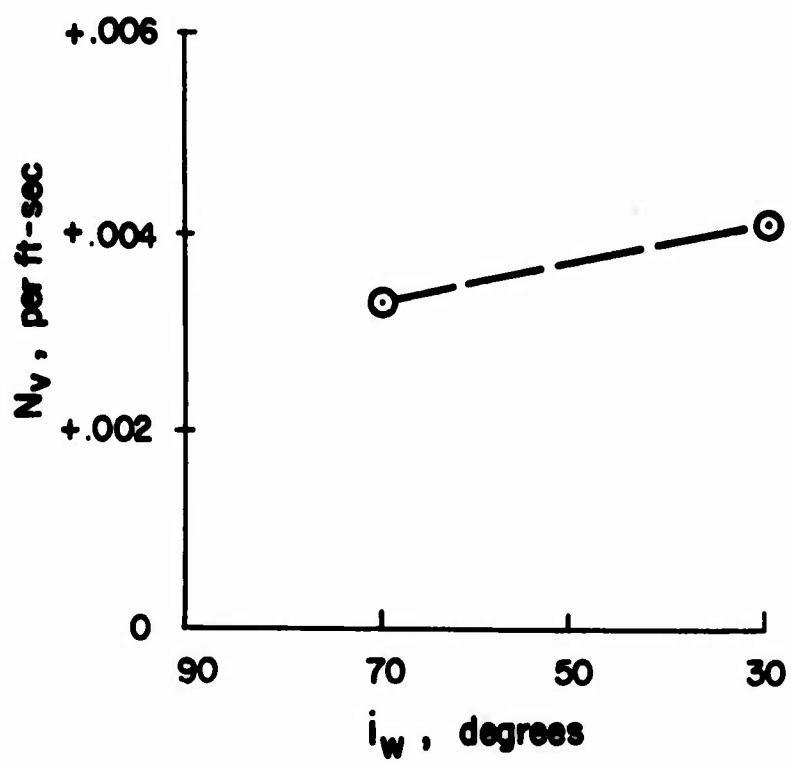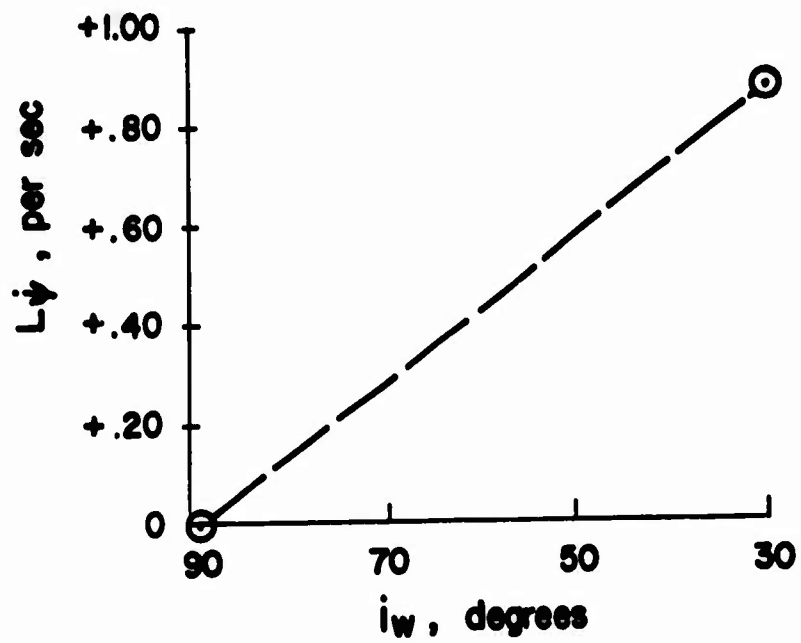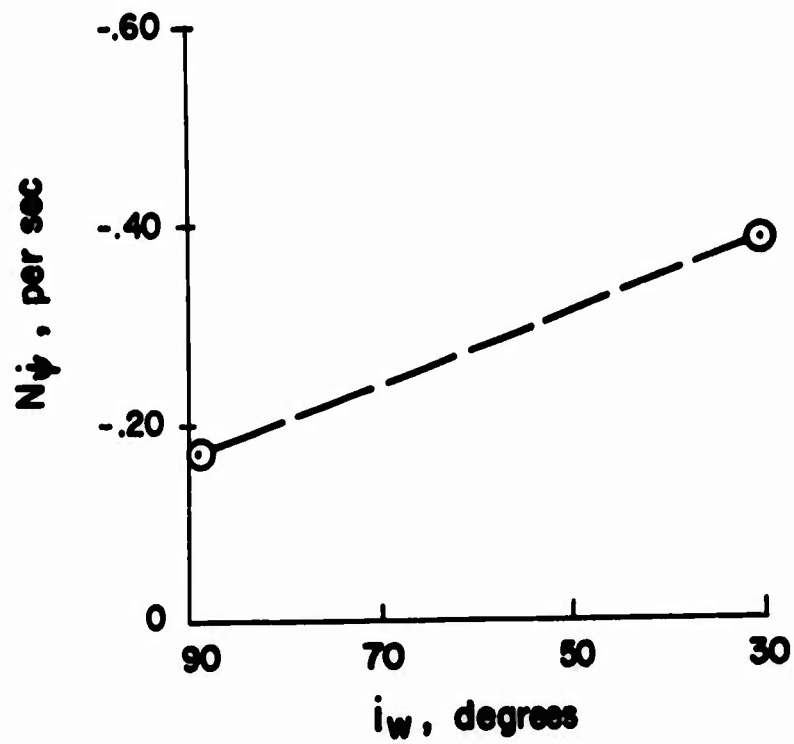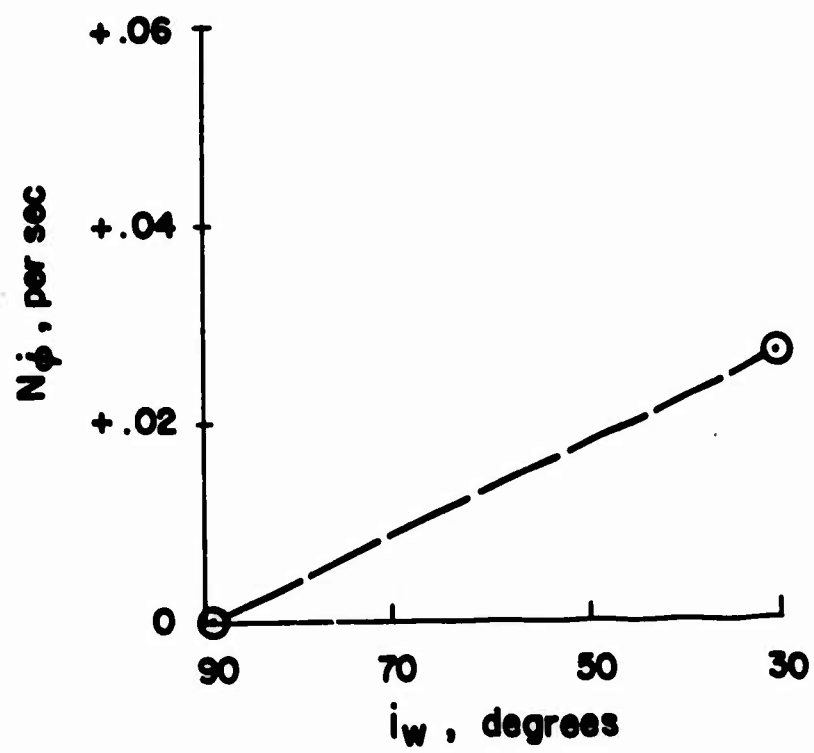
## CONCLUSIONS

1.  The model results indicate that the full-scale aircraft would have an
    unstable lateral oscillation with a period of about 13 seconds at a
    wing incidence of $89^\circ$. At $30^\circ$ wing incidence, the lateral/directional
    motion is made up of a stable, lightly damped, Dutch-roll oscillation;
    a rolling convergence; and a spiral divergence with a time to double
    amplitude of about 6 seconds.

2.  Force and moment measurements correlated to a satisfactory degree with
    the related dynamic response data. In both flight conditions analyzed
    in detail, the dihedral effect $(L_v)$ as determined from transient
    response experiments was somewhat smaller than the value obtained from
    quasi-steady-state measurements. The source of this discrepancy is
    not clear; however, it may be noted that the value of $L_v$ determined
    from dynamic response measurements is quite sensitive to accurate
    measurement of the frequency of the motion.

# RECOMMENDATIONS

1. Future lateral/directional experiments should be conducted in such a way as to eliminate mounting linkage effects. Two methods are available to accomplish this:

    a. Longitudinal force-moment instrumentation can be used to verify longitudinal trim conditions.

    b. A mounting linkage with three angular degrees of freedom could be used with the model stabilized in pitch attitude.

By either of these procedures the appearance of extraneous derivatives in the model tests, such as $N_\varphi$ in the present forward flight case, would be avoided.

The latter method is considered to be the preferable one, since the longitudinal trim of the model would be definitely established.

2. An effort should be made to correlate the results obtained herein in the form of stability derivatives and characteristics of dynamic response with full-scale flight-test data on similar configurations.

3. This series of experiments indicated clearly the need for improvement in the force and moment measurement techniques used for lateral/directional investigations. This has been accomplished since these experiments were conducted through the development of a shock mounted carriage which is in use at the present time.

# REFERENCES

1. Josephs, L. C., VHR-447 Tri-Service Transport Proposal, Volume 7 Summary Report, Part 2, Airplane Description, Chance Vought Corporation, Hiller Aircraft Corporation, and Ryan Aeronautical Company, AER-EIR-13347, April 1961.

2. Shields, M. E., Estimated Flying Qualities XC-142A V/STOL Assault Transport, LTV Aerospace Corporation, Report No. 2-53310/4R939, Dallas, Texas, May 1964.

3. Ransone, Robin K., and Jones, Gay E., XC-142A V/STOL Transport Tri-Service Limited Category I Evaluation, Air Force Flight Test Center, Technical Report No. 65-27, Edwards Air Force Base, California, January 1966.

4. Curtiss, H. C., Jr., Putman, W. F., and Martinez, E., "The Evaluation of Stability and Control Characteristics of Aircraft at Low Speeds Using Dynamically Similar Models in Semi-Free Flight", Proceedings of the American Helicopter Society Eighteenth Annual National Forum, Washington, D. C., May 1962.

5. Curtiss, H. C., Jr., Putman, W. F., and Traybar, J. J., "The Princeton Dynamic Model Track", Presented at the AIAA Aerodynamic Testing Conference, Washington, D. C., March 9-10, 1964.

6. Curtiss, H. C., Jr., Traybar, J. J., and Putman, W. F., General Description of the Princeton Dynamic Model Track, U. S. Army Aviation Materiel Laboratories, USAAVLABS Technical Report 66-73, Fort Eustis, Virginia, November 1966.

7. Curtiss, H. C., Putman, W. F., and Lebacqz, J. V., An Experimental Investigation of the Longitudinal Dynamic Stability Characteristics of a Four-Propeller Tilt-Wing VTOL Model, U. S. Army Aviation Materiel Laboratories, USAAVLABS Technical Report 66-80, Fort Eustis, Virginia, 1966.

8. Seckel, E., Stability and Control of Airplanes and Helicopters, Academic Press, New York, 1964.

9. Newsom, W. A., Jr., and Kirby, R. H., Flight Investigation of Stability and Control Characteristics of a 1/9-Scale Model of a Four-Propeller Tilt-Wing V/STOL Transport, NASA TN D-2443, Washington, D. C., September 1964.

10. Dynamics of the Airframe, Bureau of Aeronautics Report AE-61-4 II, Norair Division of Northrop Corporation, Hawthorne, California, September 1952.

11. Ashkenas, I. L., and McRuer, D. T., _Optimization of the Flight-Control, Airframe System_, Journal of the Aerospace Sciences, March 1960, pp. 197-218.

12. Breuhaus, W. O., _Résumé of the Time Vector Method as a Means for Analyzing Aircraft Stability Problems_, Wright Air Development Center, WADC Technical Report 52-299, Wright-Patterson Air Force Base, Ohio, November 1952.

APPENDIX I
ANALYSIS OF DATA


Analysis of model data to determine the stability derivatives of the air-
craft is discussed in this section.

## AXIS SYSTEM AND EQUATIONS OF MOTION

Because model data were measured with respect to a moving carriage, it is
convenient to use lateral/directional equations of motion referenced to
an axis system fixed in space (Figure 4). Precisely, the roll angle and
roll moment of the model were measured with respect to a body reference
axis, and yaw angle and yaw moment were measured with respect to a space
reference axis (Figure 4).

The space-reference roll angle and roll moment differed from body refer-
enced quantities by the cosine of the yaw angle, since all tests were
conducted with a level fuselage attitude (Appendix III). As the yaw
angle seldom exceeded $\pm 15^{\circ}$ during the responses, the cosine of the yaw
angle was approximately equal to one. Therefore, no distinction in
angular quantities between body-fixed axes and space-fixed axes is
necessary in the following. Lateral velocity and side force were
measured with respect to a space-fixed axis, perpendicular to the plane
of the gravity vector and the initial position of the longitudinal
centerline of the model.

The use of the space axis velocity $v'$ as a variable in the following
analysis makes it necessary to include derivatives dependent on yaw angle.

The functional forms of the aerodynamic forces and moments acting on an
aircraft, which depend only on the body-axis lateral velocity, the roll
rate, and the yaw rate, are

$$Y = Y(v, \dot{\phi}, \dot{\Psi})$$

$$L = L(v, \dot{\phi}, \dot{\Psi})$$

$$N = N(v, \dot{\phi}, \dot{\Psi})$$

The relationship between the body axis velocity $v$, the space axis ve-
locity $v'$, and the yaw angle is

$$v = v' - \Psi U_0$$

22

so that the relationships between the $\Psi$ and $v'$ derivatives and the $v$ derivatives are

$$\frac{\partial(\ )}{\partial \Psi} = - U_0 \ \frac{\partial(\ )}{\partial v} = - \frac{\partial(\ )}{\partial \beta} \tag{2}$$

$$\frac{\partial(\ )}{\partial v'} = \frac{\partial(\ )}{\partial v} \tag{3}$$

Therefore, the superscript may be dropped on the lateral velocity derivatives. The $\Psi$ derivatives are directly related to the $v$ derivatives, and must be included in the equations of motion when a space-fixed axis system is used. The yaw angle derivatives are directly related to the sideslip derivatives as indicated.

If the horizontal aerodynamic force $X$ is not initially zero, that is, if the model is not in level flight trim, then the side force $Y_f$, measured with respect to a space-fixed axis, will be

$$Y_f = Y - X_0 \ \Psi$$

and

$$\frac{\partial Y_f}{\partial \Psi} = \frac{\partial Y}{\partial \Psi} - X_0$$

so that equation (2) is valid only if the resultant horizontal force is zero.

The linearized, small perturbation, lateral/directional equations of motion relative to a space-fixed axis system as presented in Reference 10, including the aerodynamic derivatives discussed in Reference 8, are

$$Y_v' \ v' - \frac{m_I}{m} \ \dot{v}' + g \ \varphi + Y_\Psi \ \Psi = 0 \tag{4}$$

$$L_v' \ v' + L_{\dot\varphi} \ \dot\varphi - \ddot\varphi + L_\Psi \ \Psi + L_{\dot\Psi} \ \dot\Psi = 0 \tag{5}$$

$$N_v' \ v' + N_{\dot\varphi} \ \dot\varphi + N_\Psi \ \Psi + N_{\dot\Psi} \ \dot\Psi - \ddot\Psi = 0 \tag{6}$$

Control input terms are not included, since no dynamic tests were made with control inputs. In addition to the linearization assumption, other assumptions implicit in this form of the equations are: the vehicle is in level flight; the time rate of change of the product of inertia and moment of inertia terms is negligible; and the effect of product of inertia $(I_{xz})$ is negligible. The first assumption is justified by the test conditions. The second assumption is considered valid because of the magnitude of angular motions of the model. The third assumption was checked by the method given in Reference 11, including the product of inertia terms in a set of equivalent stability derivatives using the experimental value of the product of inertia. The difference between the values of the equivalent derivatives and the unmodified derivatives was of the order of 5 percent, and so product of inertia terms were considered to be negligible.

Stability derivatives to account for sidewash lag, $L_{\dot{v}}$ and $N_{\dot{v}}$, are neglected, as analysis of the experimental data did not indicate that they were important. The factor $\frac{m_I}{m'}$ in the sideforce equation accounts for the fact that the vertical aerodynamic force acting on the model did not equal the model weight because of the model support linkage (Figure 4) which moves with the model during lateral translation. The effect of the $\frac{m_I}{m'}$ factor is to reduce the lateral acceleration produced by a given tilt of the thrust vector, since the thrust was less than the weight of the model and mounting linkage.

A solution to equations (4), (5), and (6) may be assumed of the form $v' = \bar{v}\,e^{st}$, $\varphi = \bar{\varphi}\,e^{st}$, and $\Psi = \bar{\Psi}\,e^{st}$. Substitution of these expressions gives

$$\left(Y_v - \frac{m_I}{m'}\,s\right)\bar{v} + g\,\bar{\varphi} + Y_\psi\,\bar{\Psi} = 0 \tag{7}$$

$$L_v\,\bar{v} + \left(L_{\dot{\varphi}}\,s - s^2\right)\bar{\varphi} + \left(L_\psi + L_{\dot{\psi}}\,s\right)\bar{\Psi} = 0 \tag{8}$$

$$N_v\,\bar{v} + N_{\dot{\varphi}}\,s\,\bar{\varphi} + \left(N_\psi + N_{\dot{\psi}}\,s - s^2\right)\bar{\Psi} = 0 \tag{9}$$

24

The characteristic equation is determined by the condition that this set of equations must have nontrivial solutions for $\bar{v}$, $\bar{\varphi}$, and $\bar{\psi}$:

$$
\begin{vmatrix}
Y_v - \dfrac{m_I}{m'} s & g & Y_\psi \\[2ex]
L_v & L_{\dot{\varphi}} s - s^2 & L_\psi + L_{\dot{\psi}} s \\[2ex]
N_v & N_{\dot{\varphi}} s & N_\psi + N_{\dot{\psi}} s - s^2
\end{vmatrix} = 0
\tag{10}
$$

Values of "s" which satisfy the above expression are the roots of the characteristic equation and determine the nature of the natural modes of the aircraft. Use of a space-fixed axis system for the lateral/directional equations of motion makes equations (4), (5), and (6) a fifth order system, and consequently a fifth degree characteristic equation is obtained from the expansion of the determinant (10). However, the constant term in the characteristic equation is equal to $- g (L_v N_\psi - L_\psi N_v)$ which is

identically equal to zero from equation (2), resulting in one zero root. This root will be present whenever yaw angle rather than yaw rate is used as a variable. Certain of the terms in this determinant are determined from static measurements, and the remaining ones are found from analysis of the measured transient motion of the model.

CENTER-OF-GRAVITY LOCATION

The lateral equations of motion [(4), (5), and (6)] were derived with the origin of the axis system located at the center of gravity of the vehicle. The center of gravity of the model was located at varying distances above the pivot axes of the model, depending on the wing incidence and flap position. The pivot point is the intersection of the model roll axis and yaw axis. It is independent of wing incidence and is located somewhat ahead of the most forward center-of-gravity position of the full-scale aircraft (15-percent MAC) at 9-percent MAC with wing incidence of $90^0$. This point was taken as the origin of the axis system for the analysis, and all data presented are measured about this point. The center of gravity of the model was located nearly on the Z-axis at various distances above the X-Y plane, as shown in Figure 6c. The vertical offset of the center of gravity contributes two additional terms to the equations of motion written about the pivot axes. One is a rolling moment due to roll angle, $L_\varphi$, and the other is a rolling moment due to translational acceleration in the Y-direction, $L_{\dot{v}}$. The values of these derivatives are listed below.

25

| Wing Incidence | Flap Position | Vertical Center-of-Gravity Location | $L_\varphi$ | $L_{\dot{v}}$ |
|---|---|---|---|---|
| $90^\circ$ | $0^\circ$ | - 1.13 inches | + 1.66 | - 0.052 |
| $70^\circ$ | $15^\circ$ | - 0.88 inch | + 1.29 | - 0.040 |
| $30^\circ$ | $55^\circ$ | 0 | 0 | 0 |

## HOVER - ANALYSIS OF DATA

For hovering motions with two degrees of freedom (roll and lateral velocity), the equations of motion are obtained from equations (4), (5), and (6) by setting $\Psi = 0$, and adding $L_\varphi \varphi + L_{\dot{v}} \dot{v}$.

$$Y_v \, v - \frac{m_I}{m'} \, \dot{v} + g \, \varphi = 0 \tag{11}$$

$$L_v \, v + L_{\dot{v}} \, \dot{v} + L_\varphi \, \varphi + L_{\ddot{\varphi}} \, \dot{\varphi} - \ddot{\varphi} = 0 \tag{12}$$

From the quasi-steady-state measurements (Table VII), the following derivatives were determined:

$$Y_v = - 0.27 \text{ per second}$$

$$L_v = - 0.16 \text{ per foot-second}$$

Due to model center-of-gravity location, the terms $L_{\dot{v}}$ and $L_\varphi$ arise, and are

$$L_{\dot{v}} = - 0.052 \text{ per foot}$$

$$L_\varphi = 1.66 \text{ per second squared}$$

From the single degree of freedom in roll measurements, the roll damping was determined to be

$$L_{\dot{\varphi}} = - 0.37 \text{ per second}$$

and from the model propeller blade angle setting,

$$\frac{m_I}{m'} = 1.42$$

26

Thus, all of the terms in the two-degree-of-freedom motion described by equations (11) and (12) have been determined, and a check on the six derivatives given above may be obtained from the transient response data.

To determine the agreement between these values and the two-degree-of-freedom hover data, the dynamics predicted by the above stability derivatives are compared with the results of the model transient response measurements. Only the oscillatory roots of the dynamic response as derived from the stability derivatives can be compared to the model dynamic motions, since the real convergent root in the model response cannot be excited in such a way as to be evaluated from the transient response. Any input used to excite the convergent mode will result in model motions that rapidly exceed the response magnitude allowed by the carriage limits, because of the unstable oscillation. The characteristic equation for the two-degree-of-freedom motion is obtained from equations (11) and (12) by making the substitutions $v = \bar{v}\, e^{st}$ and $\varphi = \bar{\varphi}\, e^{st}$:

$$
\begin{vmatrix}
Y_v - \dfrac{m_T}{m'}\, s & g \\[2em]
L_v + L_{\dot{v}}\, s & L_{\varphi} + L_{\dot{\varphi}}\, s - s^2
\end{vmatrix} = 0
\qquad (13)
$$

The characteristic equation is

$$
\left(Y_v - \dfrac{m_T}{m'}\, s\right)\left(L_{\varphi} + L_{\dot{\varphi}}\, s - s^2\right) - g\left(L_v + L_{\dot{v}}\, s\right) = 0
\qquad (14)
$$

It is convenient to use root locus techniques to illustrate the effect of various parameters on the roots graphically. Placing equation (14) in root locus form considering the dihedral effect $L_v$ as the variable parameter,

$$
\frac{-\dfrac{m'}{m_T}\, g\, L_v}{s^3 - \left(L_{\dot{\varphi}} + \dfrac{m'}{m_T}\, Y_v\right) s^2 + \left(\dfrac{m'}{m_T}\, Y_v\, L_{\dot{\varphi}} - L_{\varphi} - \dfrac{m'}{m_T}\, g\, L_{\dot{v}}\right) s + \dfrac{m'}{m_T}\, Y_v\, L_{\varphi}} = -1
\qquad (15)
$$

The reason for considering the dihedral effect as the variable parameter will be clarified in the succeeding paragraphs. Recall that all of the parameters in equation (15) have been determined by other experiments.

When the preceding numerical values are substituted for all parameters except $L_v$, equation (15) becomes

$$\frac{-22.6\ L_v}{(s - 0.70)(s + 0.63 + 0.27i)(s + 0.63 - 0.27i)} = -1$$
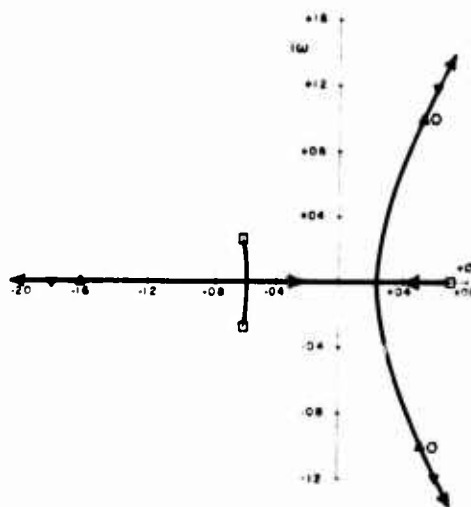


Root Locus, Effect of Variation of
Dihedral Effect, $L_v$, $i_w = 89°$.

The root locus for varying $L_v$ is shown above, where the roots for $L_v = 0$ are indicated by $\square$ . For the value of $L_v = -0.16$ per foot-second, the oscillatory roots are located at $s = +0.71 \pm 1.19i$ ($\nabla$). This corresponds to a period of 5.4 seconds contrasted to the period of 6.2 seconds measured from the transient response ($\bigcirc$). Changes in $Y_v$ and $L_{\dot{\phi}}$ influence primarily the damping of the oscillatory roots without an appreciable change in the period. The effect of $Y_v$ is small, since the dominant term in the sideforce equation is thrust vector tilt, which produces lateral acceleration. This was evident in the data, as the lateral velocity was approximately the integral of the roll angle as indicated by equation (11) with $Y_v = 0$. The dihedral effect $L_v$, though, does influence both the period and the damping of the oscillatory motion as shown above. It was necessary to reduce the value of $L_v$ from $-0.16$ to $-0.11$ to match the frequency of the oscillation. The oscillatory roots for $L_v = -0.11$ are $s = +0.52 \pm 1.00i$, and the real convergent root is $s = -1.61$ ($\triangle$).

28

The three-degree-of-freedom transient response data in hover indicated that the yawing moment equation was weakly coupled to the sideforce and rolling moment equations, since there was no oscillatory motion present in the yaw angle time histories. The equations of motion for three degrees of freedom near hover are given by equations (4), (5), and (6) and adding $L_\varphi \varphi + L_{\dot{v}} \dot{v}$.

$$Y_v \, v - \frac{m_T}{m'} \, \dot{v} + g \, \varphi = 0 \tag{16}$$

$$L_v \, v + L_{\dot{v}} \, \dot{v} + L_\varphi \, \varphi + L_{\dot{\varphi}} \, \dot{\varphi} - \ddot{\varphi} + L_{\dot{\psi}} \, \dot{\psi} = 0 \tag{17}$$

$$N_v \, v + N_{\dot{\varphi}} \, \dot{\varphi} + N_{\dot{\psi}} \, \dot{\psi} - \ddot{\psi} = 0 \tag{18}$$

where $Y_\psi$, $L_\psi$, and $N_\psi$ are identically zero in hover, as the sideforce, rolling moment, and yawing moment have no dependence on the azimuth heading for an initial velocity of zero. For the yawing moment equation to be uncoupled, any terms dependent upon yaw rate in the sideforce and rolling equations must be negligibly small. Therefore, $L_{\dot{\psi}}$ must be small. Also, since there is no indication of coupling between the yaw and roll motions, $N_{\dot{\varphi}}$ is also negligible.

Since the yawing moment equation is uncoupled, it would be expected that the roll and lateral velocity motions in two- and three-degree-of-freedom runs would be identical. However, the measured average values of the periods of these motions were 6.2 seconds for two degrees of freedom and 6.8 seconds for three degrees of freedom. The longer period for the three-degree-of-freedom motion is due to the presence of large yaw angles, which cause an increase in the period of the oscillatory motion in three degrees of freedom arising from the restraint imposed by model mounting geometry. Large yaw angles reduce (by the factor of the cosine of the yaw angle) the component of the vertical aerodynamic thrust force in the space-fixed Y-direction produced by a given roll angle. In addition, the lateral velocity component acting to produce rolling moments on the model, through the dihedral effect $L_v$, is the body-axis velocity of the model. The model motion is restrained by the carriage to a space-fixed Y-direction which will decrease (by the factor of the cosine of the yaw angle) the body-axis velocity. These two factors (reduction of the component of vertical aerodynamic thrust force and reduction of the body-axis velocity) increase the period of the oscillatory motion with yaw freedom and large yaw angles, when the motions of the model are restrained to a space-fixed direction. This difference, of course, would not be present on the full-scale aircraft.

The results of the hovering analysis in **model** scale are:

| DERIVATIVE (Symbol) | STATIC DATA (Strain gauge) | DYNAMIC DATA (Single degree of freedom) | DYNAMIC DATA (Two degrees of freedom) |
|---|---|---|---|
| $Y_v$ per second | - 0.27 | - | - 0.27 |
| $L_v$ per foot-second | - 0.16 | - | - 0.11 |
| $L_{\dot{v}}$ per foot | - 0.052 | - | - 0.052 |
| $L_{\varphi}$ per second squared | 1.66 | - | 1.66 |
| $L_{\dot{\varphi}}$ per second | - | - 0.37 | - 0.37 |
| $L_{\dot{\psi}}$ per second | - | - | 0 |
| $N_v$ per foot-second | nonlinear | - | nonlinear |
| $N_{\dot{\psi}}$ per second | - | - 0.41 | - 0.41 |
| $N_{\dot{\varphi}}$ per second | - | - | 0 |

due to C.G. location { $L_{\dot{v}}$, $L_{\varphi}$ }

It was not possible to check the value of $N_{\dot{\psi}}$ determined from single-degree-of-freedom tests because of the uncoupling of the yawing moment equation.

The difference between the value of $L_v$ measured by strain gauges and that necessary to correlate the two-degree-of-freedom data is quite large. The period predicted by the individually measured derivatives differs by 10 percent from that obtained directly from the transient response. However, since the frequency of the motion is roughly proportional to the cube root of $L_v$, the change in $L_v$ required is considerably larger.

FORWARD FLIGHT - ANALYSIS OF DATA

The analysis of the forward flight data was similar to that applied for hover. The more complex case of forward flight results in the fact that not all of the derivatives can be determined by single-degree-of-freedom experiments and static measurements. Therefore, certain derivatives may be checked, and others are determined from the forward flight transient response data.

## Static Tests - Wing Incidence Equal to $30^\circ$

The static measurements gave the following values (Table VIII):

$$L_v = -0.15 \ (L_\psi = 3.29) \text{ per foot-second}$$

$$N_v = 0.10 \ (N_\psi = -2.26) \text{ per foot-second}$$

$$Y_v = -0.44 \ (Y_\psi = 9.94) \text{ per second}$$

Because of noise in the rolling moment data, $L_v$ is considered as unknown in the analysis.

## One Degree of Freedom (Roll or Yaw)

Roll and yaw damping runs were conducted at a wing incidence of $30^\circ$ only. Time histories of the motions are given in Figures 14a and b. Mechanical springs were added for both the roll and yaw damping runs, as in hover, to provide a restoring moment so that the model was constrained to oscillate about the equilibrium condition. The values obtained for $L_{\dot\phi}$ and $N_{\dot\psi}$ (by computing the decay of the envelope of the roll and yaw traces) are (Table VIII)

$$L_{\dot\phi} = -0.74 \text{ per second}$$

$$N_{\dot\psi} = -0.92 \text{ per second}$$

Single-degree-of-freedom experiments in yaw angle $(\Psi = -\beta)$ only were also run without springs. The equation of motion applicable to these tests is

$$\ddot\Psi - N_{\dot\psi} \dot\Psi - N_\psi \Psi = 0 \quad \text{or} \quad (s^2 - N_{\dot\psi} s - N_\psi) \bar\Psi = 0 \tag{19}$$

The average period and damping were measured and used to determine the value of $N_\beta$ from the equation above. This measured value of "s" was $-0.50 \pm 1.41i$ (Table VIII). The value $N_\psi$ obtained in this fashion agrees well with that determined from strain gauge measurements.

| Stability Derivative | Quasi-Steady State (Strain Gauge) | Dynamic |
|---|---|---|
| $N_\psi$ (per second squared) | 2.26 | 2.24 |

31

The unknown derivatives appearing in equations (20) and (21) are determined using the following values of stability derivatives obtained from quasi-steady-state and single-degree-of-freedom response measurements.

### Stability Derivative

$$N_\psi = - 2.26 \text{ per second squared}$$

$$N_{\dot\psi} = - 0.92 \text{ per second}$$

$$L_{\dot\varphi} = - 0.74 \text{ per second}$$

### Two and Three Degrees of Freedom

The equations of motion describing the two-degree-of-freedom roll and yaw motion $(\Psi = -\beta)$ after the substitutions $\varphi = \bar\varphi \, e^{st}$ and $\Psi = \bar\Psi \, e^{st}$ have been made are

$$(L_{\dot\varphi} \, s - s^2) \, \bar\varphi + (L_\psi + L_{\dot\psi} \, s) \, \bar\Psi = 0 \tag{20}$$

$$(N_{\dot\varphi} \, s) \, \bar\varphi + (N_\psi + N_{\dot\psi} \, s - s^2) \, \bar\Psi = 0 \tag{21}$$

Because of noise present in the rolling moment measurements, $L_\psi$ is considered as an unknown parameter.

The fact that the single degree of freedom in yaw $(\Psi = -\beta)$ oscillatory motion was damped and the two-degree-of-freedom motion in roll and yaw had approximately zero damping indicated that the rolling and yawing motions were coupled. The method used to extract the values of $N_{\dot\varphi}$ and $L_{\dot\psi}$ from the dynamic data was based on the concept of rotating time vectors and mode ratios as discussed in Reference 12. It is more convenient here to use the mode ratios rather than the system characteristic equation.

The use of time vectors is based on the idea that the oscillatory motion of a system described by a linear differential equation can be represented by a vector which rotates about its tail. The angular velocity of rotation of the vector is the damped natural frequency of the system, and the length of the vector is proportional to the amplitude of the oscillatory motion of the system. For damped oscillatory motion, the length of the vector will decrease with time; for unstable motion, the length of the vector will increase with time. If a multiple-degree-of-freedom system is represented by a set of linear differential equations, and the characteristic equation of the system contains an oscillatory pair of roots, then it is possible to represent the oscillatory mode in each variable by its own rotating time vector. The time vectors representing the different variables in a particular mode will maintain a fixed phase relationship with each other and rotate at the same frequency. The amplitude ratio and the phase angle between two variables are constant for a given linear

system and do not depend upon the input or disturbance. The complex number which relates both the amplitudes of two variables and the phase angle between them is called a mode ratio. Note that this approach can be used when there is only one mode present in the response. That is, it is assumed in the following that any other modes of motion have damped out.

For the two-degree-of-freedom motion in roll and yaw, the relationships for the mode ratio of roll angle to yaw angle are obtained from equations (20) and (21) as

$$\frac{\bar{\phi}}{\bar{\psi}} = \frac{L_{\dot{\psi}}\ s + L_{\psi}}{s^2 - L_{\dot{\phi}}\ s} \tag{22}$$

$$\frac{\bar{\phi}}{\bar{\psi}} = \frac{s^2 - N_{\dot{\psi}}\ s - N_{\psi}}{N_{\dot{\phi}}\ s} \tag{23}$$

where "s" is a root of the characteristic equation corresponding to the mode of interest. As the mode ratio $\dfrac{\bar{\phi}}{\bar{\psi}}$ is a complex number for oscillatory motions, a maximum of four stability derivatives can be evaluated from equations (22) and (23). The phase difference between the roll angle response and the yaw angle response, as determined from the data, was $-110^\circ$. The average amplitude ratio was 1.59. Therefore, the mode ratio for this oscillatory motion was $\dfrac{\bar{\phi}}{\bar{\psi}} = -0.54 - 1.49i$. The period of the oscillatory mode was 4.8 seconds ($s = 1.31i$). Then $L_{\dot{\psi}}$ can be calculated from equation (22) using the value of $L_{\dot{\phi}} = -0.74$ obtained from the single-degree-of-freedom roll experiments. The resulting values of $L_{\psi}$ and $L_{\dot{\psi}}$ are

$$L_{\psi} = 2.38 \text{ per foot-second}$$

$$L_{\dot{\psi}} = 1.56 \text{ per second}$$

It became apparent when equation (23) was used to determine $N_{\dot{\phi}}$ with the previously determined values of $N_{\psi}$ and $N_{\dot{\psi}}$, that no solution was possible for the measured values of $s$ and $\dfrac{\bar{\phi}}{\bar{\psi}}$, unless additional terms

33

were included. The influence of variations in the angle of attack of the model due to carriage restraints (see Appendix III) arising from combinations of roll and yaw was considered, but the maximum deviation in angle of attack was found to be less than $\pm 1^\circ$.

It was concluded that the term necessary to satisfy equation (23) would arise from an unbalanced nose-down pitching moment acting on the model. An untrimmed pitching moment results in a yawing moment proportional to roll angle, since the axis about which the model is free is a space-fixed axis rather than a body-fixed axis (see Appendix III). No longitudinal experiments were conducted at $30^\circ$ wing incidence, so the longitudinal trim setting (tail rotor collective pitch) was not known. The presence of this term results in an effective stability derivative $N_\varphi$ (see Appendix III). Therefore, equation (23) was modified to include this term:

$$\frac{\bar{\varpi}}{\bar{\psi}} = \frac{s^2 - N_{\dot{\psi}}\, s - N_\psi}{N_{\dot{\varphi}}\, s + N_\varphi} \tag{24}$$

The values of $N_{\dot{\varphi}}$ and $N_\varphi$ may now be determined using the values of $N_\psi$, $N_{\dot{\psi}}$, $s$, and $\dfrac{\bar{\varphi}}{\bar{\psi}}$ previously given. The results are
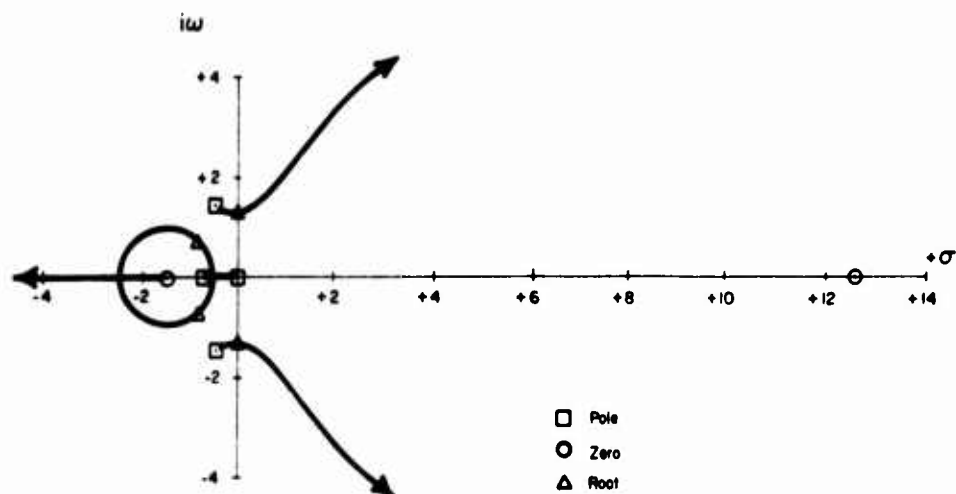
$$N_{\dot{\varphi}} = 0.066 \text{ per second}$$

$$N_\varphi = -0.83 \text{ per second squared}$$

This value of $N_\varphi$ corresponds to an untrimmed nose-down pitching moment of 2.95 foot-pounds. Extrapolated longitudinal data indicated that pitching moments of from 2 to 4 foot-pounds are possible at this flight condition.

The root locus technique was used to display the characteristic roots for two degrees of freedom in roll and yaw and three degrees of freedom using the stability derivatives found from the mode ratio equations. The characteristic equation in root locus form for two degrees of freedom is

$$\frac{N_{\dot{\varphi}}\; L_{\dot{\psi}} \left(s + \dfrac{N_\varphi}{N_{\dot{\varphi}}}\right)\left(s + \dfrac{L_\psi}{L_{\dot{\psi}}}\right)}{(s^2 - N_{\dot{\psi}}\, s - N_\psi)(s^2 - L_{\dot{\varphi}}\, s)} = +1 \tag{25}$$

34

Root Locus, Two Degrees of Freedom,
Roll and Yaw $(\Psi = -\beta)$, $i_W = 30^\circ$.

Evaluation of the two-degree-of-freedom roots is shown above. The roots
are $\pm \; ?.??$ and $-0.83 \pm 0.68i$ ($\triangle$). The characteristic equation for
the three-degree-of-freedom motion in root locus form is

$$\frac{\left(\dfrac{gL_V + Y_\Psi N_V}{\dfrac{m_I}{m'}}\right)\left[s^2 + \left(\dfrac{gN_V L_{\dot\Psi} - gL_V N_{\dot\Psi} + Y_\Psi L_V N_{\dot\phi} - Y_\Psi N_V L_{\dot\phi}}{gL_V + Y_\Psi N_V}\right)s + \dfrac{Y_\Psi L_V N_{\dot\phi}}{gL_V + Y_\Psi N_V}\right]}{-\left(s - \dfrac{Y_V}{\dfrac{m_I}{m'}}\right)\begin{vmatrix} L_{\dot\phi}\,s - s^2 & L_\Psi + L_{\dot\Psi}\,s \\[2mm] N_\phi + N_{\dot\phi}\,s & N_\Psi + N_{\dot\Psi}\,s - s^2 \end{vmatrix}} = -1 \qquad (26)$$

The portion of the denominator in determinant form is the characteristic
equation of the two-degree-of-freedom motion. The statically measured
value of $Y_V = -0.44$ per second, along with the stability derivatives
determined from the use of the mode ratio technique and the two-degree-
of-freedom data, was used to evaluate the above expression.

35
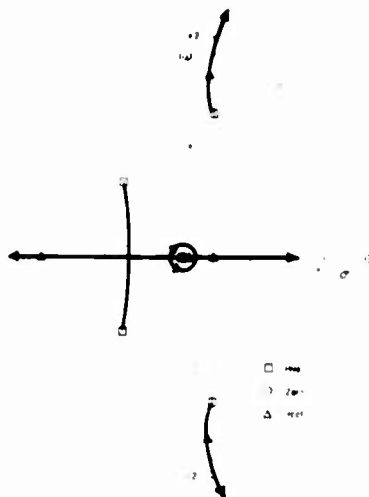
Root Locus, Three Degrees of Freedom,
Roll, Yaw, Sideslip, $i_r = 30°$.

The above root locus shows the comparison of the two-degree-of-freedom roots ( ▢ ) and the three-degree-of-freedom roots ( △ ). The three-degree-of-freedom roots are $- 0.04 \pm 1.65i$, $- 1.60$, $- 0.23$ and $0$. The lightly damped oscillatory pair of roots with a period of $3.8$ seconds compares favorably with the value of $4.0$ seconds obtained from the three-degree-of-freedom data (Figures 16d and e). The only additional derivative in equation (26) which is not in equation (25) is $Y_v(Y_\psi)$; there-fore, this agreement is a check on the values of the stability derivatives already determined. Note that there is only a small difference in the roots with $Y_v = Y_\psi = 0$. Five roots are given instead of the usual four roots, since yaw angle was used as a variable rather than yaw rate. This has the effect of introducing an additional root which has a zero value, indicating that the vehicle has no dependence on azimuth heading.

To evaluate the sensitivity of these calculations for the stability de-rivatives, the derivatives that result from the mode ratio technique for a phase angle of $- 90°$, corresponding to an error of about $0.2$ second in the measurement of phase angle, were determined. In this case, $\frac{\Phi}{\Psi} = - 1.59i$.

The stability derivatives obtained from equations (22) and (23) are
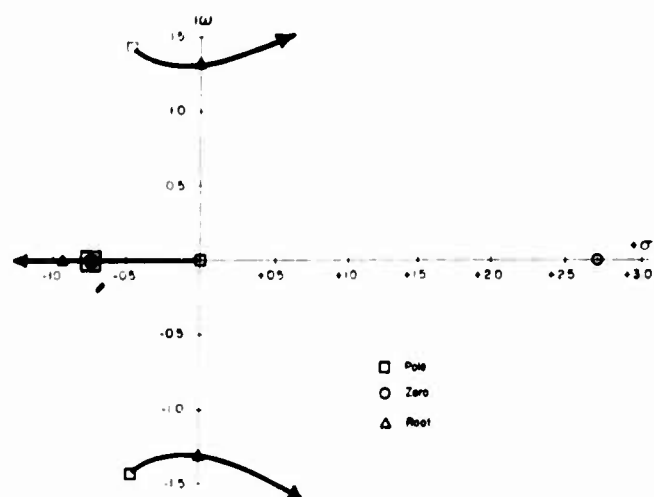
$$L_\psi = 1.54 \text{ per foot-second}$$
$$L_{\dot\psi} = 2.09 \text{ per second}$$
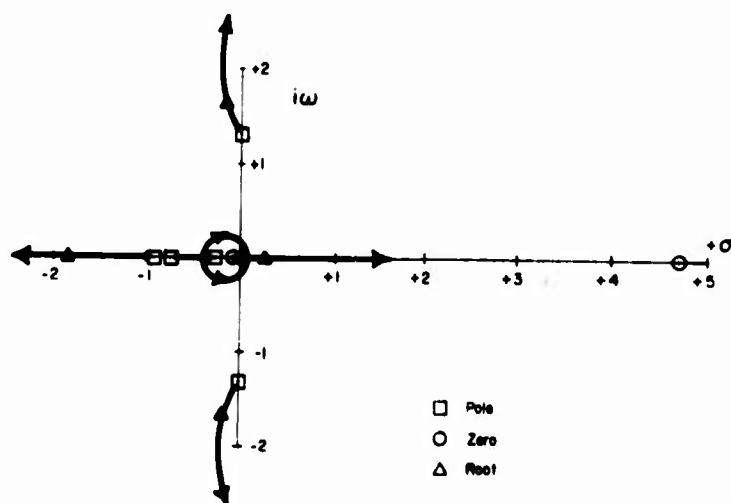$$N_\varphi = - 0.76 \text{ per second squared}$$
$$N_{\dot\varphi} = 0.28 \text{ per second}$$

36

The root locus obtained from equation (25) for two degrees of freedom, shown below, yields roots ± 1.31i, - 0.93, and - 0.74 ( $\triangle$ ).



Root Locus, Two Degrees of Freedom,
Roll and Yaw ($\Psi = -\beta$), $i_w = 30^\circ$.

The root locus obtained from equation (26) for three degrees of freedom, shown below, yields roots - 0.18 ± 1.65i, - 1.85, 0, and 0.26 ( $\triangle$ ).



Root Locus, Three Degrees of Freedom,
Roll, Yaw, Sideslip, $i_w = 30^\circ$.

The positive real root, 0.26, in this case yields a divergent motion. Since there was no divergence present in the three-degree-of-freedom response, we may assume that the previously used value of the phase angle (- 110$^\circ$) is valid. $N_\varphi$ is the only derivative that shows a large percentage change. This is due to the fact that it is small and has little

37

influence on the three-degree-of-freedom motion. Thus, the derivatives determined from the - 110° phase measurement are considered to be the best match for the dynamic response data.

A comparison of the values of the model stability derivatives for the 30° wing incidence condition as determined from the static and dynamic experiments is summarized below.

| DERIVATIVE (Symbol) | STATIC DATA (Strain gauge) | DYNAMIC DATA (Single degree of freedom) | DYNAMIC DATA (Two degrees of freedom) | DYNAMIC DATA (Three degrees of freedom) |
|---|---|---|---|---|
| $Y_v$ per second | - 0.44 | - | - | - |
| $L_v$ per foot-second | - 0.15 | - | - 0.10 | - 0.10 |
| $L_{\dot{\varphi}}$ per second | - | - 0.74 | - | - |
| $L_{\dot{\psi}}$ per second | - | - | 1.56 | 1.56 |
| $N_v$ per foot-second | 0.10 | 0.10 | - | - |
| $N_{\dot{\psi}}$ per second | - | - 0.92 | - | - |
| $N_{\dot{\varphi}}$ per second | - | - | 0.066 | - |
| $N_{\varphi}$ per second squared (linkage effect) | - | - | - 0.83 | - 0.83 |

## Static and Dynamic Tests ($i_w$ equal to 70°)

It was not possible to determine all of the stability derivatives at this wing incidence. The lack of restricted degree-of-freedom dynamic tests coupled with the uncertainty as to the magnitude of the model pitching moment during the three-degree-of-freedom tests precluded detailed analysis of the 70° wing incidence data. There were more unknown stability derivatives than there were test conditions. The only stability derivatives obtained were those determined directly from the static tests.

| | Derivative | Static |
|---|---|---|
| | $Y_v$ per second | - 0.23 |
| | $L_v$ per foot-second | - 0.17 |
| | $N_v$ per foot-second | 0.08 |
| due to C.G. location { | $L_{\dot{v}}$ per foot | - 0.040 |
| | $L_{\varphi}$ per second squared | 1.29 |

38

HOVER

The process of converting the model stability derivatives to full scale consisted of two steps. The first step was to adjust the model deriva- tives to account for the difference between the scaled-down moments of inertia of the full-scale vehicle and the actual model inertias. For the rolling moment derivatives, an increase by the factor $\frac{2.65}{1.50}$ is required; for the yawing moment derivatives, an increase by the factor $\frac{3.55}{2.70}$ is required. These adjusted derivatives are listed in Table I. Using the adjusted model derivatives and values of $\frac{m_I}{m'}$ equal to 1.00, $L_{\varphi}$ equal to 0, and $L_{\dot{v}}$ equal to 0 to correct for the addition of lifted and traveling masses (those portions of the mount that are carried or move with the model) and for the center-of-gravity location, the roots of the characteristic equation of motion for the adjusted model were found. The characteristic equation for the adjusted model with no inequality of lifted and traveling masses and no center-of-gravity location is

$$(Y_v - s)(L_{\dot{\varphi}} \, s - s^2) - g \, L_v = 0 \qquad (27)$$

The characteristic roots for the adjusted model are $s = + 0.61 \pm 1.56i$ and $s = -2.14$. The stability derivatives, period, and damping of the adjusted model correspond to those of a dynamically similar model of the full-scale vehicle. The equivalent gross weight of the full-scale air- craft in hover is 38,800 pounds for these experiments. The second step, then, was to use the scale factors for dynamic model similarity as listed in Table VI to convert the adjusted model results to those of the full-scale aircraft. These are listed in Table I. The period of the oscillatory motion of the full-scale aircraft as found in this manner is 12.7 seconds with a time to double amplitude of 3.6 seconds. The con- vergent root has a time to one-half amplitude of 1.0 second.

FORWARD FLIGHT

The results for the forward flight conditions were converted to equivalent full-scale values in a manner analogous to that described above. The model stability derivatives were adjusted to account for the differences in the roll and yaw moments of inertia between the actual model and a model that would be dynamically similar to the full-scale vehicle using the factors given above. These adjusted derivatives are listed in Table II for $70°$ wing incidence and in Table III for $30°$ wing incidence. The derivative $N_{\varphi}$ is zero for the adjusted model, since this derivative was due to the linkage restraint. The values of the roots were determined

for the adjusted model using the characteristic equation in the form given by equation (26), with $\frac{m_T}{m}$ equal to 1 and $N_\varphi$ equal to 0. The roots of the three-degree-of-freedom characteristic equation were 0, - 2.60, - 0.35 ± 2.16i, and 0.35 for $30^\circ$ wing incidence. These roots can be converted directly to full-scale values by means of the scale factors listed in Table VI. The equivalent full-scale aircraft gross weight is 38,800 pounds at a wing incidence of $70^\circ$ and 37,500 pounds at a wing incidence of $30^\circ$. The full-scale vehicle characteristic roots are 0, - 0.82, - 0.11 ± 0.68i, and 0.11. The real convergent root has a time to one-half amplitude of 0.85 second, while the real divergent root has a time to double amplitude of 6.3 seconds. The pair of oscillatory roots has a damping ratio of 0.16 and a period of 9.2 seconds. The full-scale stability derivatives for $30^\circ$ wing incidence as determined from the stability derivatives for the dynamically similar model are listed in Table III.

It was not possible to determine the characteristics of the dynamic motion of the full-scale vehicle for the $70^\circ$ wing incidence case, as it would be necessary to have the complete set of model stability derivatives evaluated in order to scale the model dynamics due to the possible linkage effects as well as model inertias. The stability derivatives which were statically determined for the $70^\circ$ wing incidence case are scaled to their relative full-scale values in Table II.

TABLE I.  STABILITY DERIVATIVES AND PARAMETERS ($89°$ WING INCIDENCE)

| | Parameter | | Model | Adjusted Model | Full-Scale Aircraft |
|---|---|---|---|---|---|
| | $Y_v$ | per second | - 0.27 | - 0.27 | - 0.085 |
| | $Y_\psi$* | feet per second squared | 0 | 0 | 0 |
| | $L_v$ | per foot-second | - 0.11 | - 0.19 | - 0.0059 |
| due to C.G. location | $L_{\dot{v}}$ | per foot | - 0.052 | 0 | 0 |
| | $L_\varphi$ | per second squared | 1.66 | 0 | 0 |
| | $L_{\dot{\varphi}}$ | per second | - 0.37 | - 0.65 | - 0.21 |
| | $L_\psi$* | per second squared | 0 | 0 | 0 |
| | $L_{\dot{\psi}}$ | per second | 0 | 0 | 0 |
| | $N_v$ | per foot-second | nonlinear | - | - |
| | $N_{\dot{\varphi}}$ | per second | 0 | 0 | 0 |
| | $N_\psi$* | per second squared | 0 | 0 | 0 |
| | $N_{\dot{\psi}}$ | per second | - 0.41 | - 0.54 | - 0.17 |
| | $Z_o$ | pounds (gross weight) | 38.8 | 38.8 | 38,800 |
| | $I_x$ | slug-feet squared | 2.65 | 1.50 | 150,000 |
| | $I_z$ | slug-feet squared | 3.55 | 2.70 | 270,000 |
| | $U_o$ | feet per second | 0 | 0 | 0 |
| | $\dfrac{m_I}{m'}$ | | 1.42 | 1.00 | 1.00 |

*Identically zero in hover.

| TABLE I - Continued | | | |
|---|---|---|---|
| Parameter | Model | Adjusted Model | Full-Scale Aircraft |
| OSCILLATORY MODE | | | |
| Period, seconds | 6.20 | 4.03 | 12.7 |
| Time to double amplitude $(T_2)$, seconds | 1.17 | 1.14 | 3.60 |
| CONVERGENT MODE | | | |
| Time to one-half amplitude $(T_{1/2})$, seconds | 0.43 | 0.32 | 1.01 |

TABLE II.  STABILITY DERIVATIVES AND PARAMETERS (70° WING INCIDENCE)

| | Parameter | Model | Adjusted Model | Full-Scale Aircraft |
|---|---|---|---|---|
| | $Y_v$ per second | - 0.23 | - 0.23 | - 0.073 |
| | $Y_\psi$* feet per second squared $(= - U_o\ Y_v)$ | 2.18 | 2.18 | 2.18 |
| | $L_v$ per foot-second | - 0.17 | - 0.30 | - 0.0095 |
| due to | $L_{\dot{v}}$ per foot | - 0.040 | 0 | 0 |
| C.G. location | $L_\varphi$ per second squared | 1.29 | 0 | 0 |
| | $L_{\dot{\varphi}}$ per second | | not evaluated | |
| | $L_\psi$* per second squared $(= - U_b\ L_v)$ | 1.61 | 2.84 | 0.284 |
| | $L_{\dot{\psi}}$ per second | | not evaluated | |
| | $N_v$ per foot-second | 0.08 | 0.105 | 0.0033 |
| | $N_\varphi$ per second squared (linkage effect) | - | 0 | 0 |
| | $N_{\dot{\varphi}}$ per second | | not evaluated | |
| | $N_\psi$* per second squared $(= - U_b\ N_v)$ | - 0.76 | - 1.00 | - 0.10 |
| | $N_{\dot{\psi}}$ per second | | not evaluated | |
| | $Z_o$ pounds (gross weight) | 38.8 | 38.8 | 38,800 |
| | $I_x$ slug-feet squared | 2.65 | 1.50 | 150,000 |
| | $I_z$ slug-feet squared | 3.55 | 2.70 | 270,000 |
| | $U_b$ feet per second | 9.5 | 9.5 | 30.0 |
| | $U_b$ knots | 5.6 | 5.6 | 17.8 |
| | $\dfrac{m_I}{m'}$ | 1.53 | 1.00 | 1.00 |

*Derivatives exist due to use of space axis system.

43

TABLE II - Continued

| Parameter | Model | Adjusted Model | Full-Scale Aircraft |
|---|---|---|---|
| OSCILLATORY MODE | | | |
| Period, seconds | 5.4 | not evaluated | |
| Time to one-half amplitude $(T_{1/2})$, seconds | 1.44 | not evaluated | |

Note: Other modes present in the response were not evaluated.

TABLE III. STABILITY DERIVATIVES AND PARAMETERS (30° WING INCIDENCE)

| Parameter | | Model | Adjusted Model | Full-Scale Aircraft |
|---|---|---|---|---|
| $Y_v$ | per second | - 0.44 | - 0.44 | - 0.14 |
| $Y_\psi$* | feet per second squared $(= - U_o\, Y_v)$ | 10.1 | 10.1 | 10.1 |
| $L_v$ | per foot-second | - 0.104 | - 0.184 | - 0.0058 |
| $L_{\dot\varphi}$ | per second | - 0.74 | - 1.31 | - 0.41 |
| $L_\psi$* | per second squared $(= - U_o\, L_v)$ | 2.38 | 4.21 | 0.42 |
| $L_{\dot\psi}$ | per second | 1.56 | 2.76 | 0.87 |
| $N_v$ | per foot-second | 0.10 | 0.13 | 0.0041 |
| $N_\varphi$ | per second squared (linkage effect) | - 0.83 | 0 | 0 |
| $N_{\dot\varphi}$ | per second | 0.066 | 0.087 | 0.027 |
| $N_\psi$* | per second squared $(= - U_o\, N_v)$ | - 2.30 | - 3.02 | - 0.30 |
| $N_{\dot\psi}$ | per second | - 0.92 | - 1.21 | - 0.38 |
| $Z_o$ | pounds (gross weight) | 37.5 | 37.5 | 37,500 |
| $I_x$ | slug-feet squared | 2.65 | 1.50 | 150,000 |
| $I_z$ | slug-feet squared | 3.55 | 2.70 | 270,000 |
| $U_o$ | feet per second | 23 | 23 | 72.5 |
| $U_o$ | knots | 13.6 | 13.6 | 43.0 |
| $\dfrac{m_\tau}{m'}$ | | 1.59 | 1.00 | 1.00 |

*Derivatives exist due to use of space axis system.

| Parameter | Model | Adjusted Model | Full-Scale Aircraft |
|---|---|---|---|
| OSCILLATORY MODE (DUTCH ROLL) | | | |
| Period, seconds | 4.0 | 2.90 | 9.2 |
| Time to one-half amplitude ($T_{1/2}$), seconds | $\infty$ | 2.0 | 6.3 |
| #1 REAL MODE (ROLLING MODE) | | | |
| Time to one-half amplitude ($T_{1/2}$), seconds | 0.43 | 0.27 | 0.85 |
| #2 REAL MODE (SPIRAL) | | | |
| Time to one-half amplitude ($T_{1/2}$), seconds | 3.0 | - | - |
| Time to double amplitude ($T_2$), seconds | - | 2.0 | 6.3 |

The linkage used to provide lateral/directional freedom is shown schematically in Figure 4. The yaw axis is a space-fixed axis, and the roll axis is a body-fixed axis. To study the idealized lateral/directional motions, it would be desirable to have both angular freedoms about body axes; however, this is not possible with a simple geometric linkage. Therefore, the simplification of one space-fixed freedom and one body-fixed freedom was made.

This geometric linkage produces the following interactions. Euler's equations for a rigid body rotating about a fixed point with respect to principal body axes are (Reference 10)

$$I_x \, \dot{p} + q \, r \, (I_z - I_y) = L_a$$

$$I_y \, \dot{q} + p \, r \, (I_x - I_z) = M_a$$

$$I_z \, \dot{r} + p \, q \, (I_y - I_x) = N_a$$

where p, q, and r are angular rates about the X, Y, and Z body axes, respectively, and $L_a$, $M_a$, and $N_a$ are the external (i.e., aerodynamic) moments acting about the body axes. The relationships between the body axes and the linkage axes are given by (Reference 10)

$$p = \dot{\phi} - \dot{\Psi} \sin \theta$$

$$q = \dot{\theta} \cos \phi + \dot{\Psi} \cos \theta \sin \phi$$

$$r = \dot{\Psi} \cos \theta \cos \phi - \dot{\theta} \sin \phi$$

where $\phi$, $\theta$, and $\Psi$ are Euler angles, that is, the angular deflections of the linkage (Figure 4). In this case $\theta = 0$, and the equations become

$$p = \dot{\phi}$$

$$q = \dot{\Psi} \sin \phi$$

$$r = \dot{\Psi} \cos \phi$$

The equations of motion in terms of gimbal deflections $(\varphi, \Psi)$ after substitution for $p$, $q$, and $r$, are

$$I_x \ddot{\varphi} + \dot{\Psi}^2 \sin \varphi \cos \varphi \, (I_z - I_x) = L_\theta$$

$$I_y (\ddot{\Psi} \sin \varphi + \dot{\Psi} \dot{\varphi} \cos \varphi) + \dot{\varphi} \dot{\Psi} \cos \varphi \, (I_x - I_z) = M_\theta$$

$$I_z (\ddot{\Psi} \cos \varphi - \dot{\Psi} \dot{\varphi} \sin \varphi) + \dot{\varphi} \dot{\Psi} \sin \varphi \, (I_y - I_x) = N_\theta$$

Now, the first equation is an equation of motion, since the model is free about the body roll axis. The latter two equations must be combined to produce the other equation of motion about the free space axis. The resulting two equations of motion are

$$I_x \ddot{\varphi} + \dot{\Psi}^2 \sin \varphi \cos \varphi \, (I_z - I_x) = L_\theta$$

$$(I_y \sin^2 \varphi + I_z \cos^2 \varphi) \, \ddot{\Psi} + (I_x \cos \varphi \sin \varphi - I_z \cos \varphi \sin \varphi) \, \dot{\Psi} \dot{\varphi}$$

$$+ \dot{\varphi} \dot{\Psi} \cos \varphi \sin \varphi \, (I_y - I_x) = N_\theta \cos \varphi + M_\theta \sin \varphi$$

These, then, are the equations of motion in terms of the angles of the model support linkage, $\varphi$ and $\Psi$, and the body moments $L_\theta$, $M_\theta$, and $N_\theta$. If the roll angle is small, these reduce to

$$I_x \ddot{\varphi} + \dot{\Psi}^2 \varphi \, (I_z - I_x) = L_\theta$$

$$(I_y \varphi^2 + I_z) \, \ddot{\Psi} + (I_y - I_z) \, \dot{\varphi} \dot{\Psi} \varphi = N_\theta + M_\theta \varphi$$

For small disturbances, the only additional first-order term due to the linkage configuration is $M_\theta \varphi$, when the initial value of $M_\theta \neq 0$. In this case an "apparent" stability derivative $\dfrac{\partial N}{\partial \varphi}$ $(= M_{\theta_0})$ would be added.

This result indicates that pitching moment instrumentation should be included to insure that $M_{\theta_0} = 0$ when lateral/directional experiments are conducted with this linkage. A later series of experiments has been conducted with the model free in pitch with a feedback loop to stabilize the attitude of the model and to eliminate this effect.

The free-stream velocity components with respect to body axes are

$$u = U_0 \cos \Psi$$

$$v = - U_0 \sin \Psi \cos \varphi$$

$$w = - U_0 \sin \Psi \sin \varphi$$

If the angular motions are small, then the angle of attack $(\alpha \cong \frac{w}{U_0})$ due to angular motions is of second order.

TABLE IV.   COMPARISON OF MODEL AND FULL-SCALE CHARACTERISTICS

|  | Model | Model Converted to Full Scale | Full Scale Aircraft |
|---|---|---|---|
| Weight, pounds | 46.7 | 46,700 | 37,000 |
| Wing span, feet | 6.75 | 67.5 | 67.5 |
| Wing area (S), feet squared | 5.34 | 534 | 534.4 |
| Moment of inertia in roll $(I_x)$, slug-feet squared | 2.65 | 265,000 | 150,000 |
| Moment of inertia in yaw $(I_z)$, slug-feet squared | 3.55 | 355,000 | 270,000 |

Horizontal center-of-gravity location:   9-percent MAC.

| Parameter | | $i_w = 89°$ | $i_w = 70°$ | $i_w = 30°$ |
|---|---|---|---|---|
| $i_w$ | degrees | 89 | 70 | 30 |
| $\delta_f$ | degrees | 0 | 15 | 55 |
| $i_r$ | degrees | 30 | 50 | 0 |
| $\beta_{.75R}$ | degrees | 15.8 | 15.7 | 13.2 |
| $\Omega$ | revolutions per minute | 4100 | 4100 | 4100 |
| $U_0$ | feet per second | 0 | 9.5 | 22.6 |
| $Z_0$ | pounds (gross weight) | - 38.9 | - 38.8 | - 37.5 |
| $I_x$ | slug-feet squared | 2.65 | 2.65 | 2.65 |
| $I_z$ | slug-feet squared | 3.55 | 3.55 | 3.55 |
| $I_{xz}$ | slug-feet squared | 0.20 | - | 0.16 |
| $\rho$ | slugs per cubic foot | 0.00225 | 0.00225 | 0.00225 |
| $\dfrac{m_7}{m'}$ | | 1.42 | 1.53 | 1.59 |

TABLE V.  SUMMARY OF MODEL TEST CONDITIONS

## TABLE VI.   SCALE FACTORS FOR DYNAMIC MODEL SIMILARITY

Multiply full-scale property by scale factor to obtain model property.

|  |  | For $\lambda = 10$ |
|---|---|---|
| Linear dimension | $\lambda^{-1}$ | .1 |
| Area | $\lambda^{-2}$ | .01 |
| Volume, mass, force | $\lambda^{-3}$ | .001 |
| Moment | $\lambda^{-4}$ | .0001 |
| Moment of inertia | $\lambda^{-5}$ | .00001 |
| Linear velocity | $\lambda^{-.5}$ | .316 |
| Linear acceleration | $\lambda^{0}$ | 1 |
| Angular velocity | $\lambda^{.5}$ | 3.16 |
| Angular acceleration | $\lambda$ | 10 |
| Time | $\lambda^{-.5}$ | .316 |
| Frequency | $\lambda^{.5}$ | 3.16 |
| Reynolds number | $\lambda^{-1.5}$ | .0316 |
| Mach number | $\lambda^{-.5}$ | .316 |

where $\lambda = \dfrac{\text{full-scale linear dimension}}{\text{model linear dimension}}$
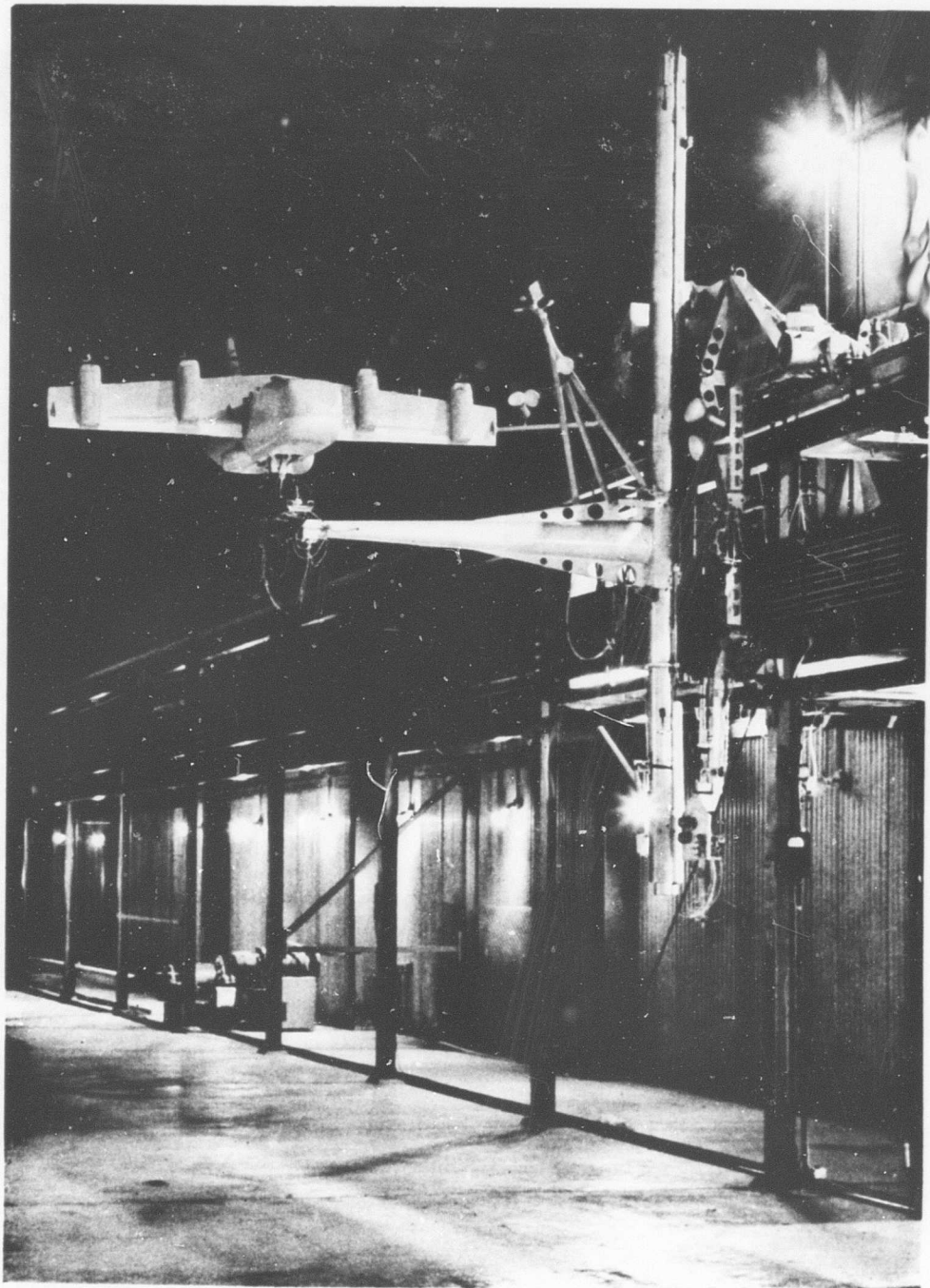
Figure 2.   Princeton Dynamic Model Track Longitudinal Mount With
            One-Tenth Scale Dynamically Similar Model.

53
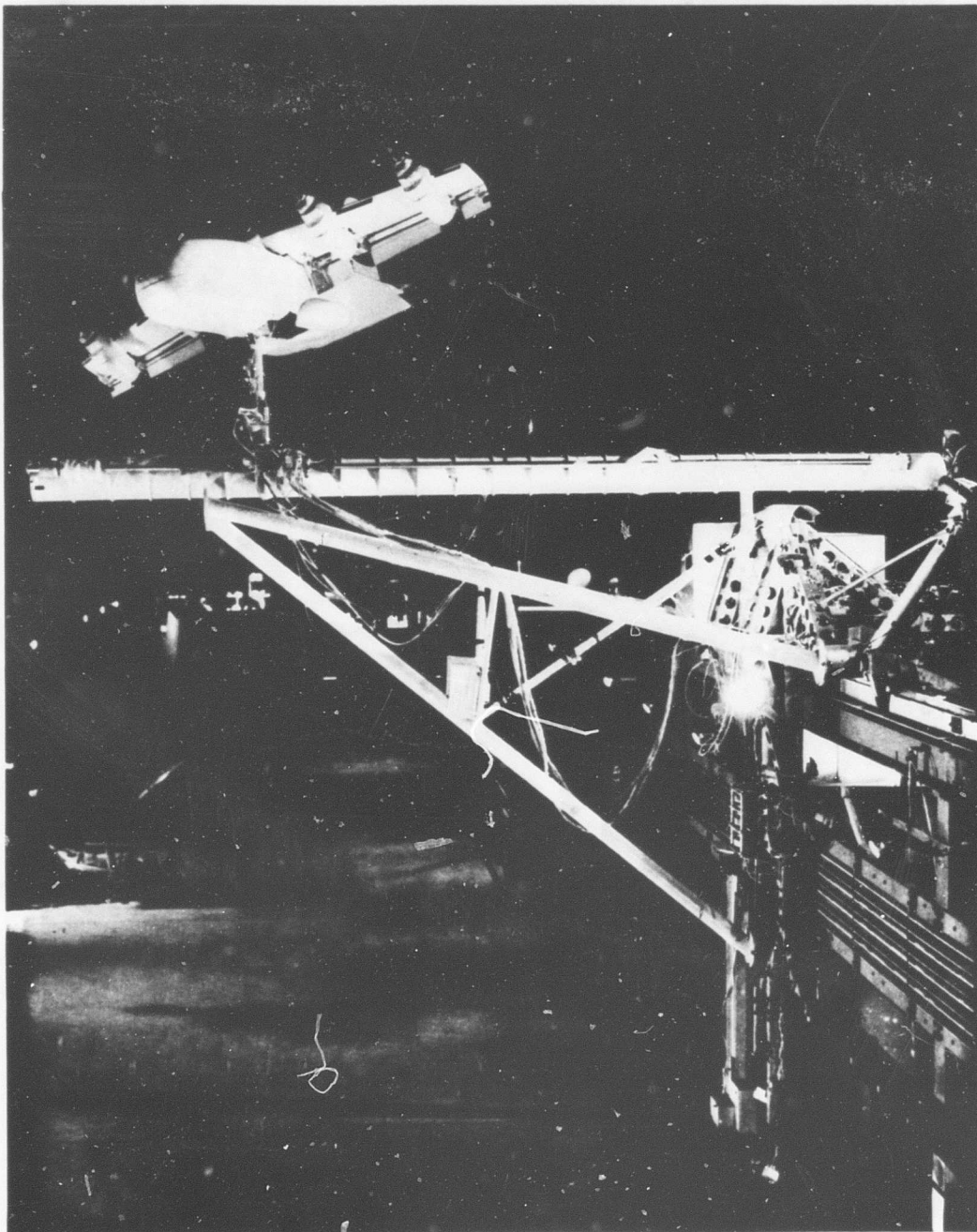
Figure 3.   Princeton Dynamic Model Track Lateral/Directional Mount With
One-Tenth Scale Dynamically Similar Model.

54
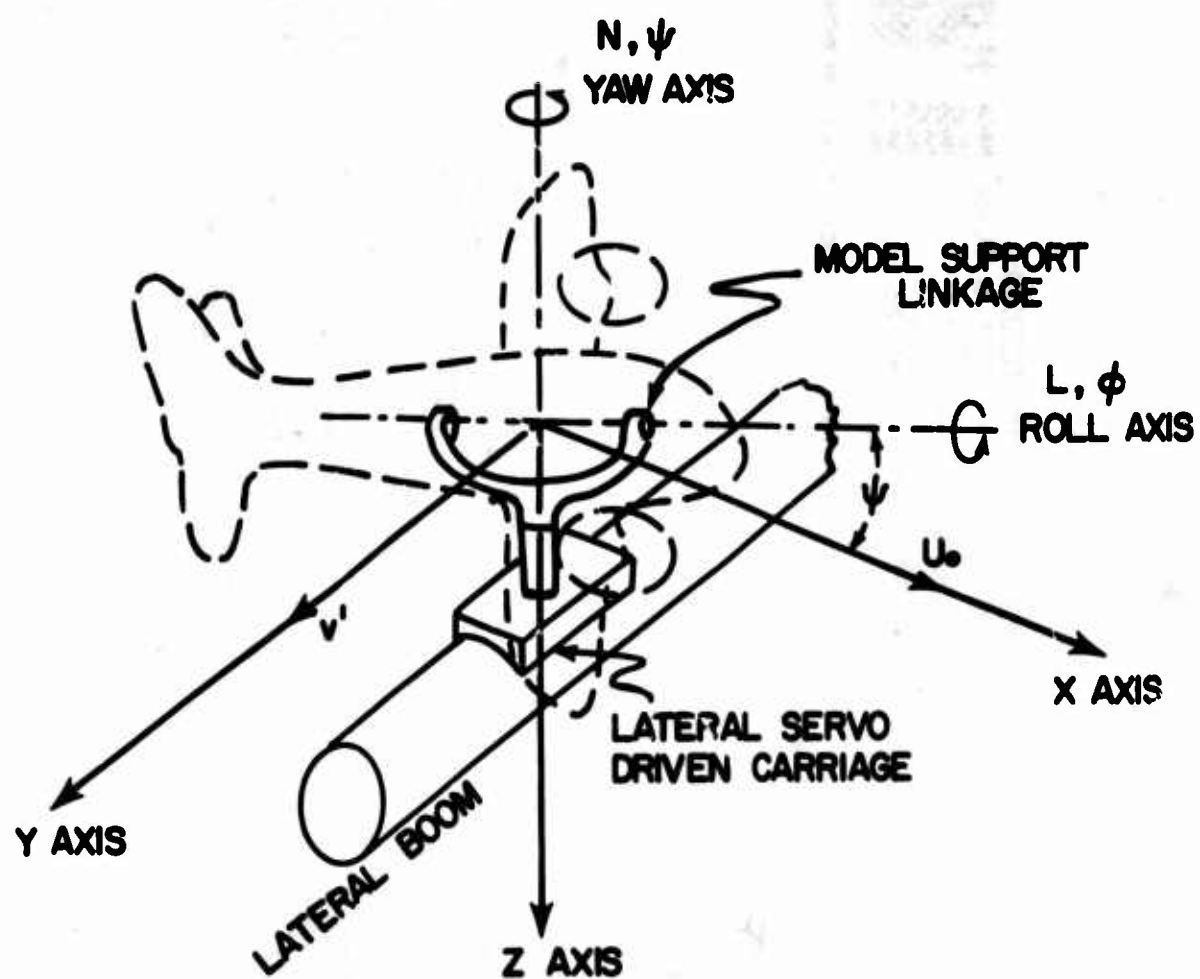
Figure 4. Schematic of Lateral/Directional Mount and Space Axis System.

Figure 5. General Arrangement, One-Tenth Scale XC-142 Model.

NOTE: WING AIRFOIL SECTION NACA 63-318
ANGULAR TRAVEL OF VANE = 1.075×ANGULAR TRAVEL AT FLAP
ALL DIMENSIONS GIVEN IN PERCENT CHORD AT ANY WING STATION
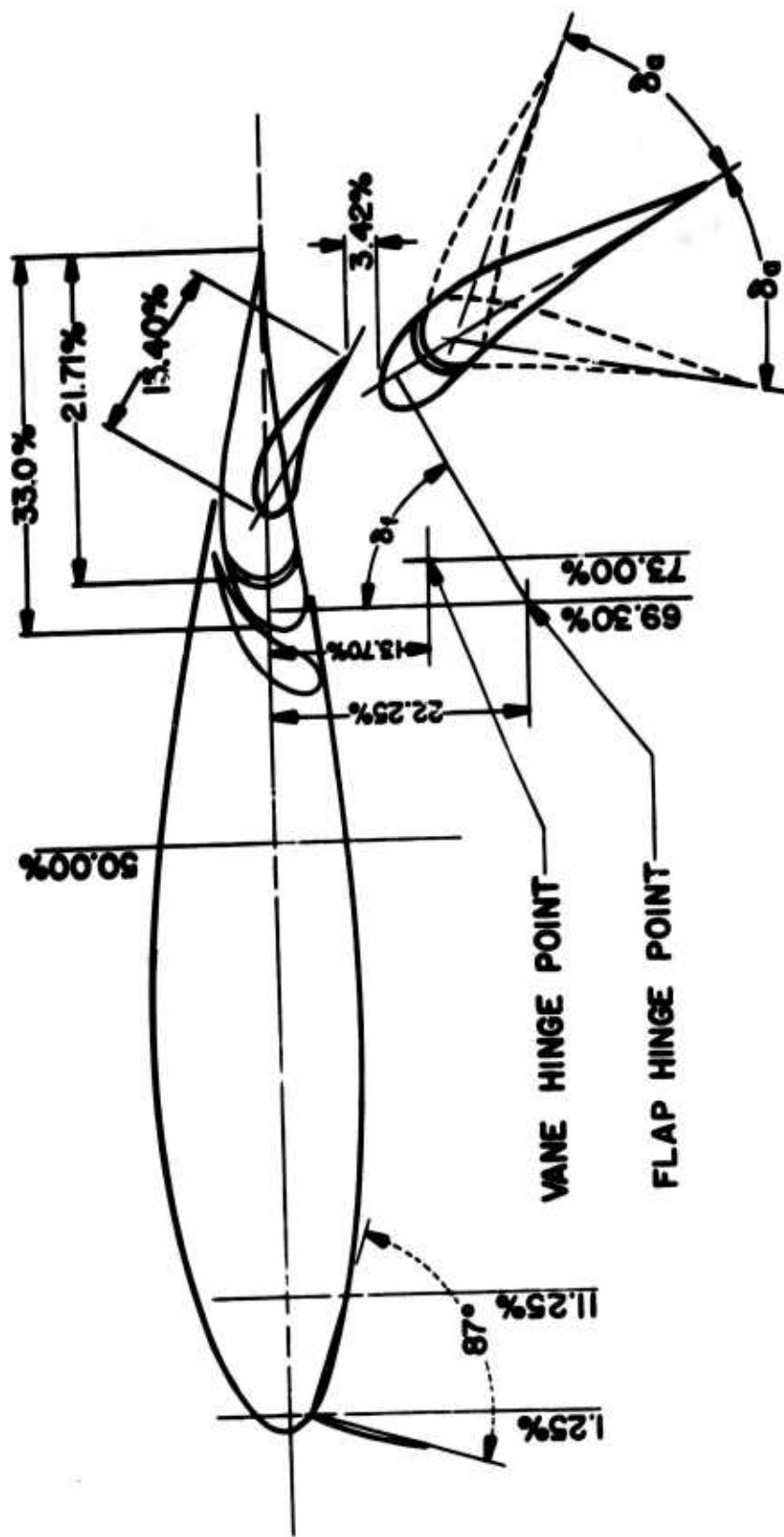
Figure 6a. Flap Arrangement.

NOTE: LEADING EDGE DEVICES EMPLOYED ONLY BEHIND UP-GOING BLADES.
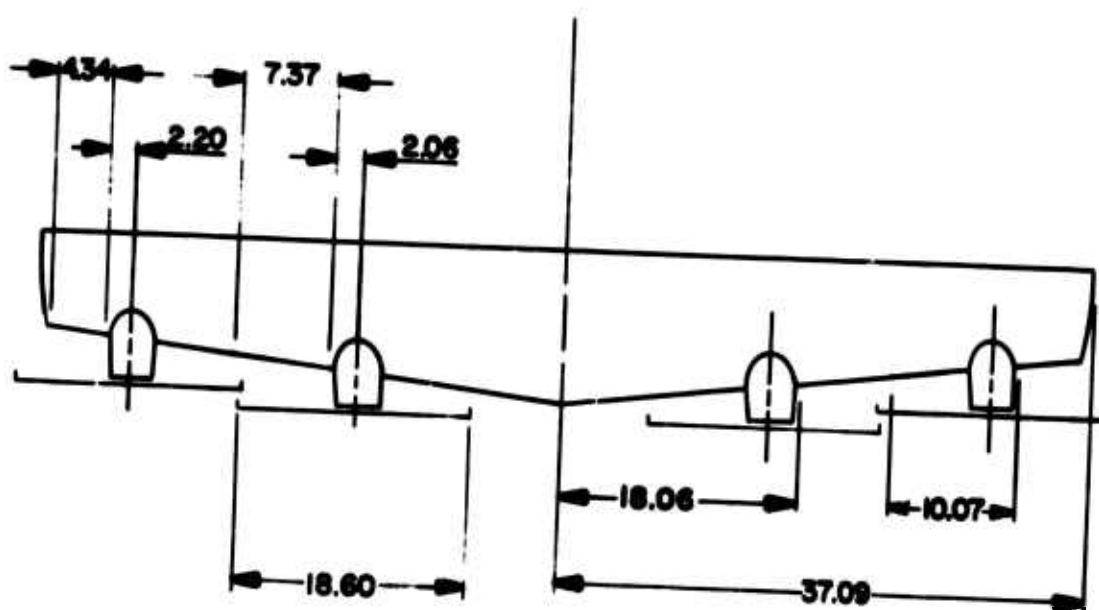
Figure 6b. Spanwise Location of Krüger Flaps.
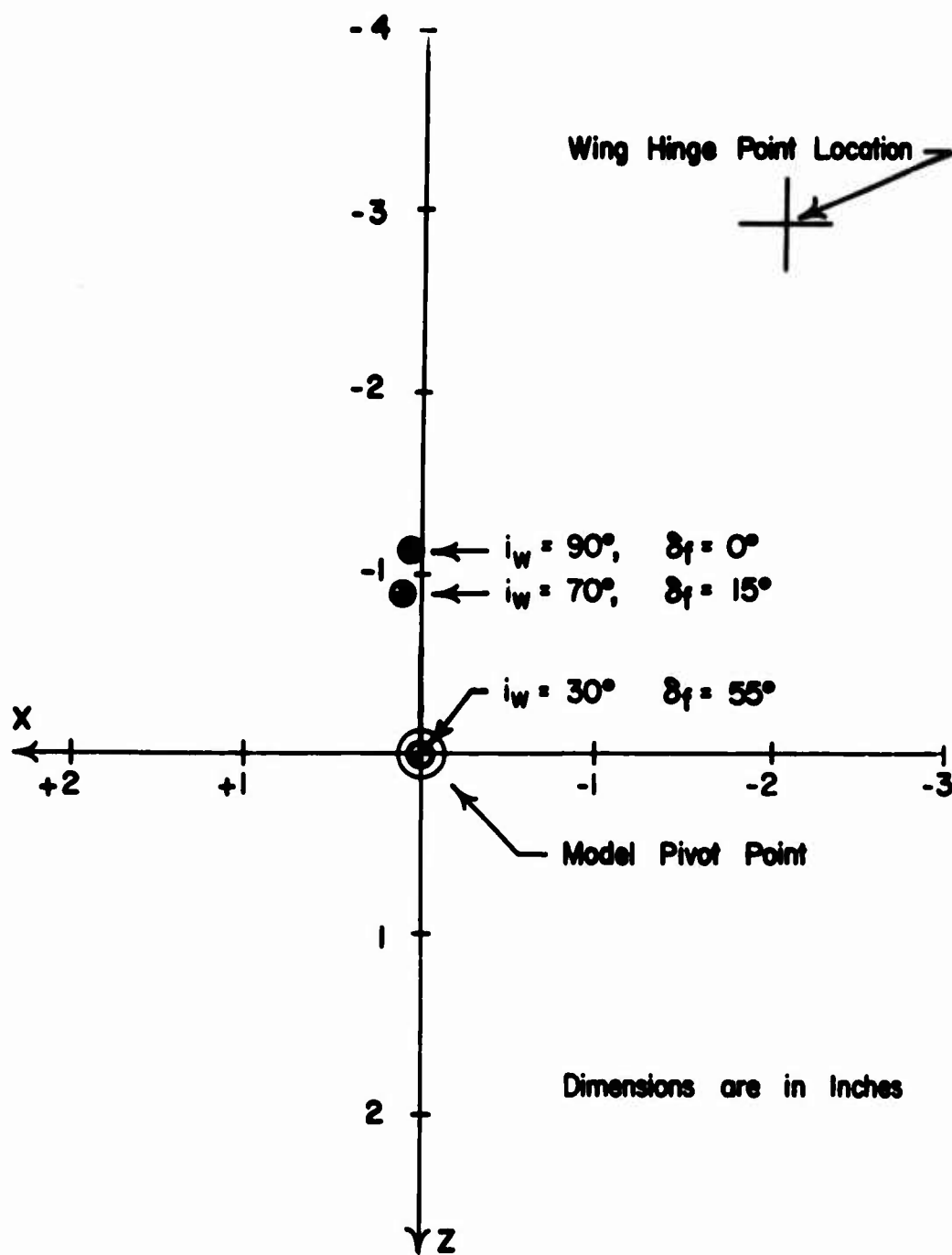
Figure 6c. Location of Center of Gravity of Model.
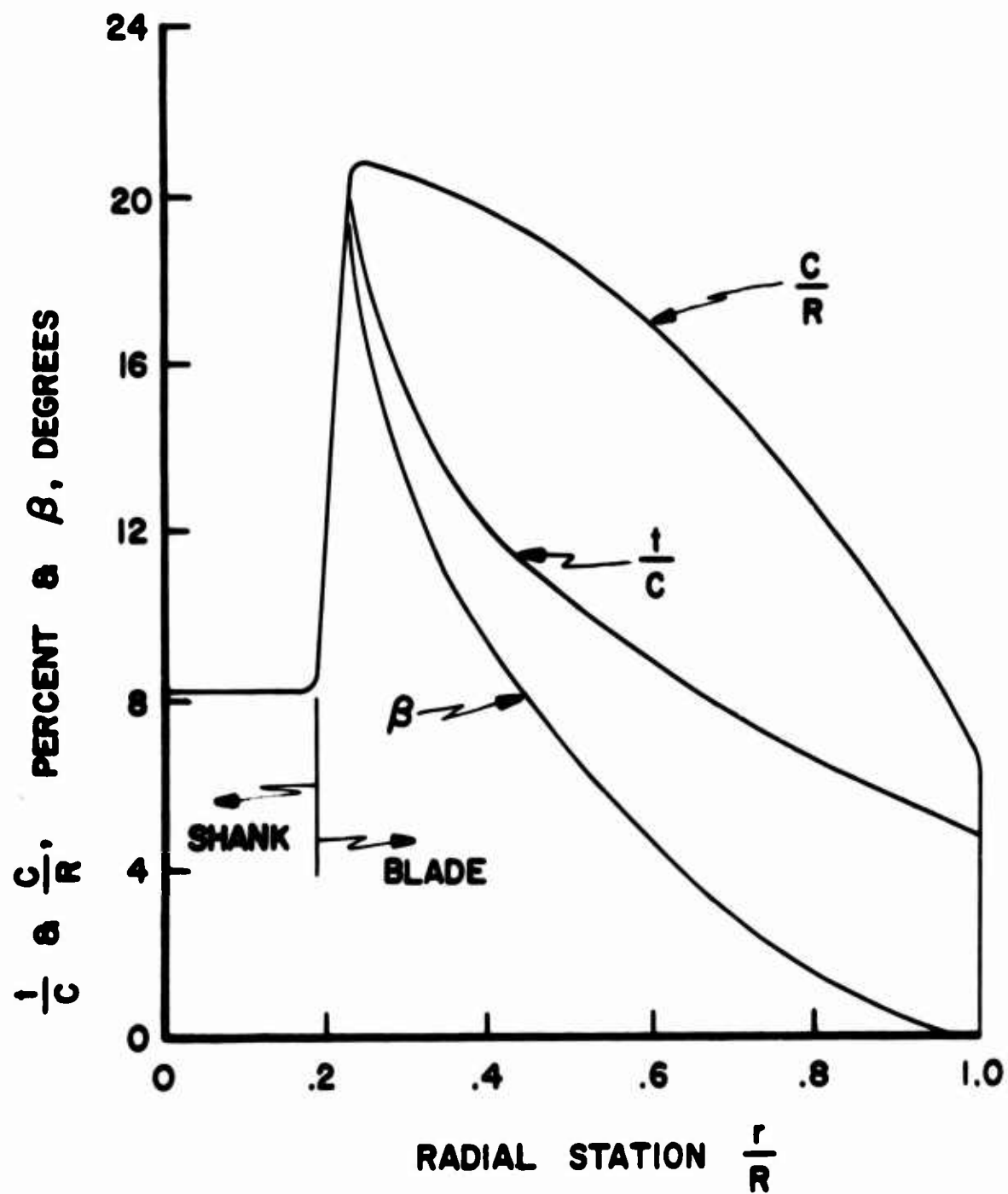
Figure 7.  Propeller Blade Characteristics, Four Blades.

60
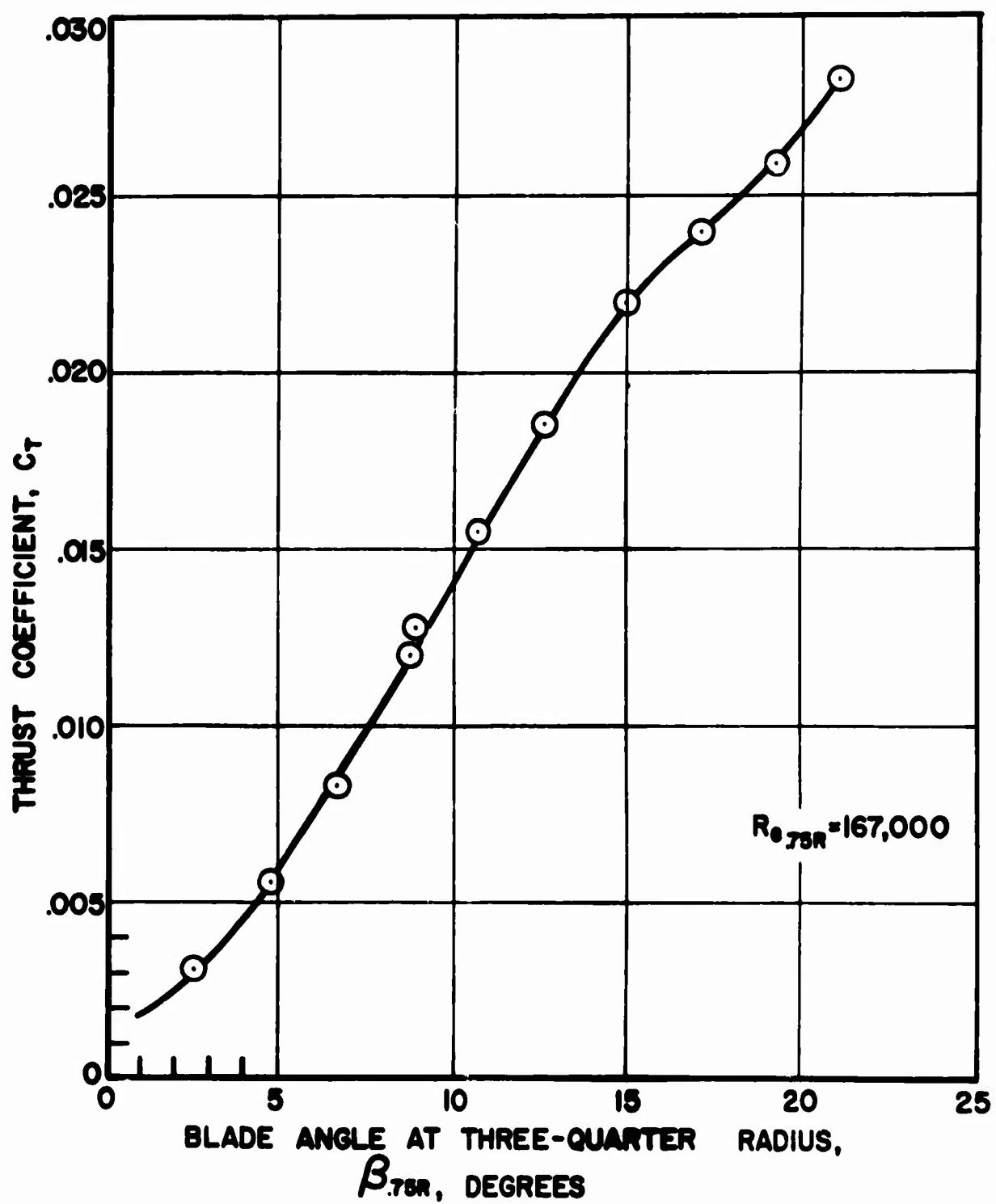
Figure 8. Propeller Static Thrust Characteristics.

61
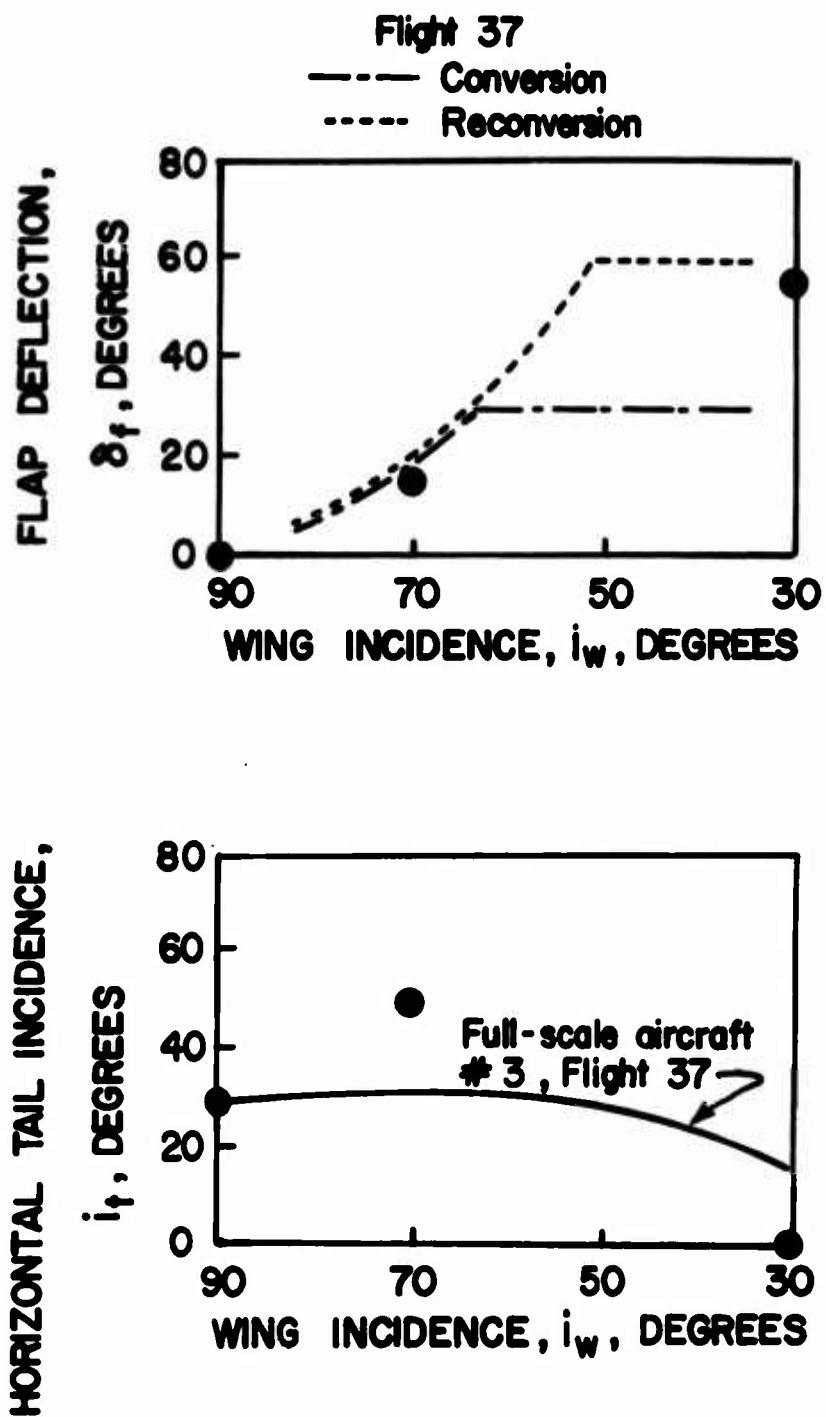
Figure 9. Model and Full-Scale Flap Deflection and Tail Incidence Versus Wing Incidence.
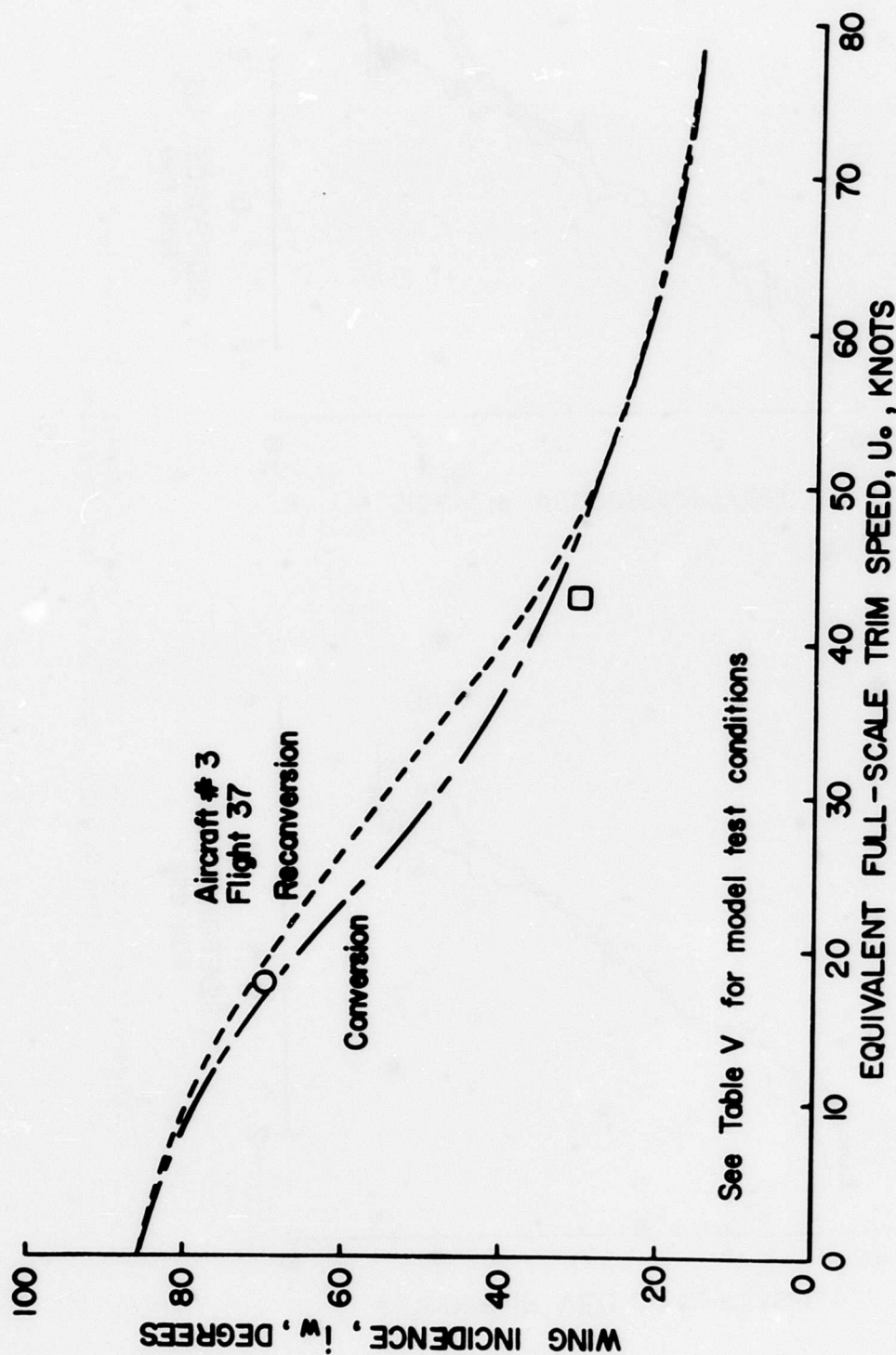
Figure 10. Comparison of Scaled Model Trim Conditions With Full-Scale Aircraft.
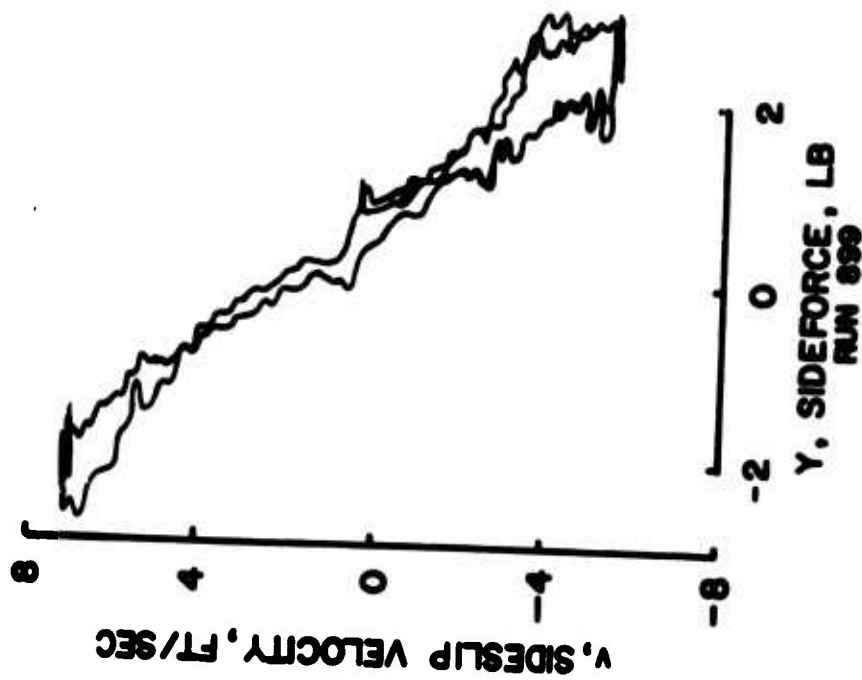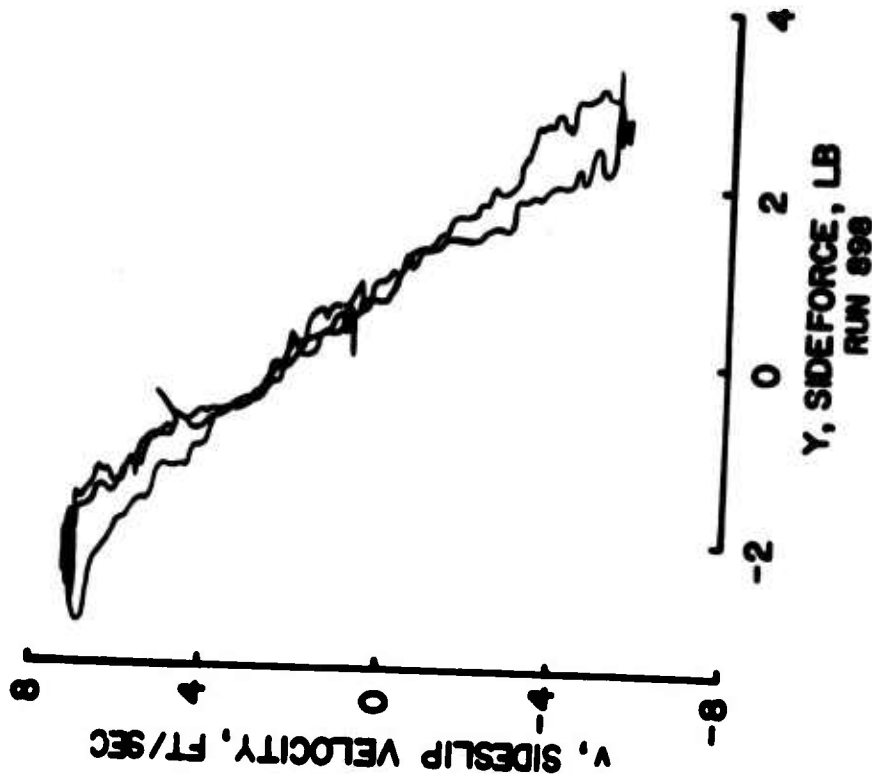
Figure 11a. Static Data: Sideforce Versus Sideslip Velocity, $i_w = 39°$.
(See Table V, Page 51, for Test Conditions)
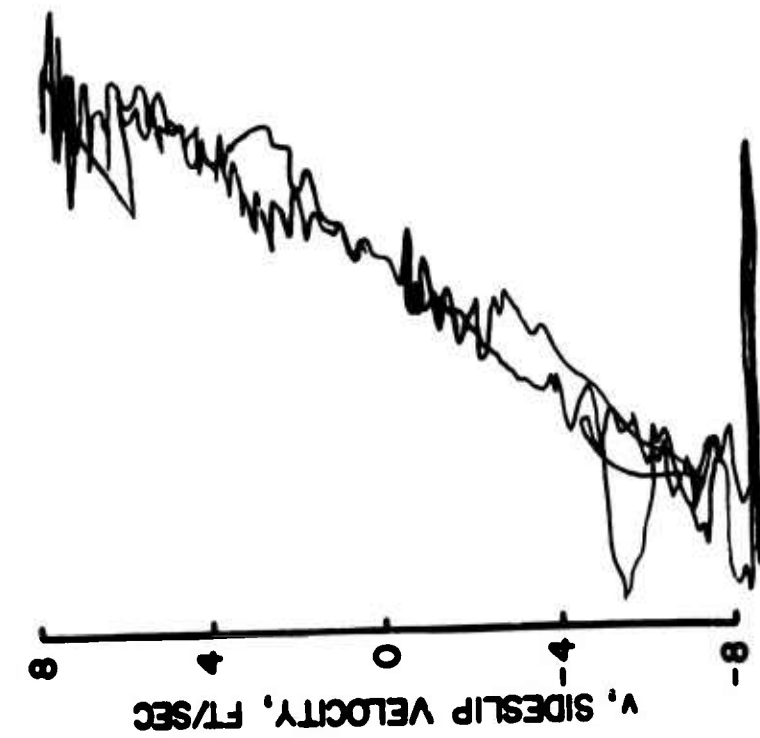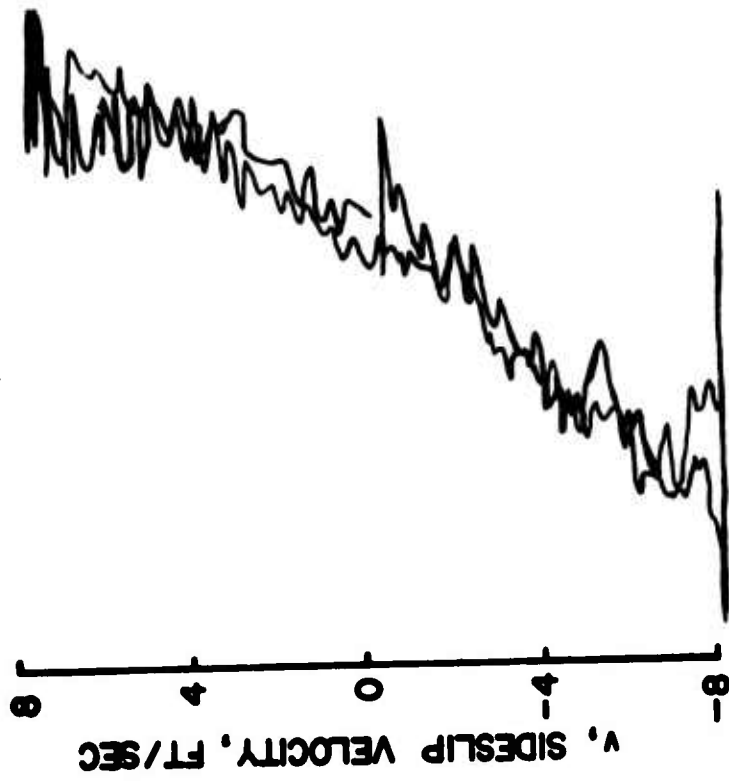
Figure 11b.  Static Data:  Rolling Moment Versus Sideslip Velocity, $i_w = 8^\circ$.
(See Table V, Page 51, for Test Conditions)
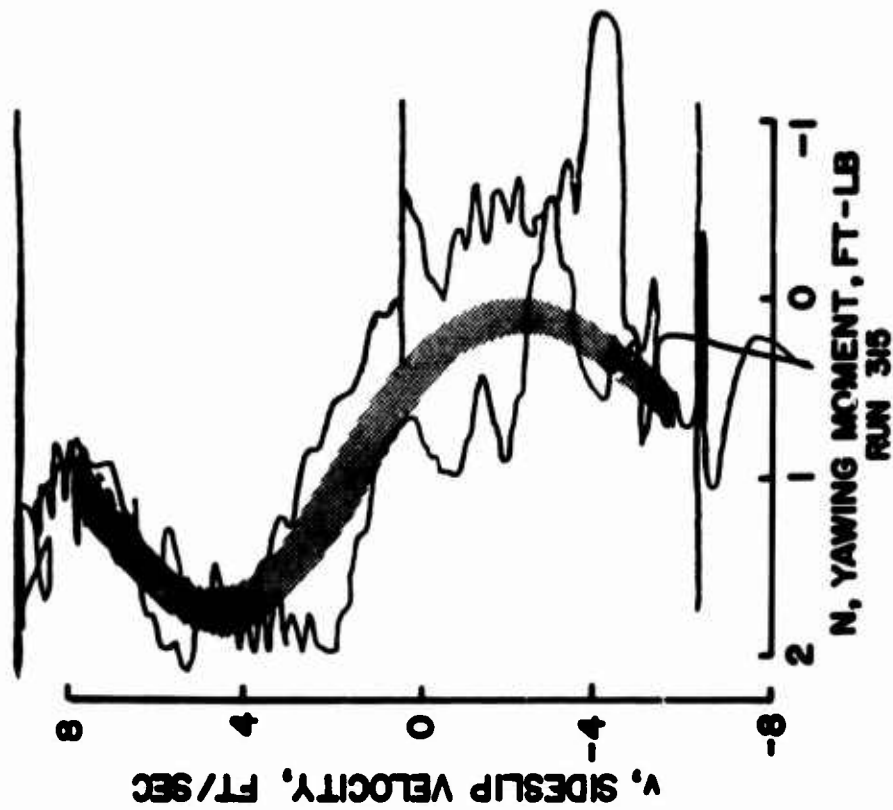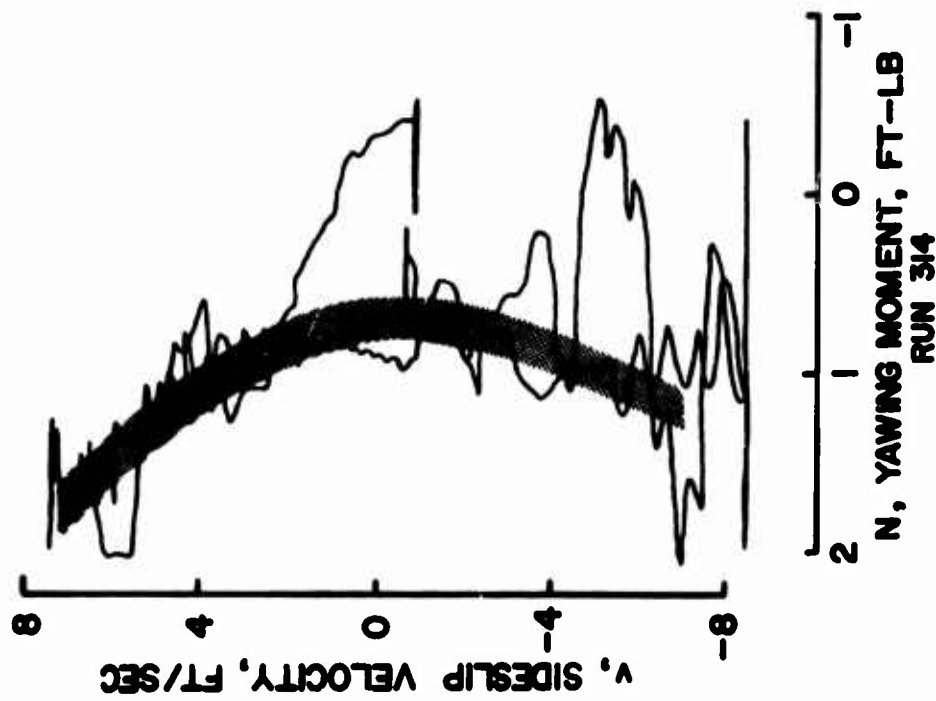
Figure 11c. Static Data: Yawing Moment Versus Sideslip Velocity, $i_w = 8°$.
(See Table V, Page 51, for Test Conditions)
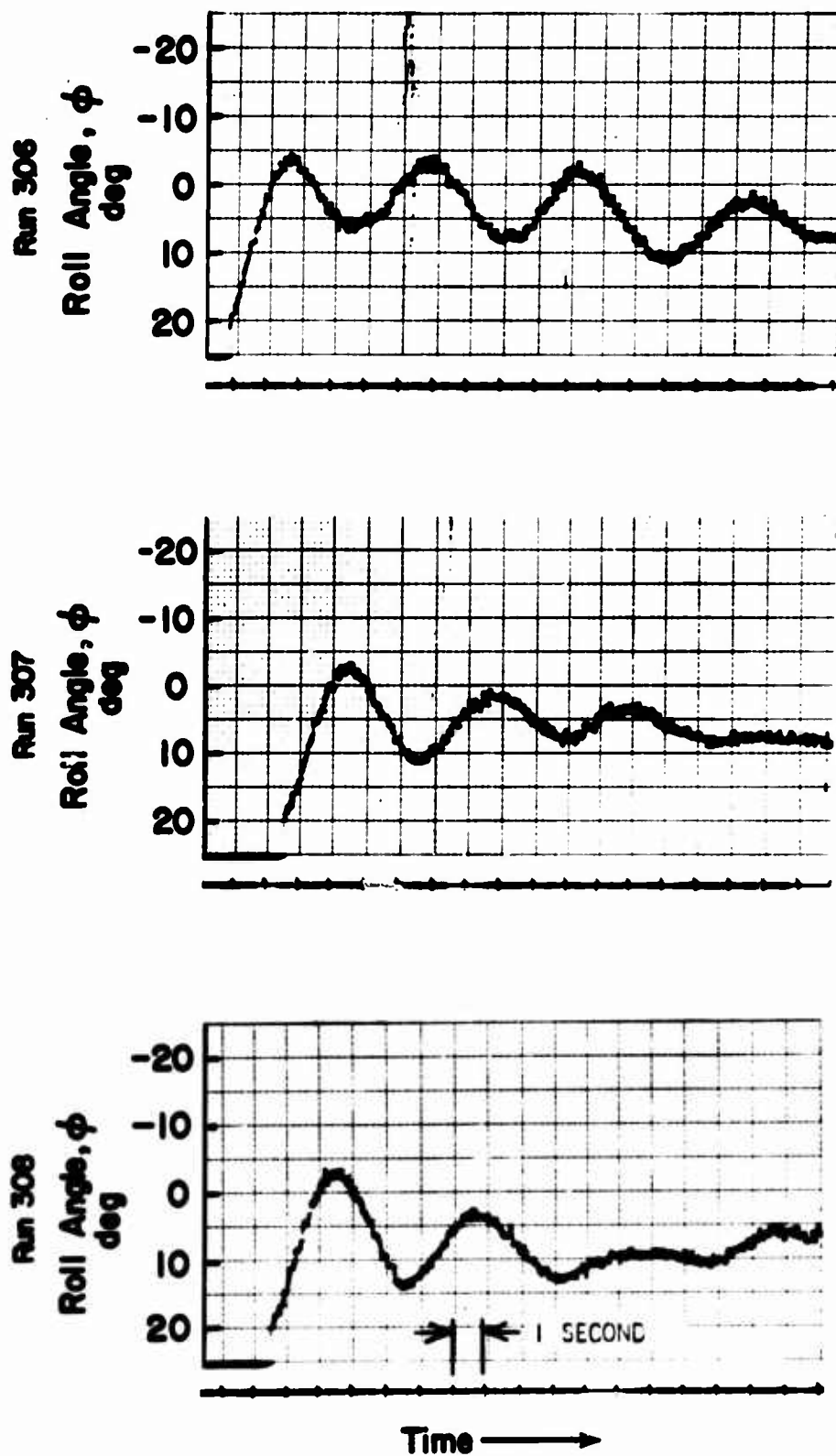
Figure 12a. Model Single Degree of Freedom in Roll Runs With Springs, $i_w = 89°$. (See Table V, Page 51, for Test Conditions)

67
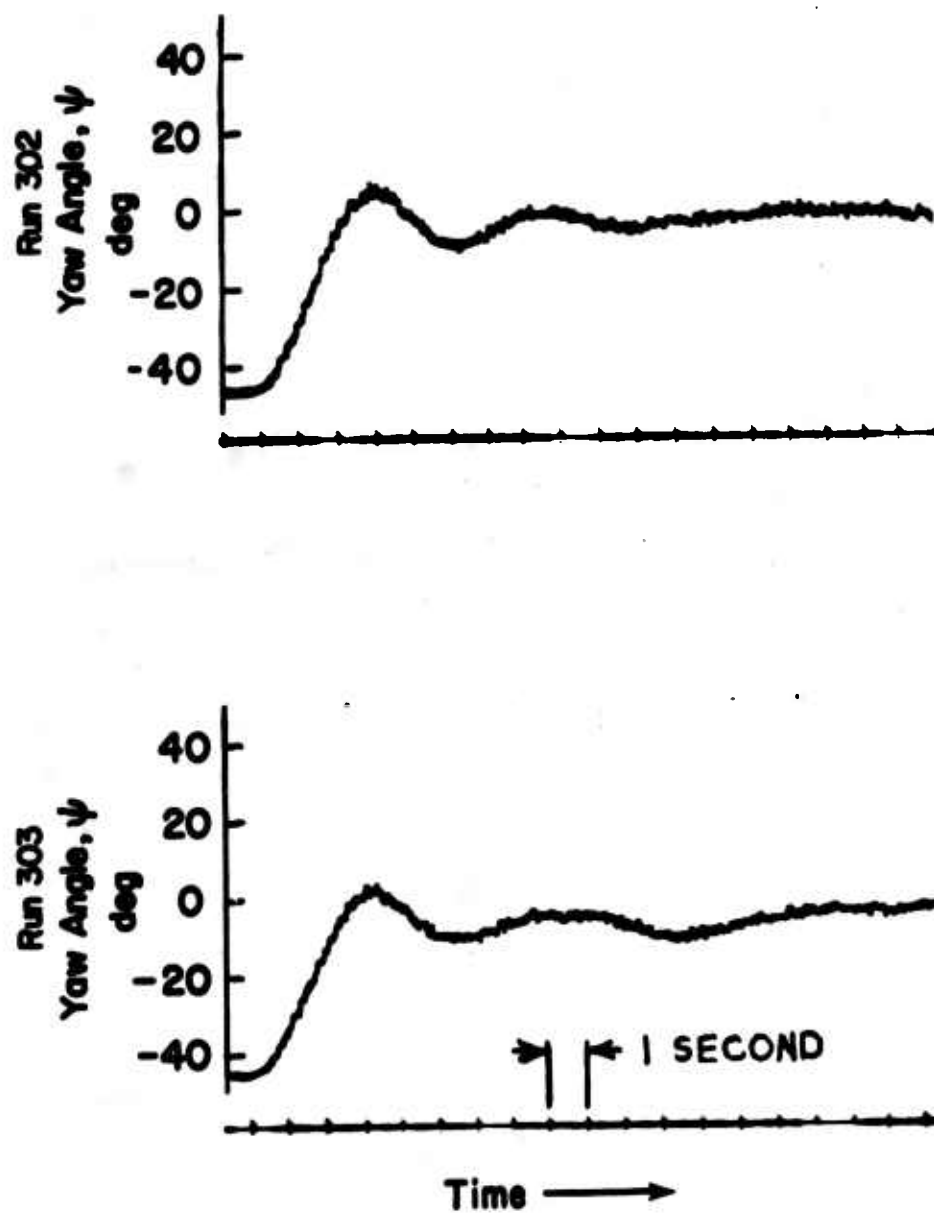
Figure 12b. Model Single Degree of Freedom in
Yaw Runs With Springs, $i_w = 8.9°$.
(See Table V, Page 51, for Test Conditions)

68
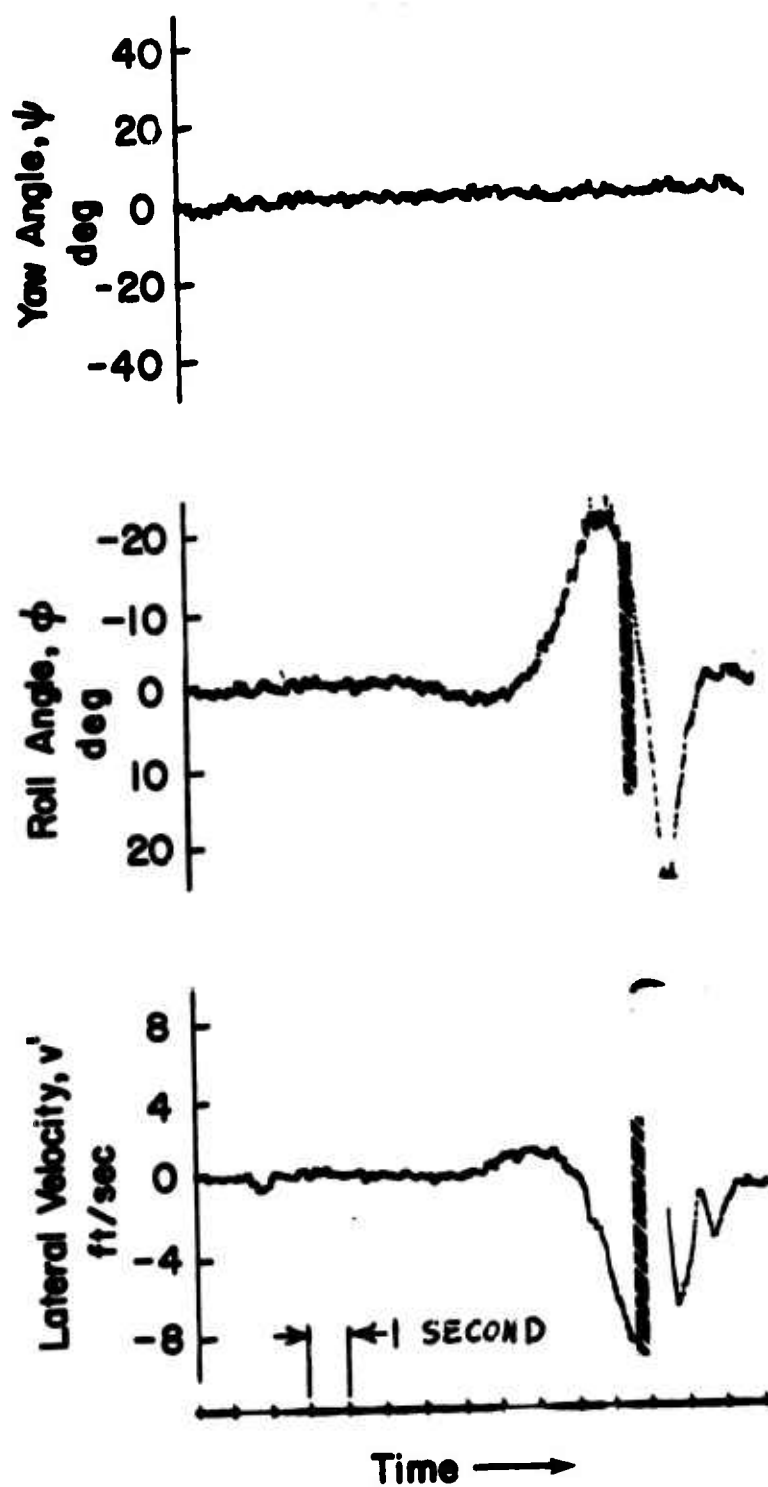
Figure 13a. Model Transient Self-Excited Response, $i_w = 89°$, Two Degrees of Freedom. (See Table V, Page 51, for Test Conditions)
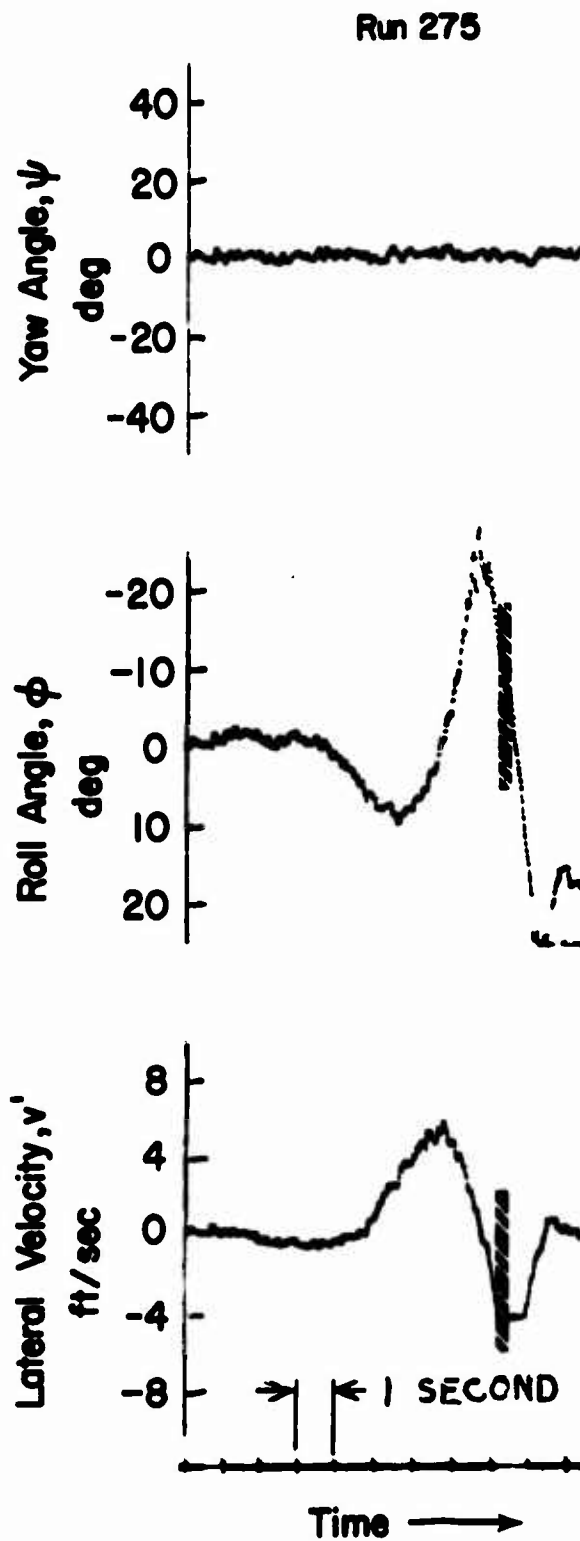
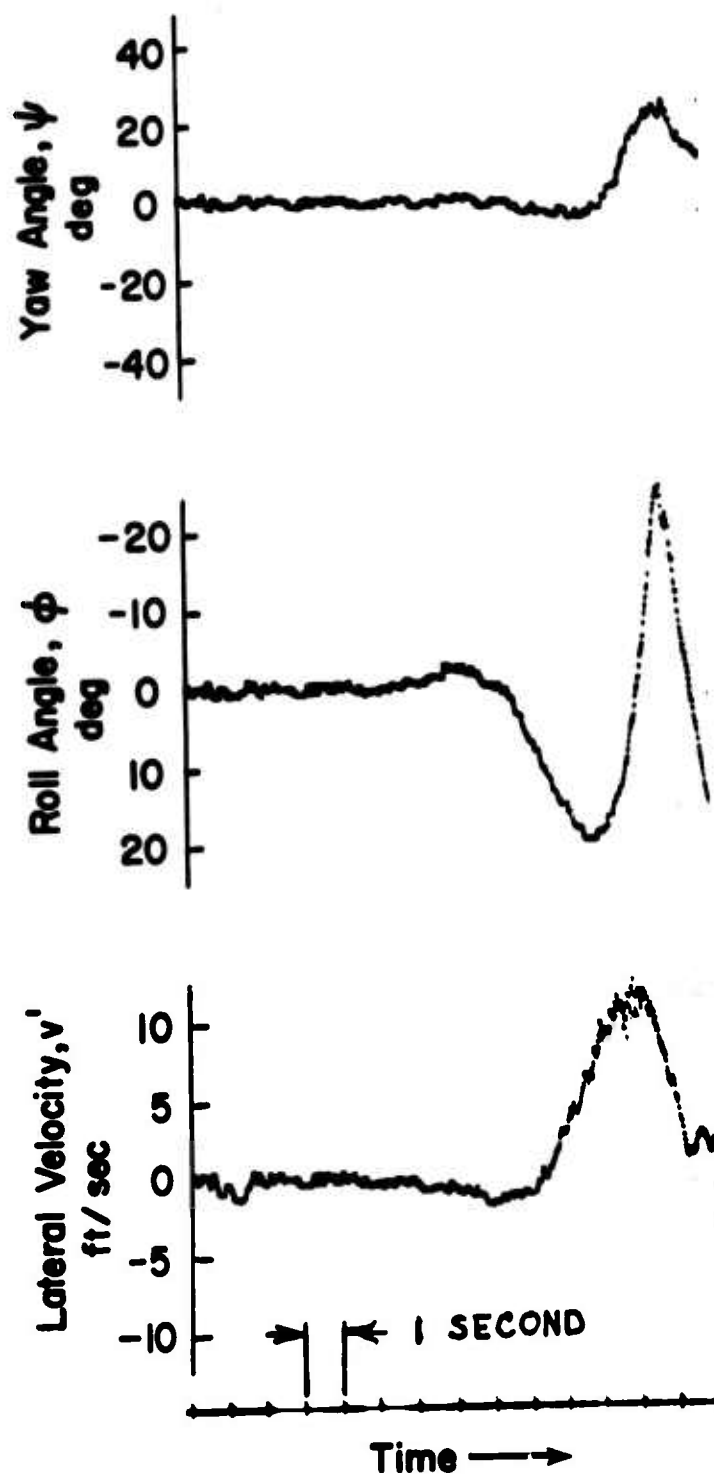Figure 13b. Model Transient Self-Excited Response, $i_w = 89°$, Two Degrees of Freedom. (See Table V, Page 51, for Test Conditions)

70
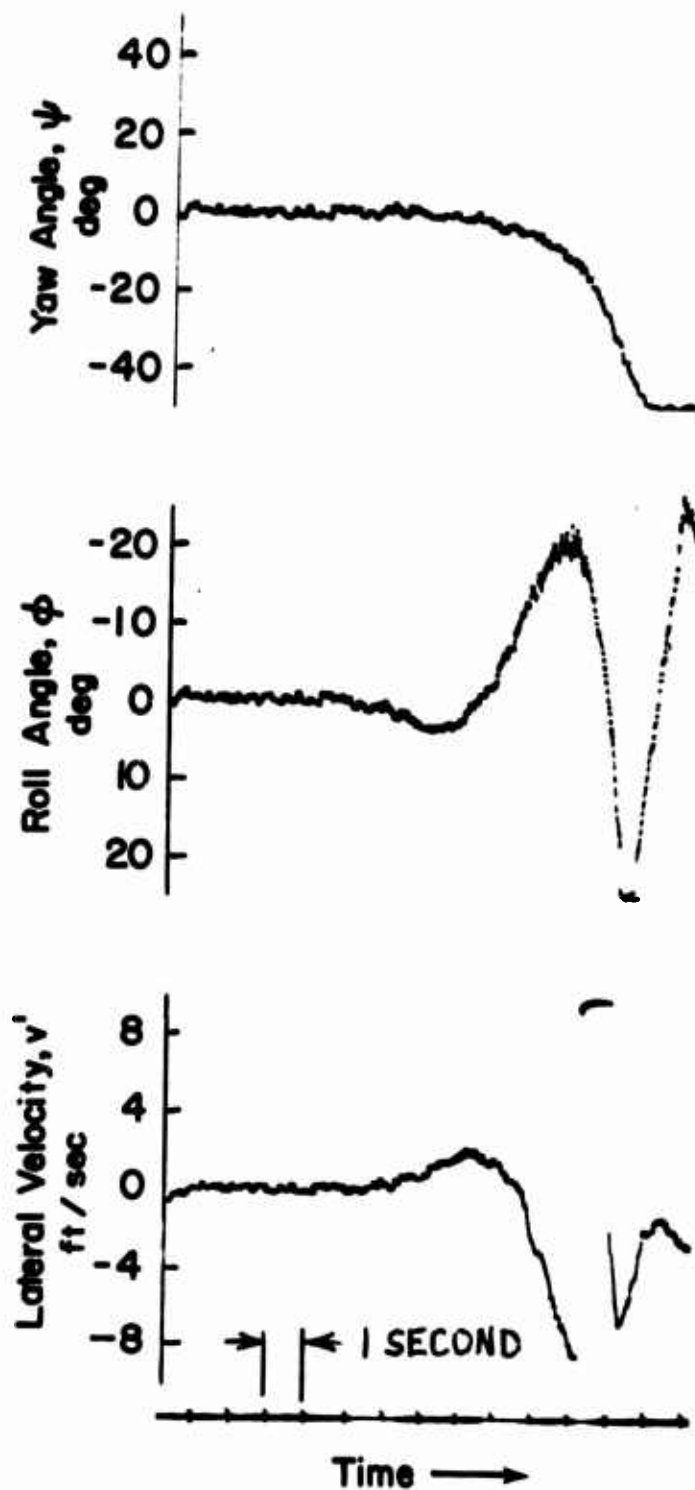
Figure 13c. Model Transient Self-Excited Response, $i_w = 89°$, Three Degrees of Freedom. (See Table V, Page 51, for Test Conditions)

Figure 13d. Model Transient Self-Excited Response, $i_w = 8^\circ$, Three Degrees of Freedom. (See Table V, Page 51, for Test Conditions)

72

## TABLE VII. SUMMARY OF HOVER DATA - MODEL SCALE

### STATIC DATA

| Run | $Y_v$ | Run | $L_v$ | Run | $N_v$ | |
|-----|-------|-----|-------|-----|-------|---|
| 898 | - 0.28 | 313 | - 0.16 | 313 | - | |
| 899 | - 0.26 | 314 | - 0.15 | 314 | - | } nonlinear |
|     |       | 315 | - 0.17 | 315 | - | |
|     |       | 319 | - 0.16 | 319 | - | |

Average value  - 0.27 per second        - 0.16 per foot-second

### ROLL AND YAW DAMPING

| Run | $L_{\dot{\varphi}}$ | Run | $N_{\dot{\psi}}$ |
|-----|---------------------|-----|------------------|
| 307 | - 0.372 | 302 | - 0.436 |
| 308 | - 0.364 | 303 | - 0.38 |

Average value  - 0.37 per second    - 0.41 per second

### TRANSIENT RESPONSE (MEASURED CHARACTERISTICS)

#### Two Degrees of Freedom

| | $\varphi$ | | $v'$ | |
| Run | Period (seconds) | $\sigma$ | Period (seconds) | $\sigma$ |
|-----|------------------|----------|------------------|----------|
| 269 | 6.2 | 0.60 | - | - |
| 275 | 6.2 | 0.60 | 6.2 | 0.58 |

#### Three Degrees of Freedom

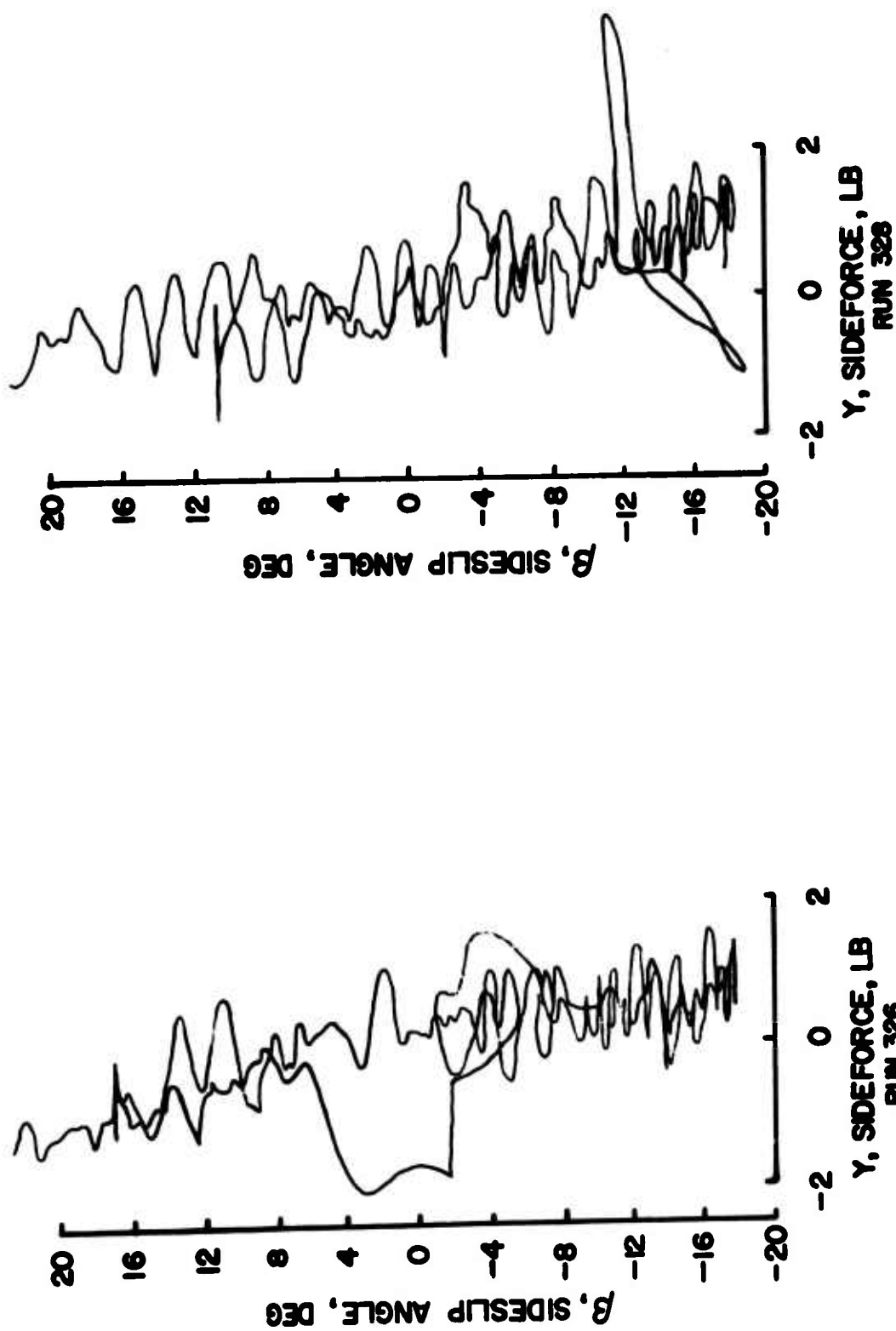| | $\varphi$ | | $v'$ | | |
| Run | Period (seconds) | $\sigma$ | Period (seconds) | $\sigma$ | $\psi$ |
|-----|------------------|----------|------------------|----------|--------|
| 289 | 6.8 | 0.46 | - | - | nonoscillatory |
| 296 | 6.8 | 0.62 | 6.8 | 0.61 | nonoscillatory |

73

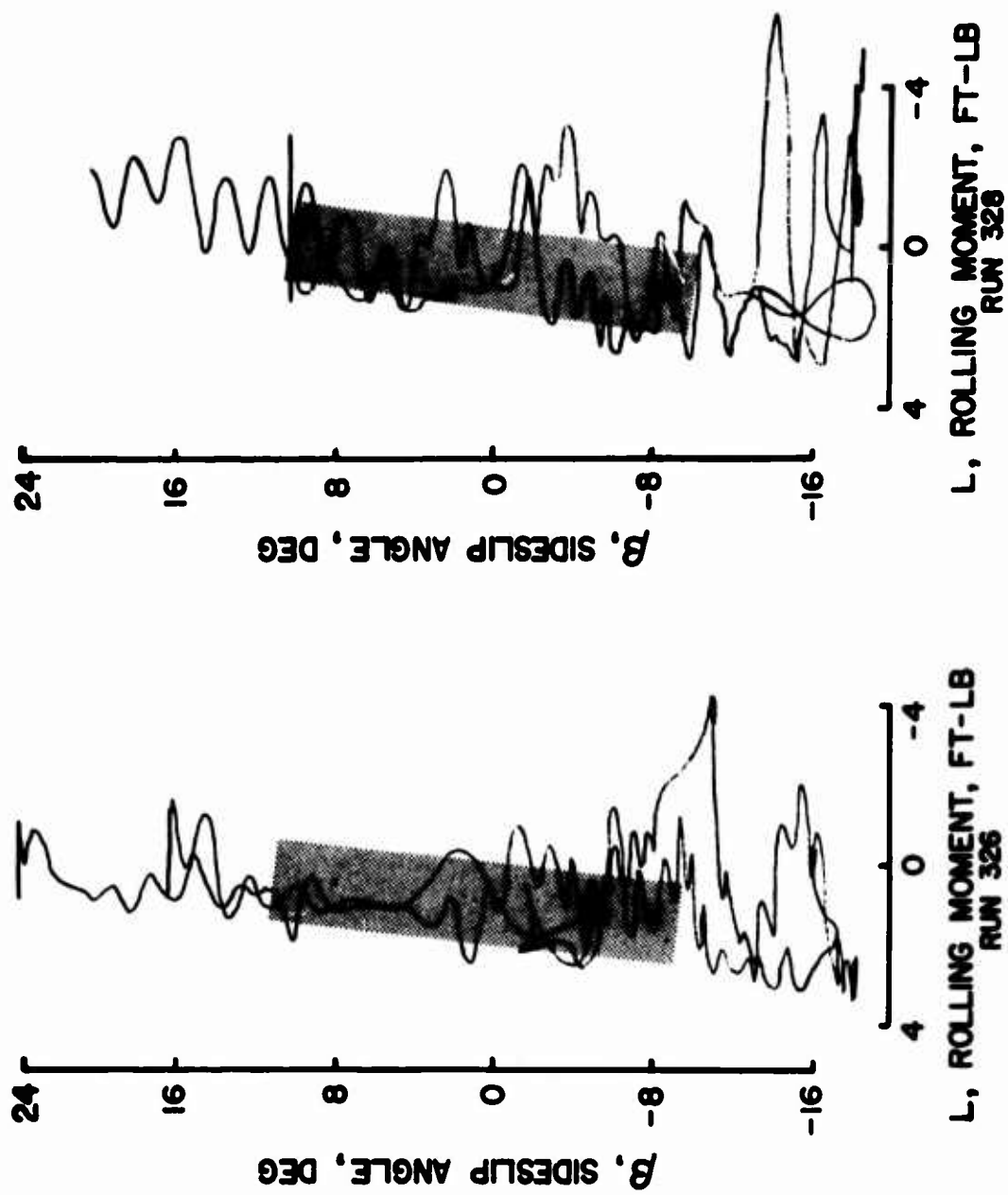Figure 14a. Static Data: Sideforce Versus Sideslip Angle, $i_w = 7^\circ$. (See Table V, Page 51, for Test Conditions)

74

Figure 14b. Static Data: Rolling Moment Versus Sideslip Angle, $i_w = 16°$.
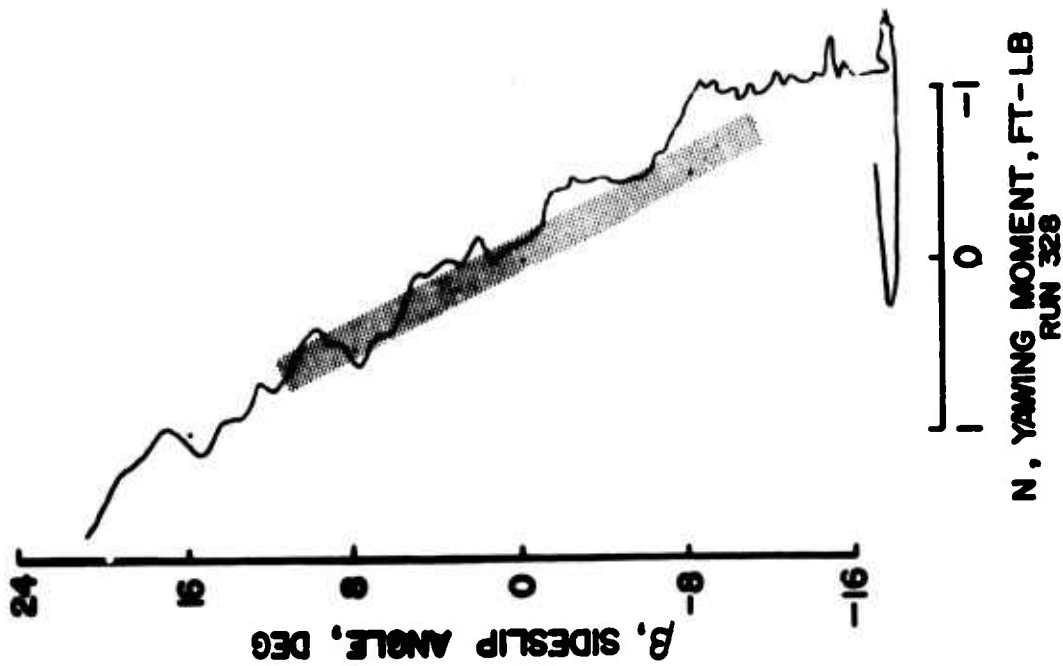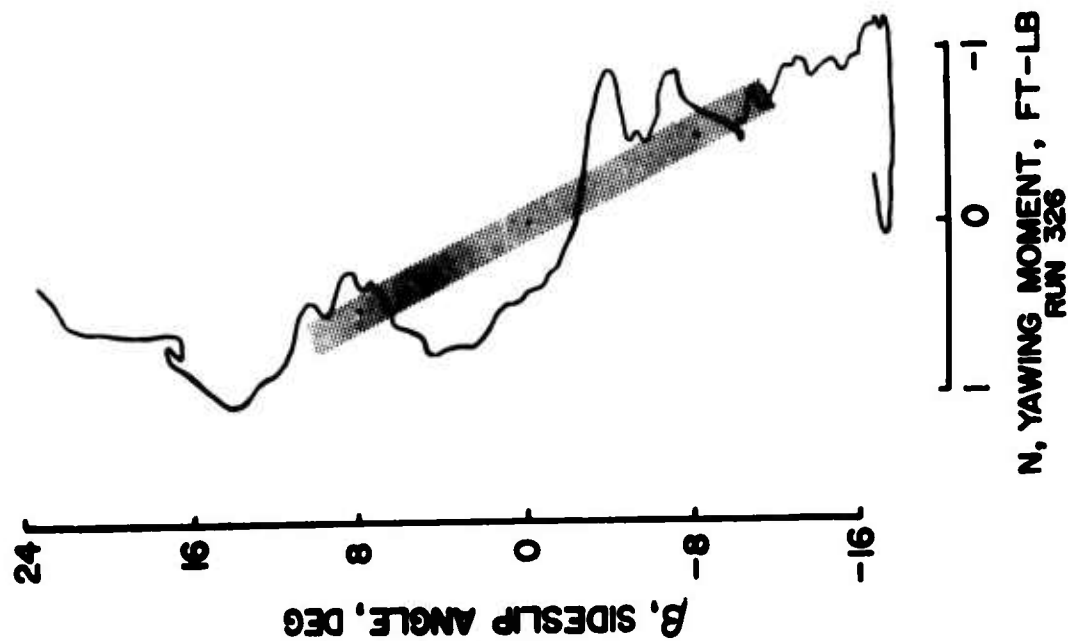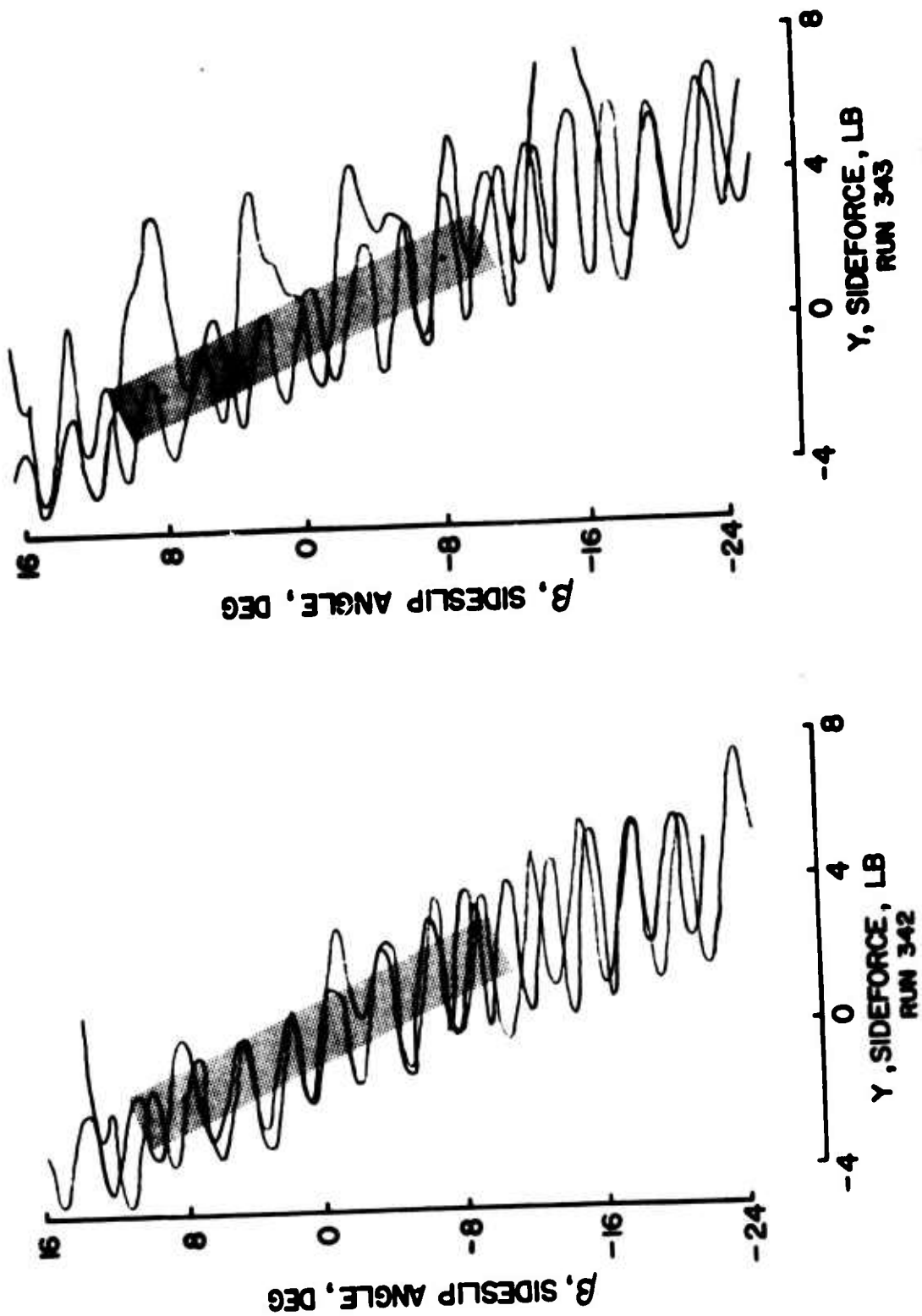(See Table V, Page 41, for Test Conditions)

N, YAWING MOMENT, FT-LB
RUN 328

β, SIDESLIP ANGLE, DEG

N, YAWING MOMENT, FT-LB
RUN 326

β, SIDESLIP ANGLE, DEG

Figure 14c.  Static Data:  Yawing Moment Versus Sideslip Angle, $i_w = 70^o$.
(See Table V, Page 51, for Test Conditions)

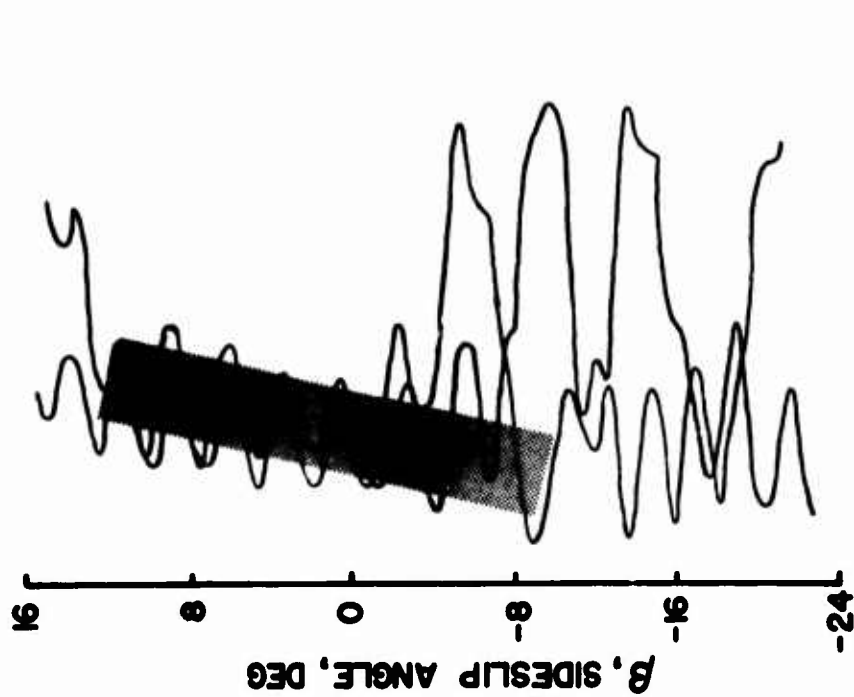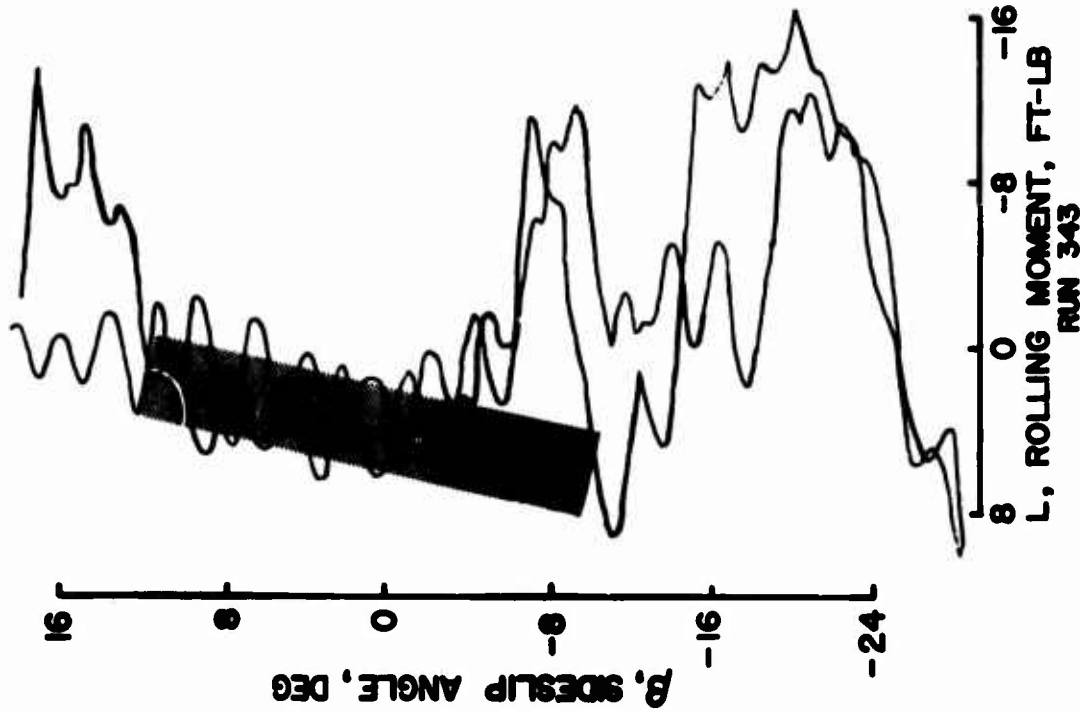Figure 14d. Static Data: Sideforce Versus Sideslip Angle, $i_w = 30°$. (See Table V, Page 51, for Test Conditions)

77

Figure 14e. Static Data: Rolling Moment Versus Sideslip Angle, $i_w = 30^\circ$.
(See Table V, Page 51, for Test Conditions)
Note: These data are presented to show a general trend only.
Values of the dihedral effect were evaluated from dynamic
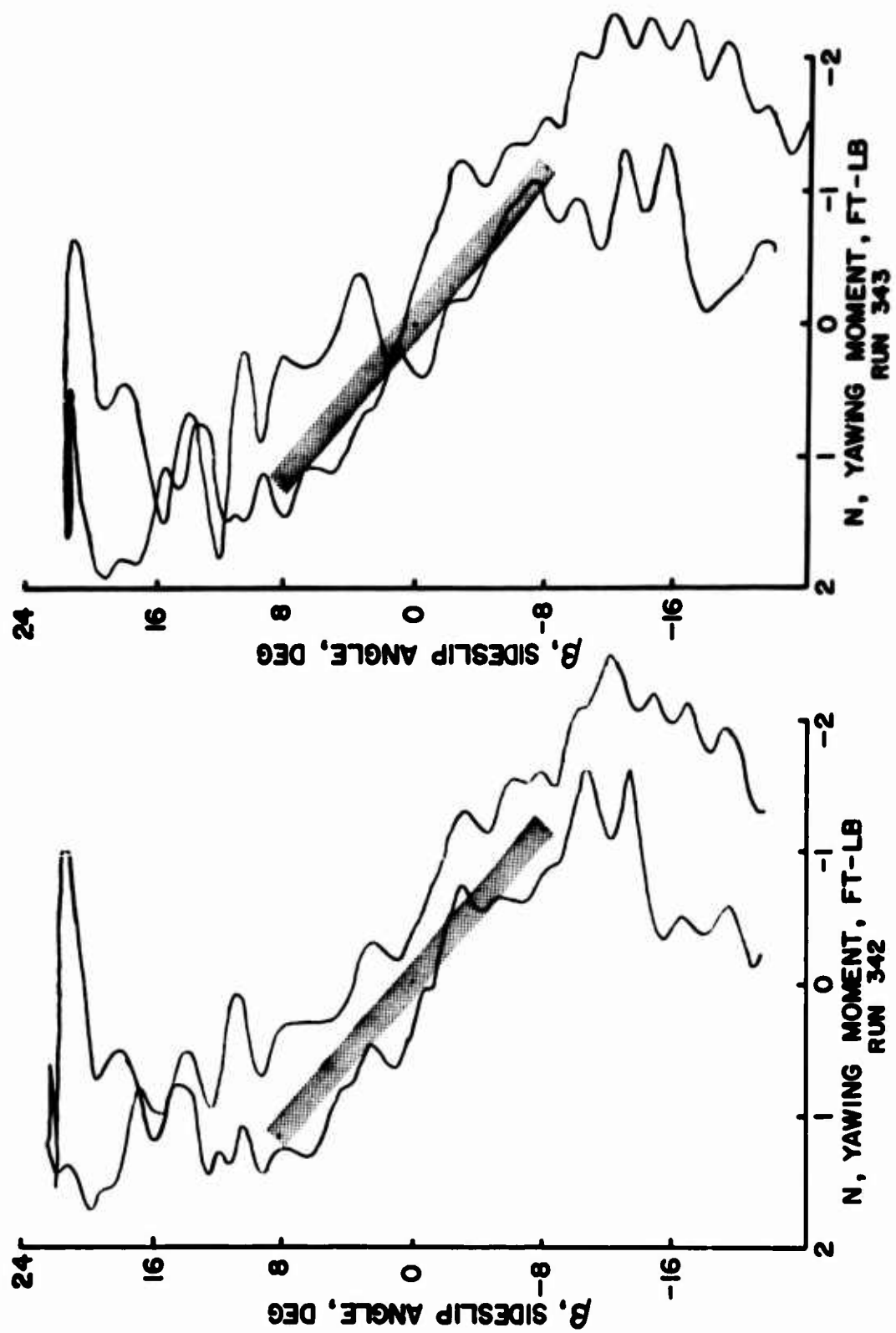data as explained in the text.

Figure 14f.  Static Data:  Yawing Moment Versus Sideslip Angle, $i_w = 30°$.
(See Table V, Page 51, for Test Conditions)

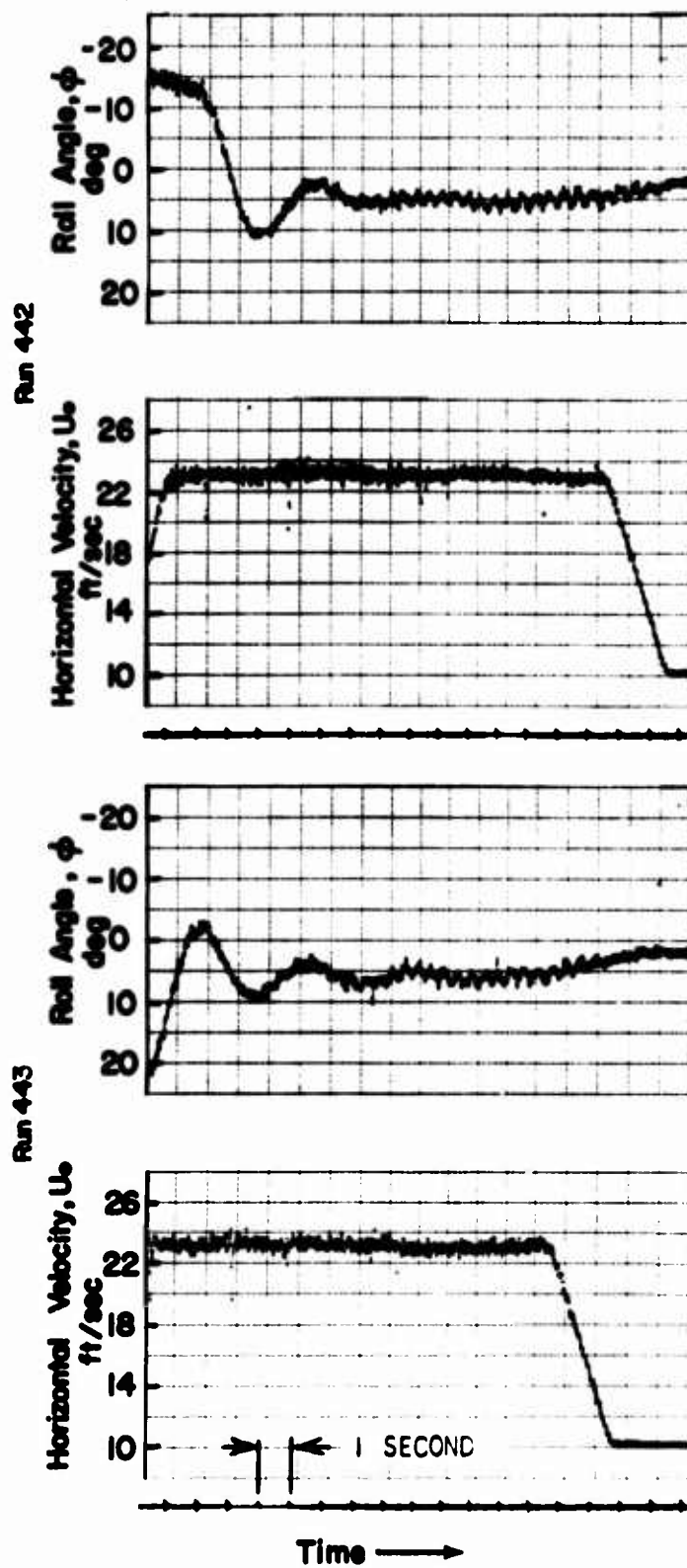Figure 15a.  Model Single Degree of Freedom in
Roll Runs With Springs, $i_w = 30°$.
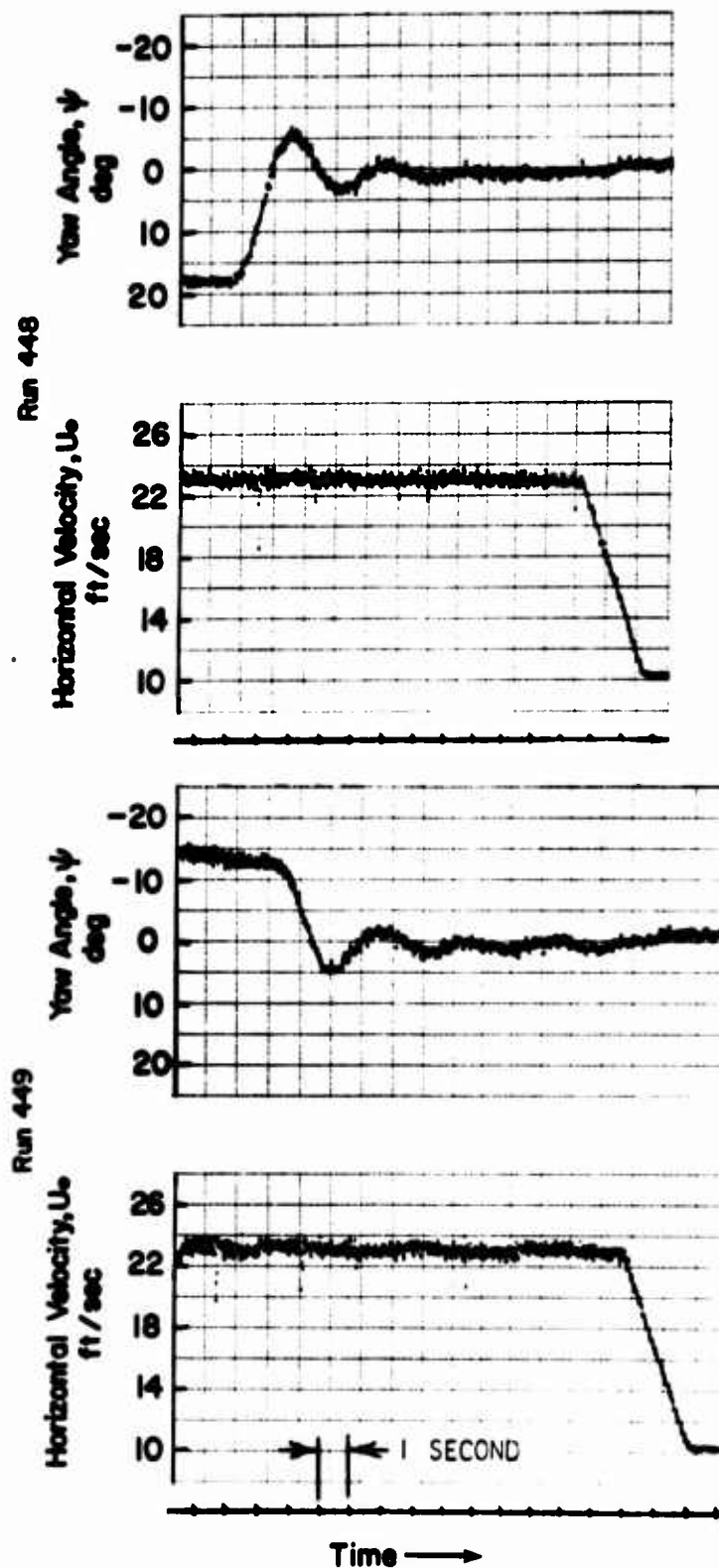(See Table V, Page 51, for Test Conditions)

80

Figure 15b. Model Single Degree of Freedom in
Yaw Runs With Springs, $i_w = 30^o$. $\Psi = -8$.
(See Table V. Page 51, for Test Conditions)

Figure 16a. Model Transient Self-Excited Response, $i_w = 70°$, Three Degrees of Freedom. (See Table V, Page 51, for Test Conditions)

82

Run 392
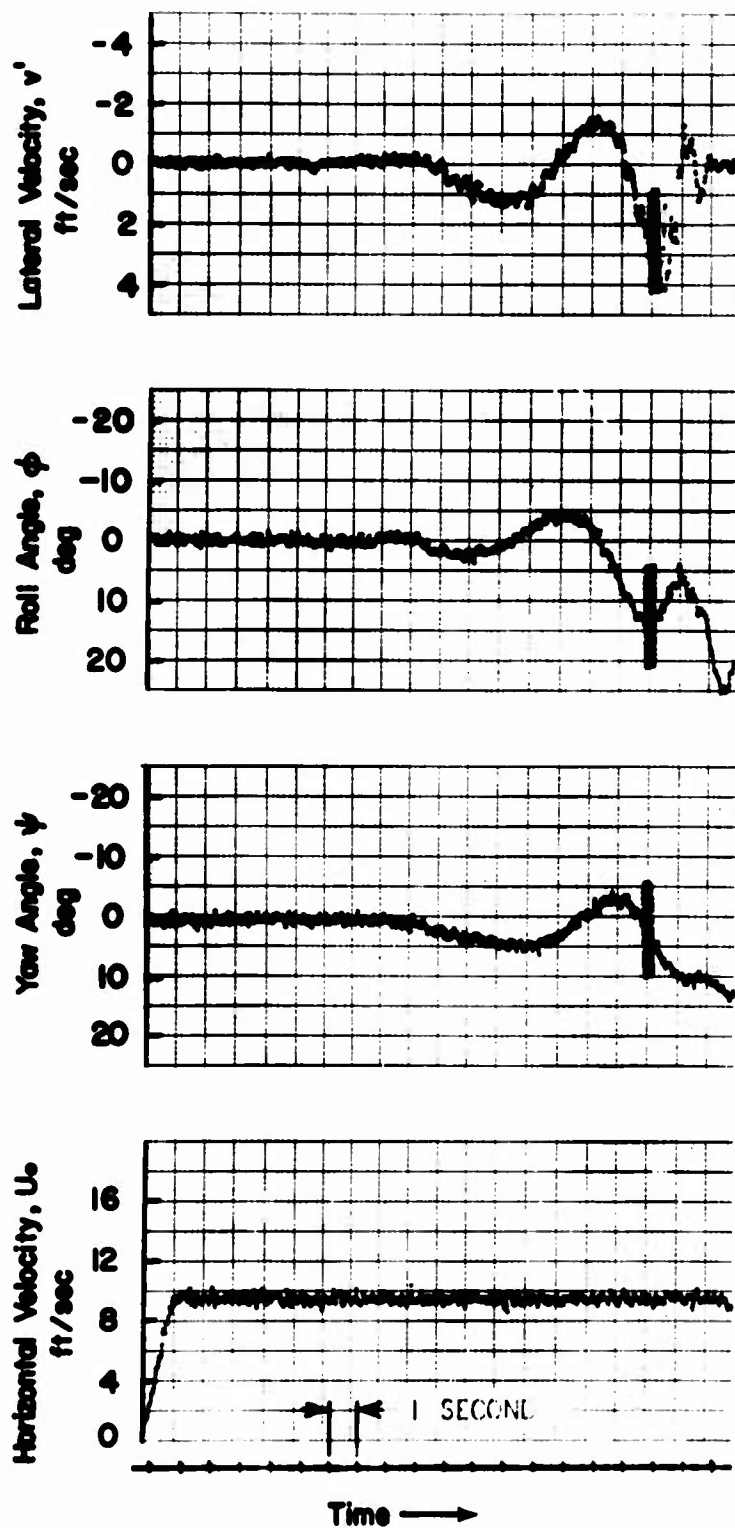


Figure 16b. Model Transient Self-Excited Response, $i_w = 70°$,
Three Degrees of Freedom.
(See Table V, Page 51, for Test Conditions)

Figure 17a. Model Transient Response, $i_w = 30^o$,
Single Degree of Freedom in Yaw, $\Psi = -\beta$.
(See Table V, Page 51, for Test Conditions)
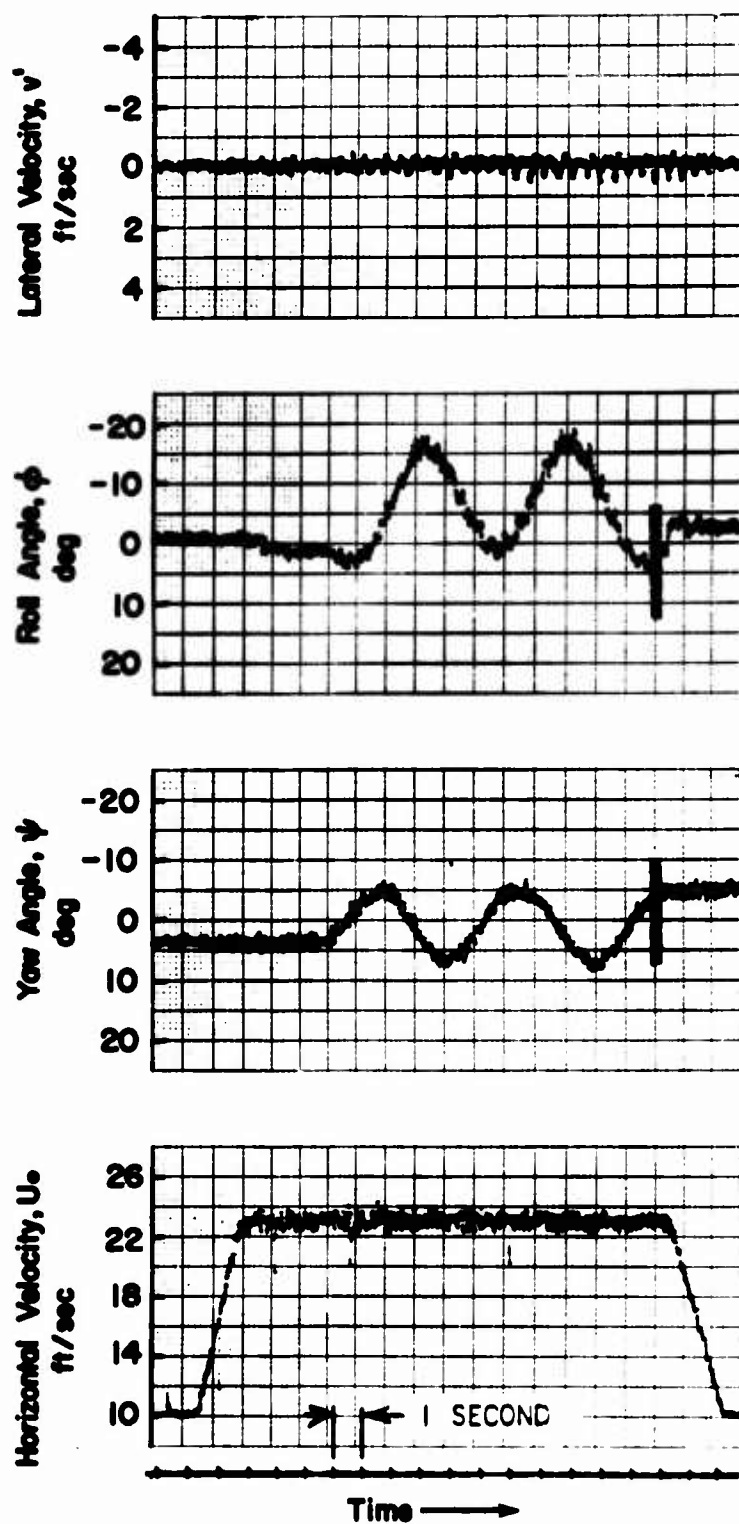
Figure 17b. Model Transient Response, $i_w = 30°$,
Two Degrees of Freedom in Roll and Yaw, $\Psi = -\beta$.
(See Table V, Page 51, for Test Conditions)

85
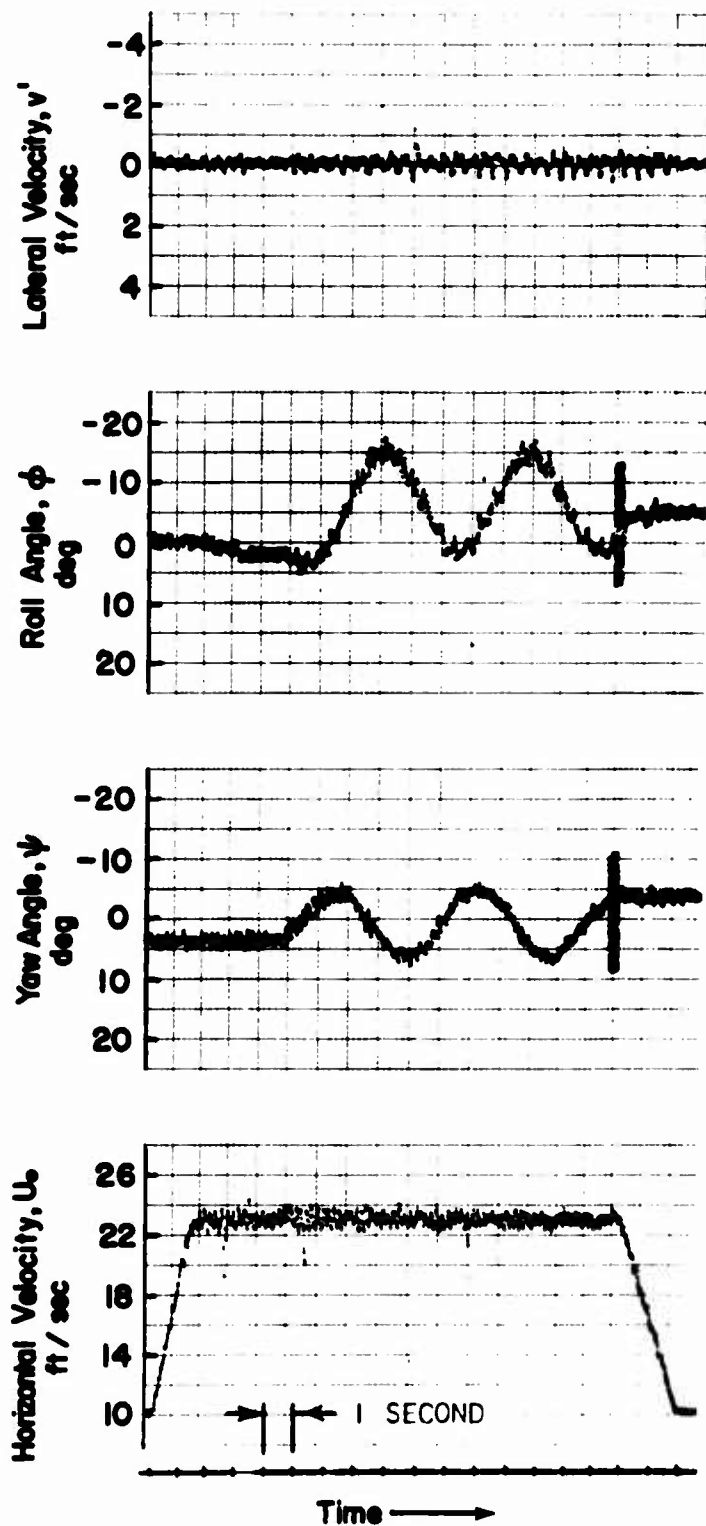
Figure 17c. Model Transient Response, $i_w = 30°$,
Two Degrees of Freedom in Roll and Yaw, $\Psi = -\beta$.
(See Table V, Page 51, for Test Conditions)

86

Run 435
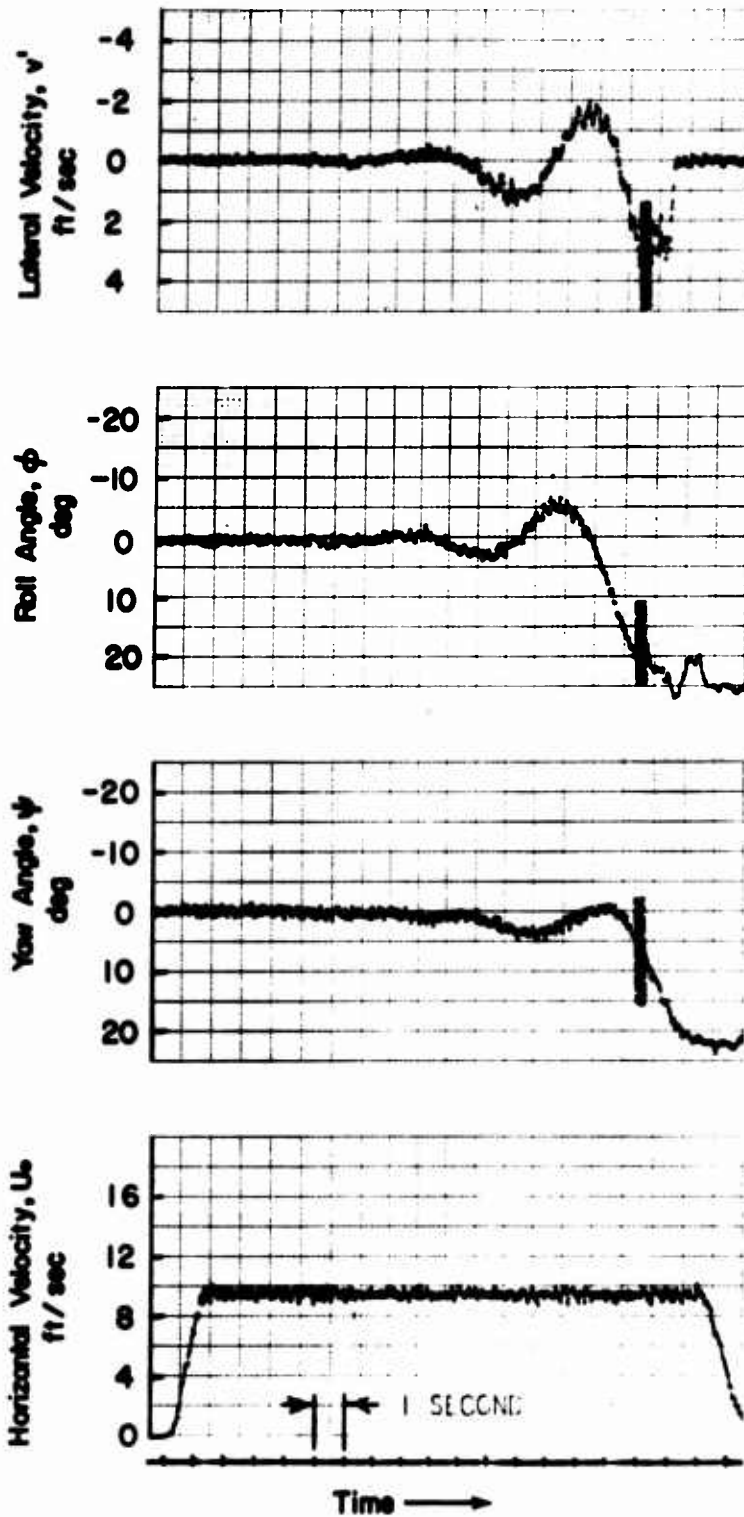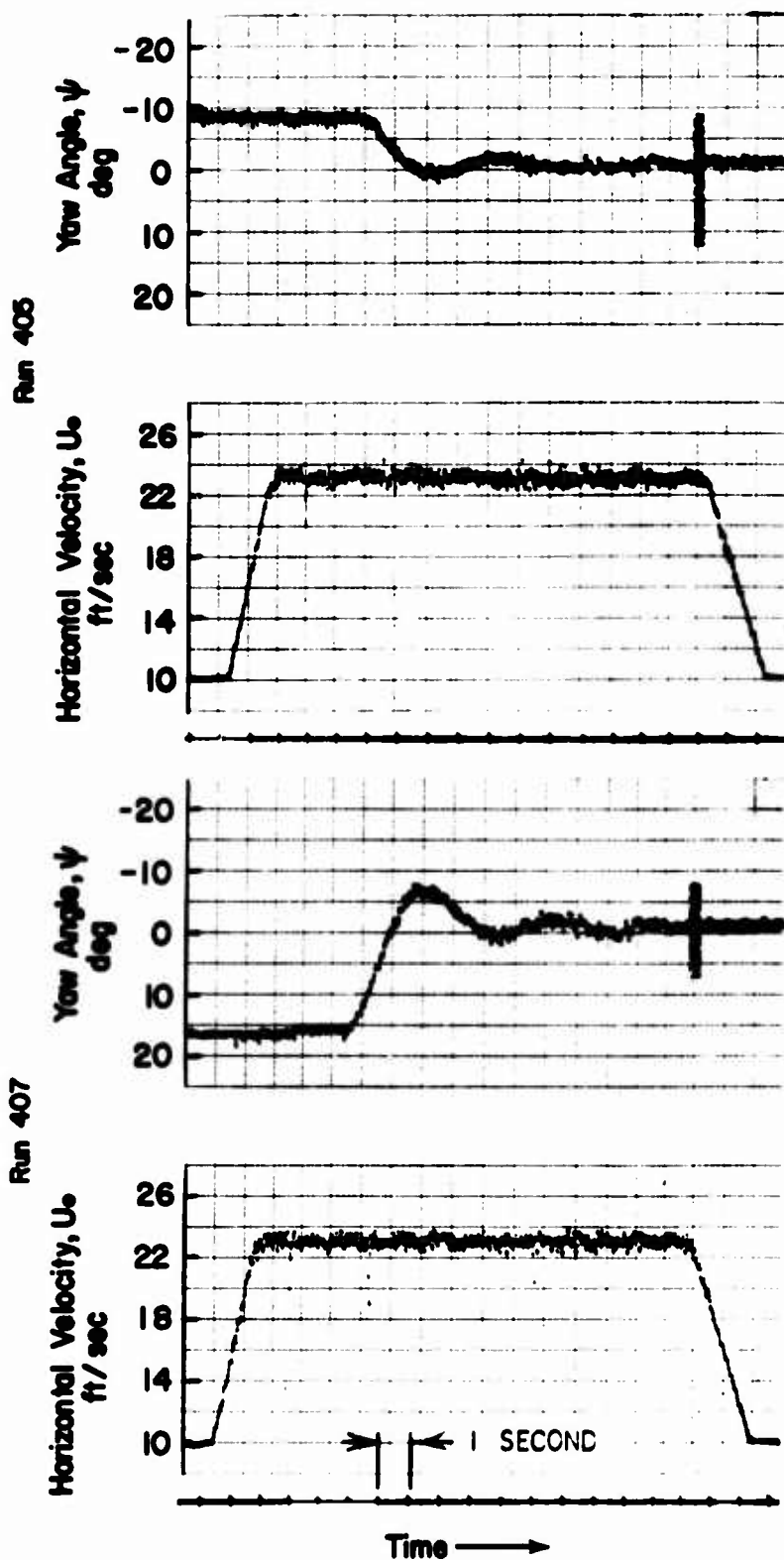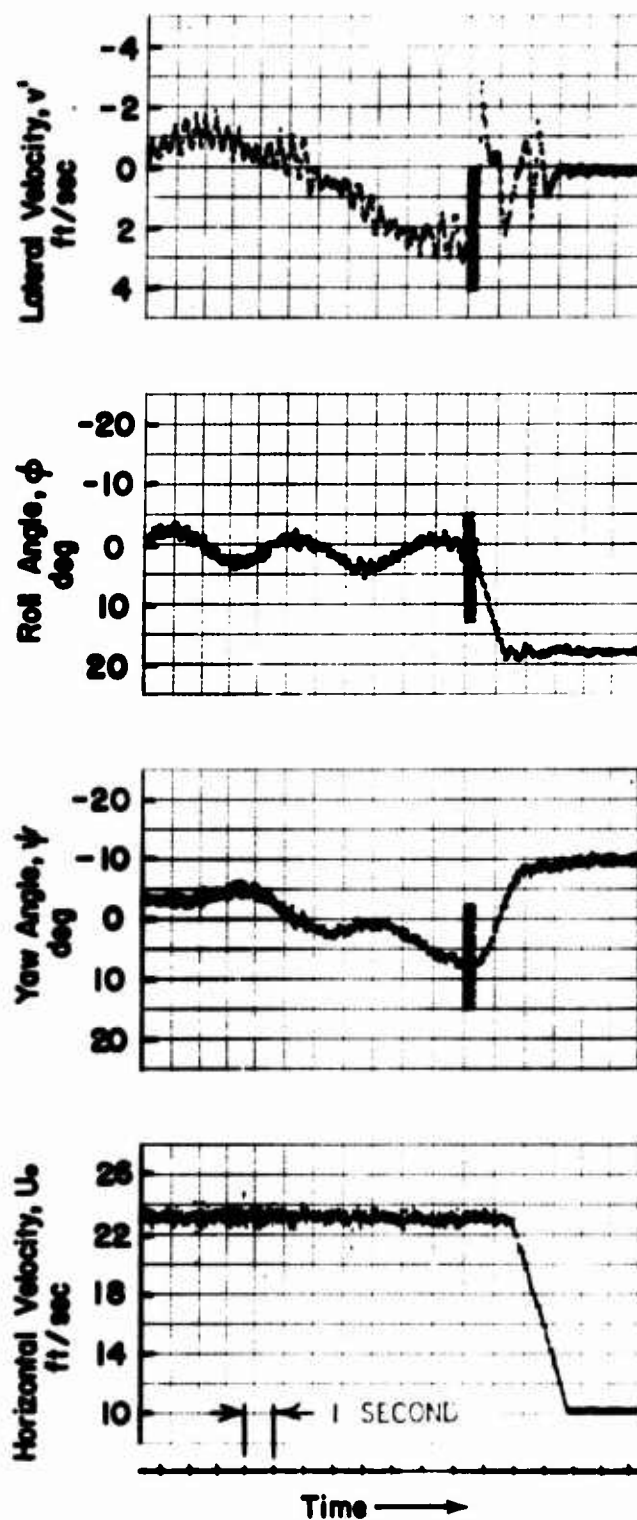


Figure 17d. Model Transient Response, $i_w = 30°$,
Three Degrees of Freedom.
(See Table V, Page 51, for Test Conditions)
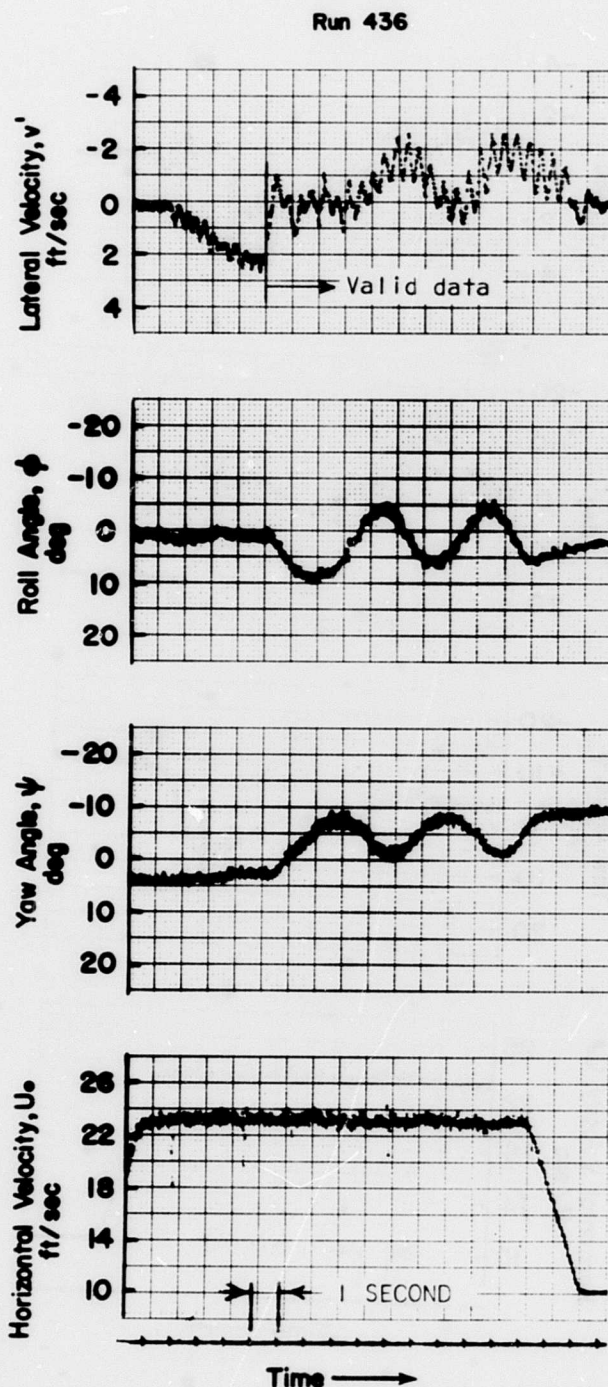
Figure 17e.  Model Transient Response, $i_w = 30°$,
Three Degrees of Freedom.
(See Table V, Page 51, for Test Conditions)

88
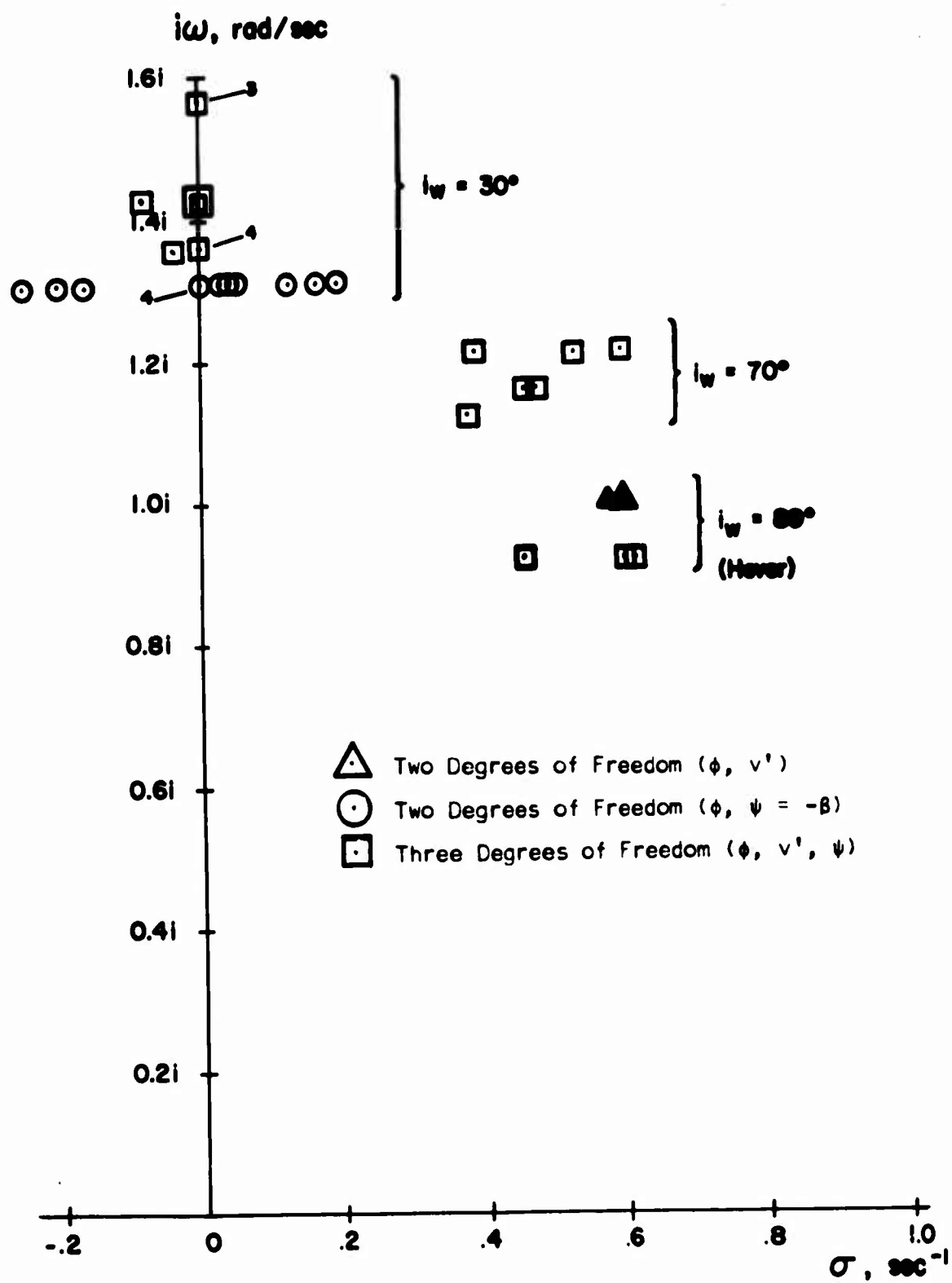
Figure 18. Summary of Model Transient Response Data.

TABLE VIII.   SUMMARY OF FORWARD FLIGHT DATA - MODEL SCALE

STATIC DATA

$i_W = 70°$

| Run | $Y_v$ | $L_v$ | $N_v$ |
|---|---|---|---|
| 322, 323, 324 | - 0.32 | - | 0.075 |
| 326, 328 | - 0.19 | - 0.14 | 0.105 |
| 331, 332 | - 0.18 | - 0.20 | 0.060 |
| Average value | - 0.23 | - 0.17 | 0.080 |

$i_W = 30°$

| 338, 339, 340 | - 0.45 | - 0.17 | 0.103 |
| 342, 343, 344 | - 0.50 | - 0.15 | 0.103 |
| 345, 346, 347 | - 0.38 | - 0.13 | 0.092 |
| Average value | - 0.44 | - 0.15 | 0.10 |

ROLL DAMPING                              YAW DAMPING

$i_W = 30°$

| Run | $L_{\dot{\phi}}$ | Run | $N_{\dot{\psi}}$ |
|---|---|---|---|
| 440 | - 0.70 | 447 | - 1.00 |
| 441 | - 0.71 | 448 | - 1.07 |
| 442 | - 0.81 | 449 | - 0.72 |
| 443 | - 0.73 | 450 | - 1.06 |
| 444 | - 0.77 | 451 | - 0.75 |
| Average value | - 0.74 | Average value | - 0.92 |

TABLE VIII - Continued

TRANSIENT RESPONSE (MEASURED CHARACTERISTICS)

$i_w = 70^o$

Three Degrees of Freedom

| | $\varphi$ | | $v'$ | | $\Psi$ | |
|---|---|---|---|---|---|---|
| Run | Period (seconds) | $\sigma$ | Period (seconds) | $\sigma$ | Period (seconds) | $\sigma$ |
| 371 | 5.2 | 0.60 | - | - | - | - |
| 372 | 5.4 | 0.48 | 5.2 | - | - | - |
| 383 | 5.2 | 0.53 | - | - | - | - |
| 389 | 5.6 | 0.38 | 5.6 | - | 6.0 | - |
| 392 | 5.2 | 0.39 | 5.4 | 0.46 | - | - |

Average period = 5.4 seconds, Average damping = 0.48

$i_w = 30^o$

One Degree of Freedom ($\Psi = -\beta$, $\varphi = 0$, $v' = 0$)

| | $\Psi$ | |
|---|---|---|
| Run | Period (seconds) | $\sigma$ |
| 404 | 4.2 | - 0.47 |
| 405 | 4.4 | - 0.56 |
| 406 | 4.4 | - 0.52 |
| 407 | 4.8 | - 0.46 |

Average period = 4.45 seconds, Average damping = - 0.50

91

TABLE VIII - Continued

$i_w = 30°$

Two Degrees of Freedom $(v' = 0, \Psi = -\beta)$

| Run | $\varphi$ Period (seconds) | $\sigma$ | $\Psi$ Period (seconds) | $\sigma$ |
|-----|------|---------|------|---------|
| 402 | 4.8 | 0.20 | 4.8 | 0.05 |
| 413 | 4.8 | 0.17 | 4.8 | 0.13 |
| 414 | 4.8 | - 0.16 | 4.8 | - 0.25 |
| 415 | 4.8 | 0.03 | 4.8 | 0.04 |
| 416 | 4.8 | - 0.20 | 4.9 | - |
| 417 | 4.8 | 0 | 4.8 | 0 |
| 418 | 4.8 | 0 | 4.8 | 0 |

Average period = 4.8 seconds,   Average damping = 0

$i_w = 30°$

Three Degrees of Freedom

| Run | $\varphi$ Period (seconds) | $\sigma$ | $v'$ Period (seconds) | $\sigma$ | $\Psi$ Period (seconds) | $\sigma$ |
|-----|------|---|------|---|------|--------|
| 398 | 4.6 | 0 | - | - | 4.6 | 0 |
| 430 | 4.6 | 0 | - | - | 4.6 | - 0.04 |
| 431 | 4.6 | 0 | - | - | 4.4 | - 0.08 |
| 435 | 4.4 | 0 | - | - | 4.4 | 0 |
| 436 | 4.0 | 0 | 4.0 | 0 | 4.0 | 0 |

Average Period = 4.4 seconds,   Average damping = 0

**DOCUMENT CONTROL DATA - R&D**

*(Security classification of title, body of abstract and indexing annotation must be entered when the overall report is classified)*

| 1. ORIGINATING ACTIVITY (Corporate author) | 2a. REPORT SECURITY CLASSIFICATION |
|---|---|
| Department of Aerospace and Mechanical Sciences Princeton University | Unclassified |
| | 2b. GROUP   - |

3. REPORT TITLE

Investigation of the Lateral/Directional Stability Characteristics of a Four-Propeller Tilt-Wing VTOL Model

4. DESCRIPTIVE NOTES (Type of report and inclusive dates)

5. AUTHOR(S) (Last name, first name, initial)

Boyden, Richmond, P.
Curtiss, Howard, C.

| 6. REPORT DATE | 7a. TOTAL NO. OF PAGES | 7b. NO. OF REFS |
|---|---|---|
| April 1968 | 106 | 12 |

| 8a. CONTRACT OR GRANT NO. DA 44-177-AMC-8(T) | 9a. ORIGINATOR'S REPORT NUMBER(S) |
|---|---|
| b. PROJECT NO. 1F125901A14233 | USAAVLABS Technical Report 68-19 |
| c. | 9b. OTHER REPORT NO(S) (Any other numbers that may be assigned this report) |
| d. | Aerospace Research Report 743 |

10. AVAILABILITY/LIMITATION NOTICES

This document has been approved for public release and sale; its distribution is unlimited.

| 11. SUPPLEMENTARY NOTES | 12. SPONSORING MILITARY ACTIVITY |
|---|---|
| - | U.S. Army Aviation Materiel Laboratories Fort Eustis, Virginia |

13. ABSTRACT

Results of an experimental investigation to determine the lateral/directional stability characteristics of a four-propeller tilt-wing VTOL aircraft using a one-tenth scale dynamically similar model are presented. Test conditions include wing incidences of $85^\circ$, $70^\circ$, and $30^\circ$. Measurements of the transient motion of the model in the lateral/directional degrees of freedom and the static lateral/directional stability derivatives were made using the Princeton Dynamic Model Track.

The transient and steady-state data are analyzed assuming that the motions of the vehicle may be described by linearized equations, and the resulting static and dynamic derivatives are presented. The characteristics of the lateral/directional dynamic motion of the full-scale vehicle as predicted by the tests of the dynamically similar model are determined and discussed. All data are presented for a center-of-gravity position of 9-percent MAC, which is ahead of the most forward C.G. position of the aircraft (15-percent MAC), and the horizontal tail and flap programs differ from those presently used on the aircraft.

The model results indicate that the full-scale aircraft would have an unstable lateral oscillation with a period of about 13 seconds at a wing incidence of $85^\circ$. At $30^\circ$ wing incidence, the lateral/directional motion is made up of a stable, lightly damped, Dutch-roll oscillation ; a rolling convergence; and a spiral divergence with a time to double amplitude of about 6 seconds.

**DD** FORM 1473 1 JAN 64

| 14. KEY WORDS | LINK A | | LINK B | | LINK C | |
|---|---|---|---|---|---|---|
| | ROLE | WT | ROLE | WT | ROLE | WT |
| Airplanes, VTOL<br>Airplanes, Tilt-Wing<br>Stability, Lateral<br>Stability, Directional | | | | | | |

## INSTRUCTIONS

1. ORIGINATING ACTIVITY: Enter the name and address of the contractor, subcontractor, grantee, Department of Defense activity or other organisation (*corporate author*) issuing the report.

2a. REPORT SECURITY CLASSIFICATION: Enter the overall security classification of the report. Indicate whether "Restricted Data" is included. Marking is to be in accordance with appropriate security regulations.

2b. GROUP: Automatic downgrading is specified in DoD Directive 5200.10 and Armed Forces Industrial Manual. Enter the group number. Also, when applicable, show that optional markings have been used for Group 3 and Group 4 as authorized.

3. REPORT TITLE: Enter the complete report title in all capital letters. Titles in all cases should be unclassified. If a meaningful title cannot be selected without classification, show title classification in all capitals in parenthesis immediately following the title.

4. DESCRIPTIVE NOTES: If appropriate, enter the type of report, e.g., interim, progress, summary, annual, or final. Give the inclusive dates when a specific reporting period is covered.

5. AUTHOR(S): Enter the name(s) of author(s) as shown on or in the report. Enter last name, first name, middle initial. If military, show rank and branch of service. The name of the principal author is an absolute minimum requirement.

6. REPORT DATE: Enter the date of the report as day, month, year; or month, year. If more than one date appears on the report, use date of publication.

7a. TOTAL NUMBER OF PAGES: The total page count should follow normal pagination procedures, i.e., enter the number of pages containing information.

7b. NUMBER OF REFERENCES: Enter the total number of references cited in the report.

8a. CONTRACT OR GRANT NUMBER: If appropriate, enter the applicable number of the contract or grant under which the report was written.

8b, 8c, & 8d. PROJECT NUMBER: Enter the appropriate military department identification, such as project number, subproject number, system numbers, task number, etc.

9a. ORIGINATOR'S REPORT NUMBER(S): Enter the official report number by which the document will be identified and controlled by the originating activity. This number must be unique to this report.

9b. OTHER REPORT NUMBER(S): If the report has been assigned any other report numbers (*either by the originator or by the sponsor*), also enter this number(s).

10. AVAILABILITY/LIMITATION NOTICES: Enter any limitations on further dissemination of the report, other than those imposed by security classification, using standard statements such as:

(1) "Qualified requesters may obtain copies of this report from DDC."

(2) "Foreign announcement and dissemination of this report by DDC is not authorized."

(3) "U. S. Government agencies may obtain copies of this report directly from DDC. Other qualified DDC users shall request through
_____."

(4) "U. S. military agencies may obtain copies of this report directly from DDC. Other qualified users shall request through
_____."

(5) "All distribution of this report is controlled. Qualified DDC users shall request through
_____."

If the report has been furnished to the Office of Technical Services, Department of Commerce, for sale to the public, indicate this fact and enter the price, if known.

11. SUPPLEMENTARY NOTES: Use for additional explanatory notes.

12. SPONSORING MILITARY ACTIVITY: Enter the name of the departmental project office or laboratory sponsoring (*paying for*) the research and development. Include address.

13. ABSTRACT: Enter an abstract giving a brief and factual summary of the document indicative of the report, even though it may also appear elsewhere in the body of the technical report. If additional space is required, a continuation sheet shall be attached.

It is highly desirable that the abstract of classified reports be unclassified. Each paragraph of the abstract shall end with an indication of the military security classification of the information in the paragraph, represented as (TS), (S), (C), or (U).

There is no limitation on the length of the abstract. However, the suggested length is from 150 to 225 words.

14. KEY WORDS: Key words are technically meaningful terms or short phrases that characterize a report and may be used as index entries for cataloging the report. Key words must be selected so that no security classification is required. Identifiers, such as equipment model designation, trade name, military project code name, geographic location, may be used as key words but will be followed by an indication of technical context. The assignment of links, rules, and weights is optional.

GPO 886-551